

**UNIVERSITY OF CATANIA**

DEPARTMENT OF CHEMICAL SCIENCES

INTERNATIONAL PhD IN CHEMICAL SCIENCES – XXXIII CYCLE

---

*Davide Gentile*

**A computational approach for the molecular  
recognition of novel ophthalmic prodrugs and  
molecular modelling of sigma receptor ligands in  
ocular diseases**

=====  
PhD Thesis  
=====

**Tutor :**  
*Prof. Antonio Rescifina*

**PhD. Coordinator:**  
*Prof. Salvatore Sortino*

---



## Abstract

In full compliance with the project financed by the European Social Fund, Action I.1 “*Innovative Doctorates with Industrial Characterization*”, some strategies have been adopted for the targeted delivery of ophthalmic drugs through the design and synthesis of prodrugs.

The physicochemical, pharmacokinetic, and pharmacodynamic properties represent, in many cases, a limitation of drugs, regardless of the pharmacological activity. For this reason, the need arises to use the prodrug approach to overcome these gaps.

Ophthalmic drug administration is generally the most common in treating many eye diseases, although the ocular bioavailability of topically applied drugs is <5%. Transporters play an important role in arranging many drugs and their metabolites in other parts of the body. Although the role of active transporters has been known for a long time, in recent years, they have drawn the attention of researchers to improve drug recognition by transporters and elucidate complex transport mechanisms.

After an overview of prodrugs (Chapter 1), ophthalmic prodrugs were designed based on the molecular recognition by two different active transporters: sodium-dependent multivitamin transporter (SMVT) for timolol transport (Chapter 2) and concentrative nucleoside transporter (CNT) for the transport of acyclovir (Chapter 3).

The SMVT transporter structure was reconstructed using a homology modeling approach. This method allowed to evaluate, *in-silico*, the stability, and the new self-immolative prodrugs' recognition quality. This study highlights for the first time the likely binding site of biotin and other physiological ligands for the SMVT transporter, detailing key interaction residues at the binding site. Furthermore, the molecular dynamics simulation (MD simulation) allowed us to evaluate the stability of every

single complex with prodrugs. The synthesized prodrugs show a better partition coefficient (logP) than timolol, with consistent corneal permeability values.

Conjugated acyclovir-uridine prodrugs have been designed and synthesized to study and evaluate the potential of these cellular transport systems that have never been considered to date. Furthermore, computational studies were carried out to evaluate the stability of the interactions between prodrugs and the recognition site of the CNT transporter. Computational analyzes revealed interesting mechanistic interactions on uridine-drug reuptake for the rational design of prodrugs recognized by CNT.

In Chapter 4, the sigma ( $\sigma$ ) receptors were treated for their biological activity in some eye diseases. Ligands of the  $\sigma$  receptors were synthesized. The new hybrid inhibitors allow having both a  $\sigma_1$  ligand and a NO donor fraction in the same scaffold. In this preliminary phase, the synthesized compounds were evaluated both for their ability to bind sigma receptors and for the release of NO. Furthermore, a computational method that could predict the agonist/antagonist activity of the  $\sigma_1$  receptor ligands has been shown in this chapter. This computational approach could facilitate pharmaceutical chemists' task for the rational synthesis of new drugs with  $\sigma_1$  activity.

This is the first prodrug design study for molecular recognition from transporters (SMVT and CNT) based on a comprehensive computational approach.

Unfortunately, the COVID-19 pandemic interfered with the period in the company (translated into smart working), slowing down both the *in vivo* experiments on cell lines to demonstrate the uptake of the newly synthesized prodrugs and the ophthalmic formulation tests.



## Summary

Chapter 1	Prodrugs: An Overview .....	1
1.1	Introduction .....	1
1.2	History And Market Of Prodrugs.....	4
1.3	Rationale For Prodrug Design.....	5
1.3.1.	Solution Of The Formulation And Administration Problems .....	6
1.3.3.	Solution Of The Distribution Problems .....	8
1.3.4.	Solution Of The Metabolism And Excretion Problems.....	9
1.3.5.	Solution Of The Toxicity Problems.....	10
1.4	Eye: Anatomy, Physiology, And Barriers To Drug Delivery.....	11
1.4.1.	Ocular Structures .....	11
1.4.2.	Ocular Pharmacokinetics .....	14
1.4.3.	Absorption .....	14
1.4.4.	Distribution .....	16
1.4.5.	Metabolism.....	16
1.4.6.	Toxicology .....	16
1.5	Aqueous Humor Dynamics And Regulation Of Intraocular Pressure .....	17
1.6	Biological Systems Of Ocular Transport.....	18
1.6.1.	Peptide Transporters .....	19
1.6.2.	Monocarboxylate Transporters .....	20
1.6.3.	Sodium-Dependent Multivitamin Transporter .....	20
1.6.4.	Organic Anions And Cations Transporters.....	21
1.6.5.	P-Glycoprotein.....	21
1.7	Prodrug Strategies In Ocular Drug Delivery .....	22
1.7.1.	Ester Prodrugs .....	23

1.7.2. Phosphate Ester .....	26
1.7.3. Carbamate Prodrugs.....	26
1.7.4. Oxime Prodrugs .....	27
1.7.5. Oxazolidine Prodrugs.....	27
1.7.6. Prodrugs Derived From Sulfonamide Groups .....	28
1.7.7. Nitrooxy Prodrugs .....	28
1.8 Transporter Targeted Prodrug Approach .....	28
1.9 Self-Immolative Prodrugs.....	31
1.9.1 Self-Immolative Prodrugs Fragmenting By 1,4, 1,6, Or 1,8 Elimination	32
1.9.2 Self-Immolative Prodrugs Fragmenting Following Cyclization .....	34
1.9.3 Kinetic Analysis Of Self-Immolative Drugs .....	36
1.9.4 Structure-Property Relationships .....	37
Chapter 2          New Self-Immolative Prodrug Of Timolol.....	40
2.1 Introduction .....	40
2.2 Therapy For Glaucoma.....	41
2.3 Ophthalmic Prodrugs.....	42
2.4 Timolol Prodrugs: State Of The Art.....	43
2.5 Design Of New Biotinylated Derivatives Of Timolol .....	46
2.6 Physiological Properties And Functions Of Sodium Dependent Multivitamin Transporter (Smt) .....	50
2.7 Computational Approach To The Transport Of Biotinylated Drugs .....	51
2.8 Homology Model And Computational Study Of Smt .....	52
2.9 Synthesis Of The New Timolol Prodrugs.....	62
2.10 Determination Of Partition Coefficient (Log P) Chemical (Non-Enzymatic) Stability .....	63

2.11 Conclusions And Perspective.....	64
Chapter 3 Cnt Transporters For New Prodrug Of Acyclovir.....	66
3.1 Introdruction.....	66
3.2 Herpes Zoster Ophthalmicus .....	67
3.3 Pharmacological Therapy And Ophthalmic Prodrugs Of Acyclovir .....	69
3.4 Structure And The Transport Mechanism Of The Concentrative Nucleoside Transporter Cnt .....	72
3.5 State Of The Art.....	78
3.6 Rational Design Of Acv Prodrugs .....	79
3.7 Computational Approach For Drug-Cnt Transporter Systems.....	83
3.8 Synthesis Of The New Acyclovir Prodrugs .....	89
3.9 Conclusions And Objectives.....	91
Chapter 4 Sigma-1 Receptors In Ocular Pathologies.....	93
4.1 Introduction .....	93
4.2 Crystal structure and binding site .....	95
4.3 Nitric oxide (no): a potential enemy against glaucoma.....	96
4.4 Sigma receptor ligands donating nitric oxide .....	100
4.5 A computational model to predict the effect of ligands on sigma $\sigma$ 1 receptors: preliminary results .....	109
4.6 Conclusion And Perspective .....	115
Chapter 5 Experimental Part.....	117
General Information .....	117
Ligand Preparation .....	130
Receptor Preparation.....	130
Homology Model.....	131
Docking Protocol.....	131



Molecular Dynamics Simulations.....	132
References .....	140



---

## CHAPTER 1 PRODRUGS: AN OVERVIEW

### 1.1 INTRODUCTION

The concept of prodrug was introduced in 1950 by Adrian Albert.<sup>1</sup> He defined prodrug a pharmacologically inactive compound that by the action of an enzymatic and/or chemical reaction is transformed into a therapeutically active drug. The conversion from prodrug to drug can occur before, during, or after absorption or at a specific site of the organism, especially if an enzyme is more abundant at a specific site.<sup>2,3</sup>

In the last ten years (2008–2017), by the US Food and Drug Administration (FDA) more than 30 prodrugs have been approved. Interestingly, in the last 3 years, 17% of approvals were prodrugs. About 10% of all marketed drugs around the world can be considered prodrugs.<sup>4</sup>

In most cases, prodrugs are simple chemical derivatives whose work of one or two chemical and/or enzymatic steps is transformed into an active drug and one or more non-toxic molecules for the body. Such modification may be, for example, oxidation or a metabolic reduction that generates a new compound generally active. There are other derivatives of the drugs called codrugs. The latter are 2 or more drugs bound together by a covalent bond.<sup>5</sup> The concept of the prodrug is shown in Figure 1.1.

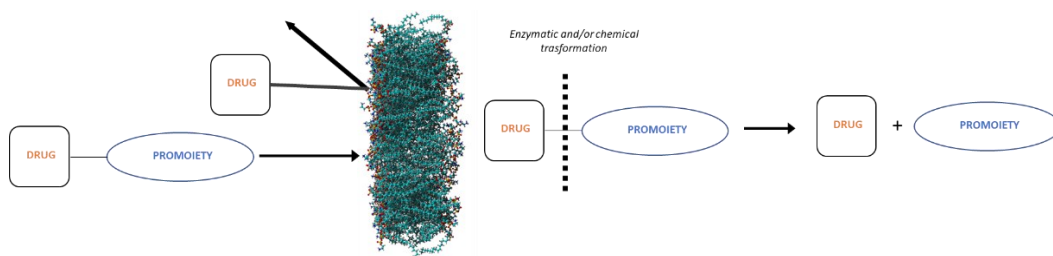


**Figure 1.1.** Schematic concept of prodrugs.

The design of a prodrug must be borne in mind that they can alter the tissue's distribution, the efficacy, and even the toxicity of the parent drug.

---

Although designing a prodrug taking into account all these factors is very demanding, at the same time, it is much more feasible than an entirely new molecule. The main factors which should be carefully considered when designing a prodrug are as follows:

- Identify the functional groups of the parent drug that can be derivatized.
  - The chemical modifications made to the drug must be reversible and must allow the prodrug to be reconverted into the parent drug by a chemical or enzymatic reaction.
  - The absorption, distribution, metabolism, and excretion (ADME) properties of the parent drug and the prodrug must be widely studied.
  - The promoiety must be non-toxic and quickly removed from the body. The choice of promoiety and its safety must also be considered in relation to the pathology, the organ of the target site, and the dose and duration of treatment.
  - The prodrug's chemical and physical stability in the galenic form (solid or liquid) is crucial for the final result and its commercialization.
-

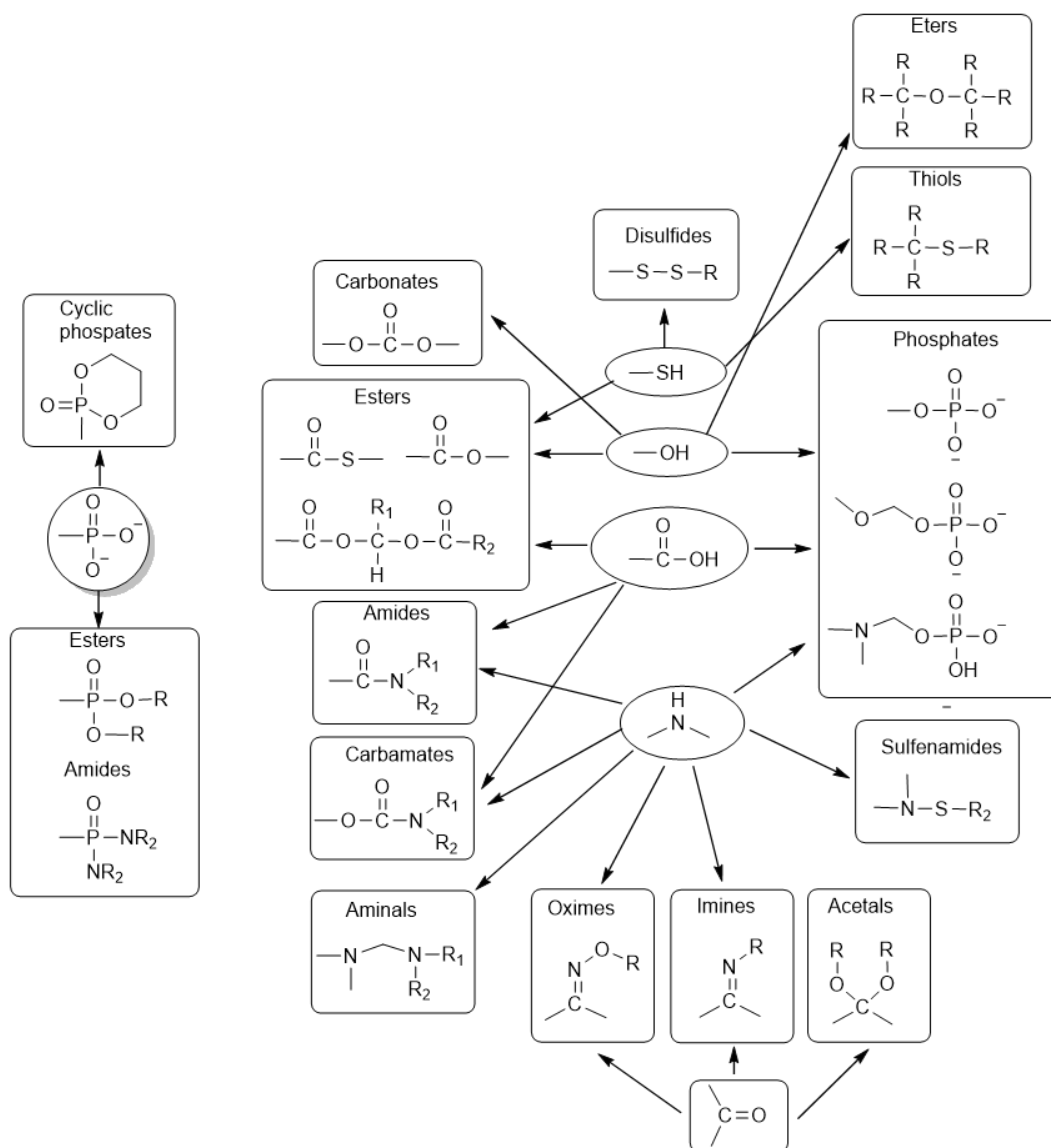


**Figure 1.2.** Prodrug strategies for the most common functional groups on parent drugs.

The most common approaches for the design of prodrugs aim at bioconversion metabolic activation by enzymes hydrolases such as peptidase, phosphatase, and carboxylesterase. In fact, these enzymes are well distributed throughout the body and are usually not involved in drug interactions. It is important to note that the esterases in some cases can prematurely hydrolyze the prodrug before it reaches the target organ, compromising the success of the design. *In-vitro* evaluation of hydrolysis rates is not always the right predictor of *in-vivo* convection due to the many biological factors that can hardly be controlled in such studies.<sup>6</sup> The most

common functional groups for the design and synthesis of prodrugs are described in Figure 1.2.

## 1.2 HISTORY AND MARKET OF PRODRUGS

Schering introduced the first prodrug in 1899; this was methanamine (or hexanamine). Methanamine releases formaldehyde and ammonium ions in urine as an antimicrobial agent. Aspirin, introduced by Bayer, is a less irritating form of salicylic acid. However, aspirin is rapidly hydrolyzed into the intestinal wall and the liver to salicylic acid. Although it was intended to function as a propellant, aspirin irreversibly inhibits cyclooxygenase, the enzyme responsible for forming the primary biological mediators, prostaglandins, and thromboxanes. The main drug, salicylic acid, is a weak reversible cyclooxygenase inhibitor and can not be considered a prodrug.

In 1935 Bayer introduced another prodrug, prontosil, capable of releasing aminophenyl sulfonamide for reduction of reducing enzymes. This led to the discovery of the most used antibacterials, sulphonamides. A few years later, Roche discovered an anti-tuberculosis prodrug.

The enzyme peroxidase catalyzes the bioactivation of isoniazid, and the compound generated inhibits the biosynthesis of mycolic acid, required for the growth of the cell wall of bacteria.

Between 2008 and 2017, 30 prodrugs were approved by the US Food & Drug Administration (FDA), representing 12% of all small-molecule new chemical entities (NCEs) and about 10% of all approved drugs. It is important to note that in the last 3 years of all NCE approvals, 17% were prodigious. After a thorough analysis of the prodrugs approved in recent years, there is a tendency to focus on design to overcome the ADMET obstacle. The prodrug strategy is a versatile and powerful method that can be applied to various pharmaceutical products whose pharmacological limitations are compromised by their clinical use. The development of

---

prodrugs is now consolidated as a strategy to improve ADMET's properties of pharmacologically potent compounds already in the early stages of drug discovery. Furthermore, the economic importance of the extension of patent protection for an existing drug may be significant. These reasons have already led to an increasing number of approved prodrugs that are on the market.

In the ophthalmic sector, two prodrugs have been approved in the last six years, namely Tafluprost in 2012, trade name Ziotan, and Latanoprostene bunod in 2017, none commercial Vyzulta. Both are used to treat glaucoma; in fact, they are prostaglandin analogs that decrease intraocular pressure. The modifications made to the progenitor drugs tend to increase the lipophilic character, which allows a more excellent corneal permeability.<sup>7</sup>

### **1.3 RATIONALE FOR PRODRUG DESIGN**

The logic behind the design of prodrugs focuses on optimizing ADME properties because they are primarily responsible for drugs' side effects. In fact, the prodrug strategy is very versatile in varying some parameters of the parent drug, such as absorption, toxicity, stability, and shelf life. It is easier and more effective for the industry to develop a prodrug to improve an existing drug's specific characteristics and effectiveness.

A drug can exert a desired pharmacological effect only if it reaches its site of action. The three main phases involved in the drug-receptor the biological interaction or bioavailability of the drug include:

- the pharmaceutical phase,
- the pharmacokinetic phase,
- the pharmacodynamic phase.

Pathological limitations such as high incidence of side effects, teratogenicity and toxicity, pharmaceutical problems such as chemical instability of the

---

formulation or product, psychological limitations such as pain at the injection site, unpleasant taste and cosmetic damage to the patient include pathological limitations. These limits can be overcome with the prodrug approach, and after passing various physiological barriers, the prodrug should rapidly convert to the active drug upon reaching the target site.<sup>8</sup>

The effective, safe, stable, acceptable and aesthetic design of targeting a drug to its site of action, overcoming various physical, chemical and social barriers, the prodrug approach has a great deal of potential.

The pharmaceutical phase is the initial phase which involves the identification of a new chemical entity with therapeutic potential and its inclusion in a drug delivery system. The delivery system can be multiple, such as capsules, tablets, creams / ointments, injections or new methods such as liposomes and installations.

The pharmacokinetic phase is considered the next phase, which involves the absorption, distribution, metabolism and excretion of the drug. Pharmacokinetic studies provide a lot of information on the properties of a drug, such as low absorption, excessively rapid elimination kinetics and pre-systemic metabolism. If these properties can be traced back to physicochemical and dosage, system properties are formed so that corrections require prodrug interventions.

### ***1.3.1. Solution of the formulation and administration problems***

The water solubility of a drug is an essential requirement for the preparation of water-based solutions for parental or injectable dosage. Several successful prodrugs show a high-water solubility compared to the original drug on the market. The most common strategy is the introduction of polar or ionizable groups in the molecule structure. One of the most used groups is the phosphoric acid ester, whose dianion increases the solubility by several magnitude orders.<sup>9</sup>

---



An excellent example of this is fosphenytoin, a phosphate ester prodrug of poorly water-soluble anticonvulsant phenytoin, which can be used in both intravenous and intramuscular administration. Although the simple sodium salt of this weakly acidic drug also has a good water solubility at high pH values, it can cause local irritation at the injection site, which is due to the drug's precipitation when the pH adjusts to the physiological range. With fosphenytoin, a phosphate ester is attached to a phenytoin acid amine functionality through an oxymethylene spacer. Therefore, this example of prodrug shows the use of a 700% increase in water solubility. Although stable at neutral pH values, fosphenytoin is completely reconverted into *in vivo* phenytoin by alkaline phosphatase through a chemically unstable intermediate (Figure 1.3), with a half-life ranging from 7 to 15 minutes in humans.<sup>10</sup>

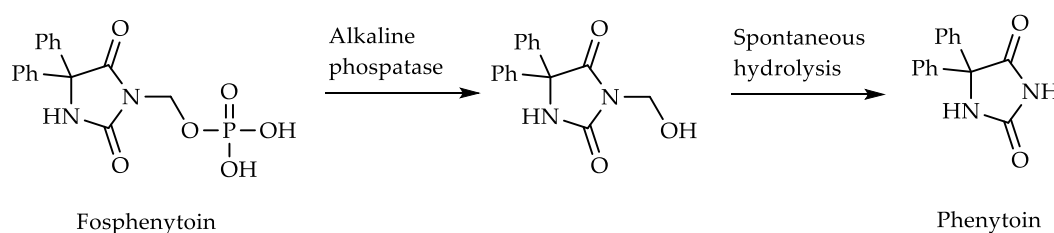


**Figure 1.3.** Bioconversion of phenytoin after activation by alkaline phosphatases.

### 1.3.2. Solution of the Absorption Barriers

To date, the most significant efforts have been focused on improving passive drug penetration through epithelial cell membranes, absorption in the gastrointestinal tract, and corneal permeability.

The most widespread solution is the derivatization of drugs related to esters. In fact, they represent about 50% of the prodrugs of the entire market. These prodrugs are activated by the enzymatic hydrolysis carried out by the ubiquitous esterases found in the blood, liver, and other organs and tissues, including carboxylesterase, acetylcholinesterase, butyrylcholinesterase, paraoxonase, and arylesterase.

For example, Enalapril, an ACE inhibitor, is used to treat hypertension in some cases of heart failure. This prodrug is converted into the active form, enalaprilat, from the esterases. The ethyl group allows a 74% absorption and a bioavailability of 44%.

Another example is famciclovir, an antiviral drug used to treat orolabial herpes. It is a prodrug of 6-deoxy-penciclovir, an analog of adenosine. Compared to the parent drug, oral availability increases by 75%, thanks to the introduction of acetyl groups. The acetyl groups are hydrolyzed by the esterases present in the liver, and by subsequent oxidation of the purine into guanidine, the active form is released, *i.e.*, the penciclovir.

An alternative way to increase oral absorption of a drug is carrier-mediated transport, mainly when a drug is polar or laden and where passive transcellular absorption is negligible. While surprisingly, many drugs already benefit from gastrointestinal tract carriers, and several prodrugs have been designed to have structural features that allow them to be recognized and detected by one of these carriers.<sup>11</sup>

### ***1.3.3. Solution of the Distribution Problems***

Some prodrugs are designed to alter the distribution in the body and reach a specific site. An interesting example is given by levodopa (L-dopa). The neurotransmitter dopamine is unable to cross the blood-brain barrier and is poorly distributed in the brain due to its hydrophilic nature. However, dopamine conversion into its  $\alpha$ -amino acid, levodopa, allows dopamine intake in the brain via the large neutral amino acid transporter (LAT1). After inserting the brain tissue, the levodopa is rapidly converted into dopamine by dopa decarboxylase (Figure 1.4) and, being a very hydrophilic molecule, it is trapped near the active site, thus allowing its pharmacodynamic effects. Although the role of LAT1 in brain intake and the distribution of levodopa has probably been discovered in hindsight, they have more recent carrier-

---

mediated prodrugs specifically designed for specific carriers, especially those that could improve intestinal absorption after oral administration.<sup>12,13</sup>

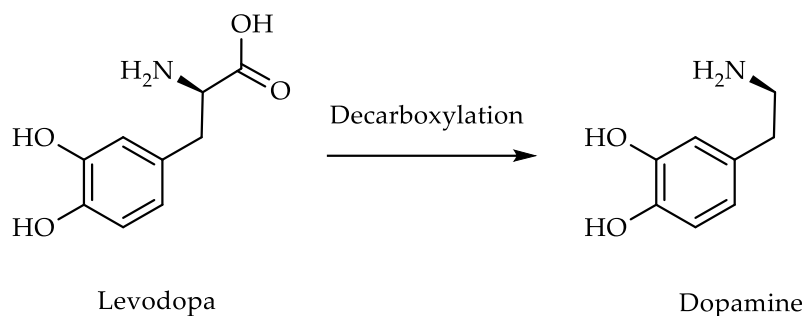


**Figure 1.4.** Bioconversion of levodopa to dopamine after activation by decarboxylation.

#### ***1.3.4. Solution of the Metabolism and Excretion Problems***

Decreasing levels of metabolism and excretion of drugs is a major challenge for pharmaceutical chemists. The strategy is to mask some metabolically labile functional groups in order to avoid rapid metabolism. An example is terbutaline, a beta 2 selective agonist, which is the active principle of specific indication against certain respiratory diseases. To obtain a prolonged action of this drug, a derivative dimethyl carbamate, bambuterol, was synthesized. Protection of phenolic units, which are sensitive to rapid and extensive pre-systemic metabolism, results in a specific avoidance of the first intestinal and hepatic metabolism pass. After oral administration, bambuterol is slowly bioconverted to terbutaline (Figure 1.5), predominantly from non-specific butyrylcholinesterase and lung tissue capable of the same metabolism. Consequently, slower release and prolonged action provide treatment to the bambuterol once a day asthma relief with a lower incidence of side effects than terbutaline took three times a day.<sup>14</sup>

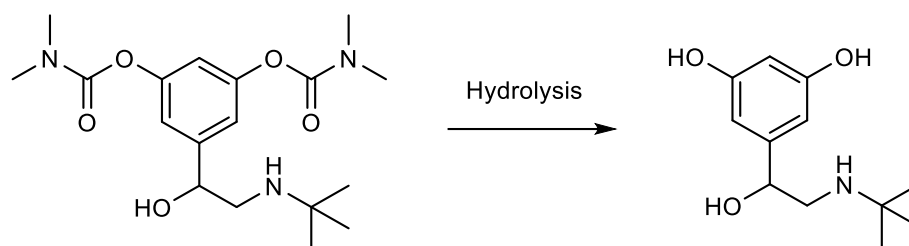


**Figure 1.5.** Bambuterol bioconversion.

### 1.3.5. Solution of the Toxicity Problems

The prodrugs designed to increase absorption, for the specificity of action for the stability and a slow-release, also reduce the drug's toxicity. For example, epinephrine, used in glaucoma treatment, presents many ocular and systemic side effects correlated with its use. The dipivaloyl epinephrine prodrug proved to be more powerful than epinephrine in dogs and rabbits and as effective as epinephrine in humans with a significantly increased toxicological profile.

Another example of the prodrug's utility to reduce the toxicity of a drug can be observed in aspirin analogs' design. The side effects associated with the use of aspirin are gastric irritation and ulceration. Esterification of aspirin ( $R = \text{alkyl}$ ) and the use of other non-steroidal anti-inflammatory drugs significantly reduce gastric activity. Unfortunately, the esterification of aspirin makes the acetyl group of aspirin extremely susceptible to enzymatic hydrolysis. The esters of some 2-hydroxyacetamides  $N,N$ -disubstituted ( $R = \text{CH}_2\text{CONR}_1\text{R}_2$ ) are very chemically stable but are hydrolyzed very rapidly in the plasma from the pseudocholinesterases and, therefore, they are proven suitable as aspirin prodrugs to reduce irritant effects of this drug at the gastric level<sup>15</sup>.

## 1.4 EYE: ANATOMY, PHYSIOLOGY, AND BARRIERS TO DRUG DELIVERY

The eye is the sense organ of phototransduction; it is almost spherical and is housed in the orbital cavity, consisting of an adipose body and bounded by bones of the skull and splanchnocranium.

The eye is a complex system that is relatively isolated from systemic access by the blood-retinal, blood-aqueous and blood-vitreous barriers. Thanks to its particular anatomy, the eye represents an exclusive organ-specific pharmacological laboratory for studying the effects of inflammation and the autonomic nervous system. No other organ in the body is so accessible and so visible for the study of pharmacological effects.

### 1.4.1. Ocular Structures

Inside the eye, there are cavities with different physicochemical properties, delimited by a wall organized into three overlapping tunics: fibrous, vascular, and nervous. The eye can be divided into two segments, front, and rear. The cornea, the limbo, the anterior chamber, the posterior chamber, the trabecular reticular, the Schlemm channel, the lens, the zonula, and the ciliary body are recognizable at the front. The posterior segment includes the vitreous, the retina, the choroid, the sclera, and the optic nerve.<sup>16,17</sup>

- *Anterior Segment*

The cornea is an entirely avascular tissue and, for the most part, is formed by the stroma, a hydrophobic layer characterized by collagen lamellae, synthesized by keratocytes and immersed in a glycoprotein matrix with a refractive index equal to that of the fibers. Below the stroma is the basal membrane of the corneal endothelium, called the Descemet membrane. Internally it consists of endothelium, a monolayer of cells that maintain the cornea's integrity by acting as a hydrophobic barrier. Externally, it is coated with stratified floor epithelium, a barrier for external agents and drugs. The hydrophobic epithelial layer comprises five to six layers of cells. The basal

---

epithelial cells rest on a basal membrane adjacent to Bowman's membrane, a collagen fibers layer.

The iris is the most anterior portion of the grape tract, including the ciliary body and the choroid. The iris's anterior surface consists of a layer of fibrocytes and melanocytes below the stroma of connective tissue lasso with pigmented cells and smooth muscle cells to form the pupil's constrictor muscle whose contraction determines myosis, blood vessels, and parasympathetic and sympathetic nerves. A double epithelial leaflet covers the iris's posterior surface with pigmented cellular elements and myoepithelial cells, which have numerous radially directed cytoplasmic projections containing contractile myofilaments, which together form the dilator muscle of the pupil whose contraction determines mydriasis.

The ciliary body consists of the ciliary orbit, the ciliary crown, and the ciliary muscle. The ciliary body's anterior portion is a ring-shaped structure, which rises to form the ciliary processes. These are composed of strongly vascularized loose connective tissue and covered with a double epithelial leaflet, involved in the secretion of aqueous humor. Externally there is a ring of smooth muscle cells that give rise to the ciliary muscle, the contraction of which is responsible for the accommodation process. This phenomenon allows one to focus on nearby objects and can be blocked pharmacologically by cholinergic muscarinic antagonists through cycloplegia.

The ciliary muscle contraction also exerts traction on the scleral spur, widening the spaces within the trabecular network. This phenomenon explains, at least in part, the reduction of intraocular pressure using parasympatheticomimetic drugs, both direct and indirect action.

The crystalline lens is a transparent, avascular structure of epithelial and biconvex nature, with elastic properties that allow it to modify the radius of curvature of the front and rear surfaces, depending on the accommodation

---

needs. The crystalline lens has a diameter of about 10 mm and consists of three elements: a capsule, thin and elastic, an epithelial layer of cubic cells, and a substance of its own, consisting of elongated epithelial cells. The more superficial cells that form the anterior epithelium slowly proliferate and continue to produce new fibers throughout life. However, aging, taking certain medications, such as corticosteroids, and certain diseases, such as diabetes mellitus, make the crystalline lens opacity, a condition that is referred to as a cataract.<sup>18,19</sup>

- *Posterior segment*

Due to the whitish color conferred by the fibers, the sclera or white of the eye is formed by dense connective tissue, with collagen and elastin fibers, and has the function of protection as of seat for the insertion of the extrinsic muscles.

The outer surface of the scleral capsule is coated by the vascular episcleral layer, the Tenon capsule, and the conjunctiva. Also, the tendons of the six extra-ocular muscles fit on the surface collagen fibers of the sclera. The numerous blood vessels, which perforate it, provide the choroid's blood circulation, the ciliary body, the optic nerve, and the iris. Hydrated, the scleral fibers stay opaque, while the corneal fibers do not retain the water become transparent. The corneal lendelion helps to maintain its openness by removing water. The sclera, being the eyepiece's outer coating, is subject to numerous changes in the outer environment and intraocular pressure.

The rods are about 20 times more numerous than the cones and are more sensitive to light, ensuring twilight vision in low visibility conditions. The cones are primarily dedicated to daytime vision, chromatic sensitivity, spatial discrimination. Each stick contains a special light-sensitive pigment, rhodopsin, which consists of a large protein, opsin, and the retinal; when light rays hit the retina and are absorbed by the rhodopsin, the retinal is isomerized and activates the enzymatic activity of the opsin, which then

---

initiates a phototransduction process, generating action potentials that then travel along the optic nerve. The cones, on the other hand, have iodopsin, which absorbs the intense and colored light. Due to the anatomical and vascular barriers of the posterior part of the eye, which hinder the passage of drugs, administered both topically and systematically, the posterior pole's pharmacological treatment is complicated.<sup>20</sup>

#### **1.4.2. Ocular Pharmacokinetics**

Numerous factors influence the bioavailability of the ophthalmic drugs; these factors are mainly determined by the drug's chemical and physical characteristics, that is, the drug's molecular structure, pH, and logP. Other factors concern the vehicle's characteristics: osmolarity, osmolality, density, viscosity, etc.

Numerous formulations can prolong the pharmacological agent's residence time on the eye's surface: gels, ointments, solid preparations, contact lenses, and collagen protections.

Pharmacokinetic theory based on studies of systemically administered drugs cannot be applied to all ophthalmic drugs. Although similar principles of absorption, distribution, metabolism and excretion determine the disposition of the drug in the eye, alternative routes of drug administration, in addition to the oral and intravenous routes, introduce other alternatives in the compartmental approach. Most ophthalmic drugs are formulated to be applied topically.

#### **1.4.3. Absorption**

The rate of absorption of an active ingredient through topical ocular depends on the following variables: the time in which the active ingredient remains in the *cul-de-sac* and in the precorneal tear layer, elimination through nasolacrimal drainage, drug interactions with tear proteins, drug

---



metabolism by tear and tissue proteins and diffusion through the conjunctiva and cornea.

Transconjunctival and transcorneal / scleral absorption are the best routes for local ocular drug effects. The time between the instillation of the drug and its appearance in the aqueous humor is defined as the *latency time*. The driving force for passive diffusion is provided by the drug concentration gradient between the tear film and the cornea and conjunctival epithelium. Other characteristics that influence the diffusion of a drug are the chemical structure, the size of the molecule and the steric configuration. The transcorneal penetration of the drug is a process of differential solubility; the cornea can be seen as a "fat-water-fat" trilamellar structure corresponding to the epithelial, stromal and endothelial layers. While the stroma is a barrier for hydrophobic compounds, the epithelium and endothelium represent barriers for hydrophilic substances. Hence, a drug with both hydrophilic and lipophilic properties is more suitable for transcorneal absorption.

The permeability of drugs in the eye is mainly related to the tear film concentration and can be altered by some subjective pathological aspects from the experimental point of view. Preliminary tests can be carried out to evaluate the corneal permeability; these tests combined with the water octanol partition coefficient crossed with the octanol-water distribution measures or with the distribution coefficient provide a parabolic correlation that represents a valid preventive parameter regarding ocular absorption should be borne in mind that data obtained from these studies are influenced by many factors often challenging to control as the lacrimal nose drainage the binding of the drug with proteins and tissues corneal absorption and transconjunctival absorption.

---

#### ***1.4.4. Distribution***

Administration of topically administered drugs topical administration of drugs may lead to nasal mucosal uptake or local ocular absorption by transconjunctival transcorneal absorption transcorneal absorption leading to a concentration of the aqueous drug with subsequent distribution in the other structures with possible distribution in the systematic circulation through the filter trabeculae. The bonds that can establish melanin drugs are particularly important; for example, alpha-adrenergic agonist drugs' effect appears more slowly in subjects with dark irises than in those with clear irises. This explains how atropine can have more prolonged effects in some subjects than in others because the link with melanin is a potential deposit for the drug that allows a prolonged release.

#### ***1.4.5. Metabolism***

Pharmacokinetics and pharmacodynamics of a drug are primarily influenced by enzymatic biotransformation. The enzymes found in ocular tissues are numerous, including oxidoreductases, esterases, peptidases, lysosomal enzymes, glucuronide, glutathione-conjugating enzymes, sulfate transferases, monoamine oxidase, catechol-*O*-methyl-transferase and 11 $\beta$ -hydroxysteroid dehydrogenase are found in the eye. As the design of the prodrugs is taken into account the enzymatic activity so that the active ingredient can be successfully released into the ocular tissue; in fact, the bond that will be hydrolyzed by tissue-specific enzymes must be free from steric hindrance that can influence the hydrolytic process.

#### ***1.4.6. Toxicology***

Ophthalmic drugs can enter the systemic circle and cause side effects; in most cases, ophthalmic drugs are released only locally, and local toxic effects are limited hypersensitivity reactions or toxic effects directly on the cornea. During the drug design, it is essential to consider the probable toxic

---

effects that may cause the new groups included in the structure of the parent drug; in fact, it is crucial to monitor this parameter for the design's successful outcome.<sup>21</sup>

### **1.5 AQUEOUS HUMOR DYNAMICS AND REGULATION OF INTRAOCULAR PRESSURE**

Aqueous humor (or watery humor) is a colorless and transparent liquid in the eye's anterior segment. It is formed by secretion from the ciliary body at a 2.0–2.5  $\mu\text{L}/\text{mL}$  rate and is predominantly made up of water, salts, and protein substances. Cellular elements, on the other hand, are almost absent. It passes from the posterior chamber to the inner one passing through the pupil, subsequently flowing through the filtering trabeculae; the Sharm channel is subsequently drained into an episcleral venous plexus to flow into the systematic circulation finally. This system manages to drain 80–95% of the total humor volume and represents one of the significant targets of cholinergic drugs used in glaucoma therapy. The rate of production and reabsorption of the aqueous humor is accomplished in such a way as to determine a pressure between 10 and 21 mmHg (normal range) within the eye. To maintain this stable value, the eyeball continuously produces a small amount of aqueous humor, while an equal level of this liquid is drained through a complex network of cells and tissues.

However, considering that the aqueous humor is a continually renewed and circulating liquid, intraocular pressure is not an immutable constant. Excessive production of aqueous humor or an obstacle to its outflow can lead to ocular hypertension, a condition that predisposes to the onset of glaucoma (a subtle ocular disease that compromises visual function following optic nerve pain). Furthermore, there are pathological changes characterized by hypotonia, lower production of aqueous humor, or excessive drainage. The peripheral part of the anterior chamber delineates

---

essential differences in the two types of open-angle and angle-closure glaucoma; the current therapy of open-angle glaucoma aims to decrease the production of aqueous humor and increase the outflow of the same instead, in the case of angle-closure glaucoma, the therapy is performed by laser or scalpel.<sup>22</sup>

Aqueous humor performs multiple functions:

- Participates in the refraction process, being one of the diopter means of the eyeball.
- Contributes to give consistency and volume to the eye and stabilizes the shape of the cornea, thanks to the pressure it exerts on the inner walls (ocular physiological tone).
- Has a nutritive function towards the crystalline lens and cornea (ocular structures without vessels).
- Has the task of keeping the lens intact and transparent.
- Avoid significant temperature changes to the cornea, to the crystalline lens, and the iris.
- It has a fundamental role in the regulation of intraocular pressure.

## **1.6 BIOLOGICAL SYSTEMS OF OCULAR TRANSPORT**

Transporters are membrane proteins that have an essential role in the active transport of nutrients or other exogenous and endogenous substances in humans transporters play a significant role in the processes of absorption, metabolism, distribution, and elimination of drugs has been shown that in the ocular tissue the role membrane proteins are indispensable for a correct delivery of the active substance at the target site. Also, transporters allow the translocation of nutrients and endogenous substances through cell membranes; these include peptides, vitamins, glucose, and amino acids. The integrity of cell membranes is fundamental for the excellent transport of substances inside and outside the cell. Usually, the transporters are

---

cytosolic membrane proteins that are an integral part of all organisms. In humans, according to about 2000 genes, many of these specialized codify membrane transporters are divided into two superfamilies: SLC (solute carrier) transporters and ABC (ATP-binding cassette). ABC transporters act by ATP hydrolysis to actively pump their substrates across the lipid bilayer. These proteins are encoded by 49 genes and are grouped into seven subclasses (from ABCA to ABCG). The best transporter documented in the ABC superfamily is the P-glycoprotein (P-gp) encoded by the MDR1 gene and is responsible for the efflux of several endogenous molecules, including drugs. The superfamily SLC includes 43 families and contributes to the absorption of drugs.

Furthermore, the role of membrane transporters in drug-drug interactions and multiresistant resistance has been well documented. In addition to drug delivery, some carriers also act as a protective barrier for particular organs or cell types. Recently, the Food and Drug Administration and the International Transporter Consortium have identified some organic anion transporters (OAT), organic anion transport polypeptides (OATP), organic cation transporters (OCT), peptide transporters (PEPT), P-gp, multidrug resistance-associated protein (MRP) and breast cancer resistance protein (BCRP) - which are critical for drug-drug interactions.

### ***1.6.1. Peptide transporters***

Peptide transporters are capable of translocating dipeptides and tripeptides into cells and a wide variety of molecules such as Beta-lactam antibiotics and cephalosporins. Types of transporters use the  $\text{Na}^+/\text{H}^+$  exchanges as the driving force for peptide uptake. Studies to date have identified two peptide transporters: peptide transporter 1 (PEPT1, SLC15A1) and peptide transporter 2 (PEPT2, SLC15A2). These carriers have 12 membrane domains with N-C terminals oriented towards the cytosol. 708 amino acid residues

---

encode the PEPT1 protein, while 729 residues encode PEP2. These proteins transport dipeptides and tripeptides independently of their amino acid sequence and their charge at physiological pH. Furthermore, they can transport  $\beta$ -lactam antibiotics and peptide-related drugs. Possible translocation mechanism is proposed: (A) outward-facing conformation, (B) occluded state, and (C) inward-facing conformation. In stage A, the peptide (Pep) and the proton enter the cavity facing outwards or towards the extracellular domain. In the occluded stage, the Pep is occluded in the central cavity, closing both the central cavities, while the proton binding region is still facing the extracellular side. Below, both Pep and  $H^+$  are released towards the intracellular side of the membrane.<sup>23</sup>

### ***1.6.2. Monocarboxylate transporters***

Carriers of monocarboxylates catalyze monocarboxylates' transport, such as lactate, into pyruvate; therefore, they play an essential role in cell metabolism. These carriers can also move ketone bodies (acetoacetate and  $\beta$ -hydroxybutyrate) across the plasma membrane. These compounds are considered the chief energy substrates for specific cell types and act as crucial fuel when low glucose levels persist. Lactic acid is quantitatively not only the essential oxidizable substrate but also the preferred substrate of photoreceptor inner segments.<sup>24</sup>

### ***1.6.3. Sodium-dependent multivitamin transporter***

Sodium-dependent multiple vitamin transporter (SMVT) has a high capacity to transport drugs into ocular tissue, translocating vitamins such as biotin, pantothenic acid, and cofactors such as lipoic acid. SMVT is a sodium-dependent electrogenic system transcribed by the SLC5A6 gene. This system comprises 635 amino acids that form 12 transmembrane domains with *N*- and *C*-terminals facing the cytoplasm.<sup>25</sup>

---

Said et al. identified seven histidine residues across the species (human, mouse, rabbit, rat). These residues are essential for the absorption of biotin and other vitamins. Also, four *N*-glycosylation sites and two potential phosphorylation sites were identified.<sup>26</sup>

#### ***1.6.4. Organic anions and cations transporters***

An organic anion transporter polypeptide (OATP) is a transmembrane transport protein, substantially a transporter, which mediates transport primarily of organic anions through the cell membrane. It follows that OATP transporters are present in the lipid bilayer of the cell membrane. OATPs are expressed in the liver and many other tissues on the basolateral and apical membranes, carry anions, neutral compounds, and even cations. They also carry an incredibly diverse range of pharmacological compounds, including anti-cancer substances, antibiotics, lipid-lowering drugs, anti-diabetic drugs, and toxins and poisons.<sup>27</sup>

Organic cation transporters are among the leading classified transporters of the superfamily SLC22A. Three members of the subfamily of the OCTs were cloned, including OCT1, OCT2, and OCT3. OCT proteins are usually 500–600 amino acids in length. Furthermore, the SLC22A family contains cation and organic carnitine transporters (OCTN1 and OCTN2). These transport proteins are expected to contain 12 transmembrane domains with *N*- and *C*-intracellular end groups.<sup>28</sup>

#### ***1.6.5. P-glycoprotein***

P-glycoprotein is a membrane protein that belongs to the superfamily of ABC carriers. ABC proteins transport various substances through the intra- and extracellular membranes. The ABC genes are divided into 7 subfamilies (MDR / TAP, MRP, ABC1, ALD, GCN20, OABP); this protein is a member of the MDR / TAP subfamily. Like all members of its subfamily, Pgp is involved in multi-drug resistance processes. It is an efflux pump for

---

xenobiotic substances that accept a broad spectrum of substrates. It is responsible for the reduced accumulation of the drug in multidrug-resistant cells and often mediates resistance against anticancer drugs. P-glycoprotein also acts as a transporter in the blood-brain barrier.

The glycoprotein-P (P-gp) has a significant role in the transport of drugs, and therefore in their permeability. P-gp is localized in the apical (luminal) membrane surface in polarized cells, while in the eye appears on the corneal epithelium's apical surface, which is localized on the basolateral membrane of the retinal epithelium. P-gp shows three essential sites of glycosylation and phosphorylation. Furthermore, these carriers can recognize the substrates selectively. The recognition elements concern two large class groups: Type I and Type II. Those of Type I show electron donor groups with a separation of 2.5 Å, while those of Type II show two or three electron donors separated by 4.6 Å.<sup>29</sup>

### **1.7 PRODRUG STRATEGIES IN OCULAR DRUG DELIVERY**

Local administrations for ocular drugs are the most common because the drug's action is localized in the eye's anterior segment. However, the low penetration and rapid loss of the drug are the significant limitations of this route.<sup>30</sup> To overcome this problem, two different approaches are generally used: either to develop new pharmaceutical formulations and modify the structure of the parent drug by optimizing the physicochemical properties to increase the ocular bioavailability. The design of prodrugs is a chemical approach to increase the bioavailability of the parent drug. The prodrug must be designed to release the active substance at the desired site after undergoing a biochemical transformation (enzymatic hydrolysis, oxidation or enzymatic reduction, etc.). Increased solubility in the aqueous phase, decreased toxicity and increased lipophilicity are just some of the advantages of the prodrug strategy.<sup>6</sup>

---



When designing an ophthalmic prodrug, it is important to take into account some aspects related to the characteristics of the parent drug so that it can be clinically useful:

- The parent drug must have at least one group susceptible to chemical derivatization.
- The chemical modification made must be reversible.
- The new chemical group must be non-toxic.
- Promoiety must be easily eliminated from the body.
- The prodrug bioconversion must be regulated by enzymes present in the ocular tissue rapidly, such as esterase and peptidase.
- The new prodrug must have good stability in the formulations for eye drops.
- Most ocular preparations are in the form of eye drops, so the new molecule must have good solubility in water.
- Lipophilicity must be sufficient to pass the corneal barrier.

The functional groups are commonly used in the design and synthesis of ophthalmic prodrugs are the hydroxyl, carbonyl, amino and carboxy groups. The modification of these functional groups in carbamates, esters, oximes and phosphates leads to ophthalmic prodrugs.

### ***1.7.1. Ester Prodrugs***

The most common ophthalmic prodrugs developed so far are esters derived from the COOH or OH functional group. Carboxylic acids exist in the ionized form under physiological conditions, which does not favor drug passage through the lipid membrane, resulting in inadequate drug bioavailability. The esterification of these groups allows an increase in lipophilicity, therefore an increase in corneal permeability. To synthesize ester prodrugs, mostly Steglich esterification reaction conditions have been

---

applied with *N,N'*-dicyclohexylcarbodiimide (DCC) or ethyl-3-(3-dimethylaminopropyl) carbodiimide (EDC) as a coupling reagent and 4-dimethylaminopyridine (DMAP) as a catalyst (Figure 1.6). In 1976, Hussain et al. reported the first ophthalmic prodrug dipivefrin, where two hydroxyl functional groups of epinephrine have been esterified to prepare dipivalyl epinephrine. Dipivefrin showed enhanced corneal penetration with 10 times improved therapeutic index compared to epinephrine.

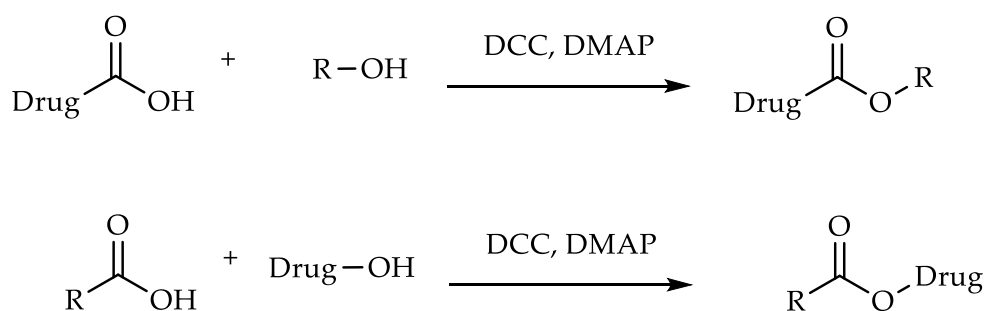


**Figure 1.6.** Methods for ester synthesis.

Ganciclovir is an antiviral that inhibits cytomegalovirus virus activity, but the low distribution coefficient results in poor ocular bioavailability. Mitra et al. reported that the mono-drug prodrug derivatives have a significantly improved permeability. The derivative with a side chain with 4 carbon atoms gave the best results, increasing the permeability of 6 times compared to the parent drug. These prodrugs also underwent rapid enzymatic hydrolysis, which increased heterogeneously as the length of the aliphatic chain increased (Figure 1.7).<sup>31,32</sup>

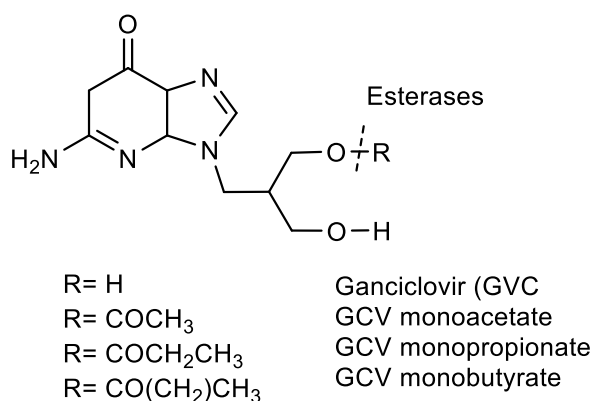
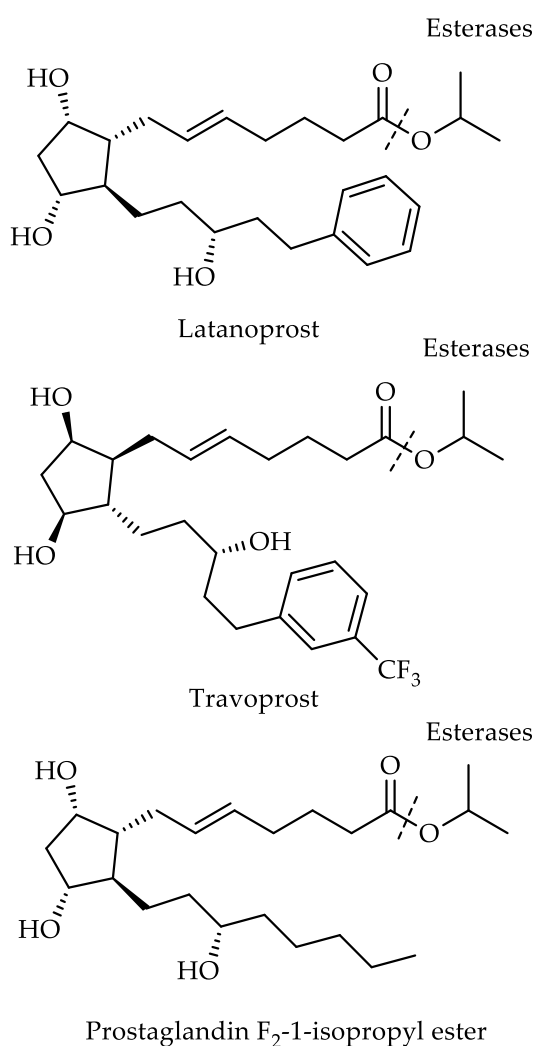


**Figure 1.7.** Ganciclovir derivatives.

Prostaglandin analogs,  $\text{PGF}_2\alpha$  have been widely used as ocular hypotensive agents. In carboxylic acid forms of these compounds exhibit low permeability and irritate the eye. The carboxylic acid functionality of prostaglandins ( $\text{PGF}_2\alpha$  and its analogs) has been utilized to develop various alkyl/aryl ester prodrugs, which resulted in 2–3 fold higher lipophilicity and 25–40 fold enhanced in vitro corneal permeability. These agents were 10–30 times more potent ocular hypotensive agents than their parent molecules. However, due to ocular side effects such as conjunctival hyperemia and superficial irritation, these prodrugs have limited clinical application.



---

**Figure 1.8.** Chemical structure of Latanoprost, Travoprost, and Prostaglandin F2-1-isopropyl ester.

Later on, two isopropyl ester derivatives of modified PGF2 $\alpha$  analogs were developed (latanoprost, travoprost) where the modification was made on one side chain (omega chain) of PGF2 $\alpha$  backbone by attaching phenyl ring at the 17-position. Latanoprost, travoprost, and one other PGF2 $\alpha$  analog, unoprostone isopropyl, are currently being used clinically<sup>33</sup> (Figure 1.8). Latanoprost and travoprost undergo facile hydrolysis by esterases present in the cornea to biologically active latanoprost acid and travoprost acid, respectively. Cornea slowly releases latanoprost acid into anterior parts of the eye<sup>34</sup>. The maximum concentration of latanoprost acid has been detected in aqueous humor 1-2 hrs after topical application.<sup>35</sup> Travoprost and other ester prodrugs of PGF2 $\alpha$  analog hydrolyze during passage through the cornea by butyrylcholine esterase and carboxylesterases.

### **1.7.2. Phosphate ester**

Prodrugs are typically designed to make some drugs with hydroxyl functionality more soluble. In fact, the dianionic phosphate group's presence considerably increases the drugs' water solubility, making them very stable in solution and easily hydrolyzable by alkaline phosphatases present in the ocular tissue.<sup>36</sup>

### **1.7.3. Carbamate Prodrugs**

Carbamate prodrugs can be prepared from amine and carboxyl functionalities. Although amines can be easily acylated, prodrug carbamate is rarely used in ophthalmic prodrugs due to low in vivo stability. This problem can be overcome by introducing an ester group to have an *N*-(acyloxy)alkyl carbamate as the final structure, which is highly stable in aqueous solutions. These prodrugs are very stable in solution and have high corneal permeability and enzymatic hydrolysis rate. The hydroxyl

---

catalyzed by the esterases generates a very unstable intermediate (acyloxy) alkyl-carbonyl, which decomposes spontaneously to regenerate the amine of the parent drug<sup>37</sup>.

#### **1.7.4. Oxime Prodrugs**

Drugs with hydroxyl groups can be converted into oximes or methoxime by oxidation of the secondary alcohol into ketone and subsequent reaction with hydroxylamine or mesoxyamine. Some beta-blockers such as alprenolol, betaxolol, propranolol, and timolol to treat glaucoma were derivatized using this approach. The new prodrug is regenerated by initial hydrolysis and ketone reduction due to ketone reductase. An oxime limitation approach is due to a low presence of ketone reductase in the ocular tissue<sup>38-40</sup>.

#### **1.7.5. Oxazolidine Prodrugs**

Oxazolidines are cyclic condensation products of  $\beta$ -amino alcohols, present in various drugs and carbonyl-containing compounds, *i.e.*, aldehydes or ketones. These derivatives increase the amino alcohol concentration and, therefore, the ocular penetration. These compounds undergo hydrolysis in aqueous solutions within pH 1–11 at 37 °C. The hydrolysis rate depends on several factors: steric effects of the carbonyl substituent and on the nitrogen atom, and electronegativity of the substituents. At neutral and basic pH, hydrolysis rate decreases with increasing steric effects within carbonyl moiety or amino alcohol moiety and increases with increasing electronegativity of substituents at the nitrogen atom. Unfortunately, the low solubility in water makes these compounds challenging to use to formulate ophthalmic solutions.<sup>41</sup>

---

### ***1.7.6. Prodrugs Derived from Sulfonamide Groups***

Drugs like carbonic acid inhibitors (such as acetazolamide, methazolamide and ethoxzolamide) do not contain functional groups that are amenable to prodrug derivatization. As a result, the sulphonamide group was used to prepare new prodrugs. Several sulphonamide derivatives have been synthesized, including *N*-acyl, *N*-alkoxycarbonyl, *N*-sulfonylurea, *N*-sulfonylimidate, *N*-sulfonylamidine, *N*-sulfonyl pseudourea, *N*-sulfonyl sulfoximines, and *N*-sulfonyl sulfilimines. They are very stable in solution, but the low enzymatic hydrolysis *in vivo* did not allow their use in the ophthalmic formulation.<sup>42</sup>

### ***1.7.7. Nitrooxy Prodrugs***

Recently, a new prodrug (Latanoprosten Bunod) similar to prostaglandins has been approved in the USA to treat ocular hypertension. The dual mechanism of action derives from its metabolite latanoprost acid, analogue of prostaglandin F<sub>2</sub>-alpha, and from its ability to release NO due to the effects of tissue relaxation. After topical ocular administration, latanoprostene bunod is hydrolyzed to latanoprost acid and butanediol mononitrate, subsequently reduced to 1,4-butanediol and nitric oxide.<sup>43</sup>

## **1.8 TRANSPORTER TARGETED PRODRUG APPROACH**

Recent developments on transporters have shifted their focus to the derivatization of drugs to improve their absorption. Conveyors are essential for the passage of exogenous and endogenous substances through the cell through active mechanisms. Various influxes and efflux transporters have been identified in the various region of the eye.

The flow transporters can carry the therapeutic molecules in the eye, passing certain limits linked to the corneal barriers' complex structure.

---

Instead, an efflux transporter could reduce the drug's bioavailability by pushing it out of the cell.

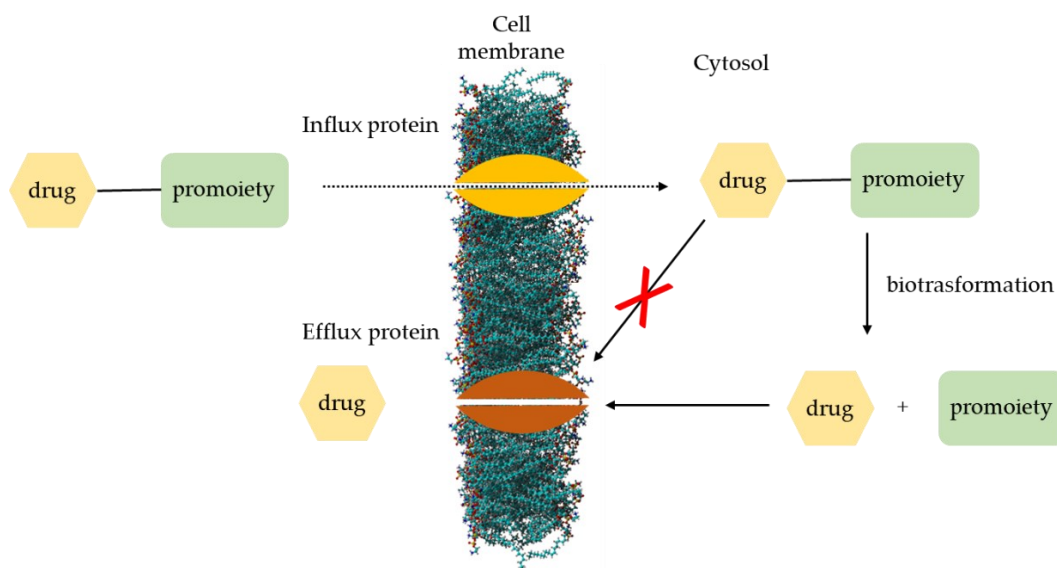


**Figure 1.9.** The intracellular influx of prodrugs mediated by active transport systems.

Prodrugs have been synthesized in such a way that (a) chemically modified drug will have a lower affinity towards efflux transporters such as quinidine prodrugs, or (b) chemically modified drug will have a higher affinity towards influx transporter which otherwise are not recognized as such as a transporter such as a peptide and amino acid prodrugs (acyclovir and ganciclovir). In addition to peptide, amino acid, and monocarboxylic acid transporters, recently, various vitamin transporters such as biotin and ascorbic acid have been utilized to deliver various ocular prodrugs.<sup>44-46</sup>

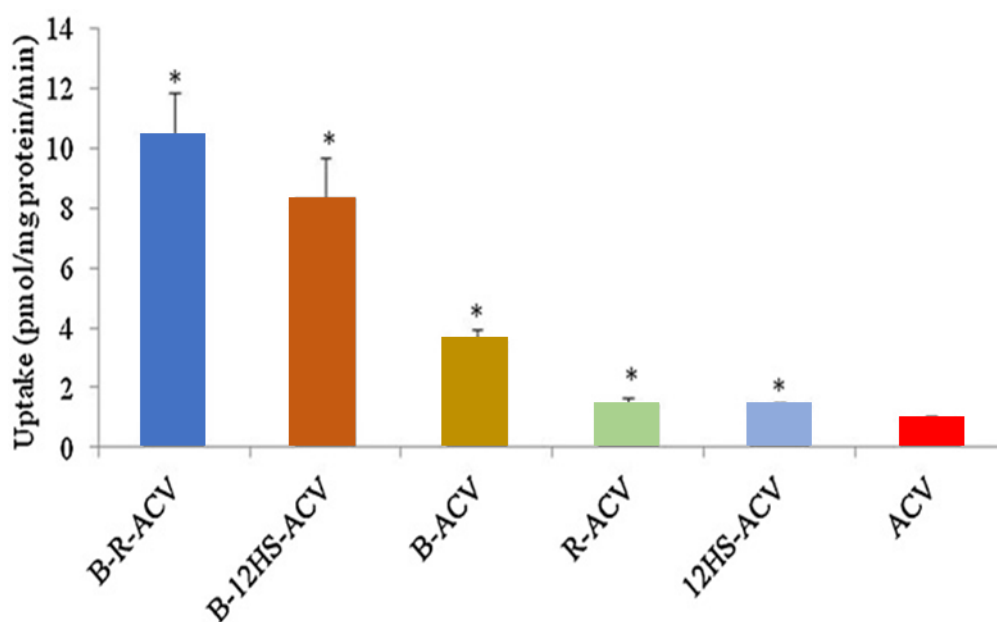
The transporter targeted delivery approach appears to be clinically very valid for drug delivery (Figure 1.9). This new approach has been extensively studied for the delivery of antitumor drugs using the folate receptor as a target. In recent years, the folate receptor's interest rate has increased considerably, registering an increase in anticancer drug licenses.

Kumar G. et al. have proposed a new Ganciclovir conjugate to biotin to study its absorption into the ocular tissue using albino rabbits. Studies have

shown that multivitamin transport systems have recognized the new prodrug by improving the parent drug's pharmacological profile.<sup>47</sup>

In 2012, Vadlapudi et al.<sup>48</sup> developed new acyclovir prodrugs to increase bioavailability in ocular tissue. In this study, the drug was conjugated to the biotin (transporter) via a lipid raft (ricinoleic acid) to confer an increase of lipophilia to the new molecule. Targeted lipid prodrugs, *i.e.*, biotin-ricinoleic acid-acyclovir (BR-ACV) and biotin-12-hydroxystearic acid-acyclovir (B-12HS-ACV), were synthesized with ricinoleic acid and 12-hydroxystearic acid as the lipophilic rafts and biotin as the targeting moiety. Biotin-ACV (B-ACV), ricinoleic acid-ACV (R-ACV), and 12hydroxystearicacid-ACV (12HS-ACV) were also synthesized to delineate the individual effects of the targeting and the lipid moieties. The results showed that the time increases in B-R-ACV absorption compared to the parent drug, ACV. B-ACV and R-ACV showed a 6 times increase in absorption.

Compared to ACV, the absorption of B-R-ACV and B-12HS-ACV increased by 10 and 8.3 times, respectively, while the absorption of B-ACV, R-ACV, and 12HS-ACV were higher than 3.5, 1.4, and 1.3 times respectively (Figure 1.10).





---

**Figure 1.10.** Cellular accumulation of B-R-ACV, B-12HS-ACV, B-ACV, R-ACV, 12HS-ACV, and ACV on Caco-2 cells.

Transepithelial transport studies suggest that biotinylated lipid prodrugs have a higher affinity towards sodium-dependent multivitamin transporter (SMVT). This new strategy demonstrates how it is possible to increase the corneal absorption of hydrophilic drugs by exploiting the two effects of synergistic action: increased lipophilicity and corneal recognition.

### 1.9 SELF-IMMOLATIVE PRODRUGS

Dual prodrugs can be ineffective because the link is too labile (for example, some esters) or very stable. To solve this problem, Katzenellenbogen et al.<sup>49</sup> developed a three-component prodrug (also known as self-immolative). In a three-component prodrug, the promoiety is not connected directly to the drug but rather to a self-immolative spacer related to the drug. This allows incorporating different types of functional groups to varying the stability and remove the drug from the site of hydrolysis, decreasing the steric interference by the conveyor. However, the drug-spacer connection must be designed so that it breaks spontaneously (*i.e.*, it is self-immolative) after the promoiety has come off.

The linker's primary function is to quickly release the active drug in a spontaneous fragmentation process after enzymatic activation. The linker design is crucial for activation kinetics and cytotoxicity differential; it can influence the prodrug's stability, the selectivity for the target enzyme, and pharmacokinetic properties.<sup>50</sup> The advantages of self-immolating prodrugs are: (i) a wide range of drugs can be designed without limitations on the structural requirement; (ii) decrease of the electronic or steric effects that cause activation problems; (iii) the pharmacokinetic properties can be modulated by modifying the linker structure; (iv) the drug can be conjugated to a promoiety to increase molecular recognition.

---

Introduced initially to overcome limits for drug delivery, self-immolative spacers have earned broad interest in medicinal chemistry, material science and analytical chemistry.

Two main mechanisms of fragmentation of self-immolative prodrugs have been employed: elimination and cyclization. Both are triggered by an electronic switch, the generation or unmasking of an electron-donating group/nucleophile.

### ***1.9.1 Self-Immolative Prodrugs Fragmenting by 1,4, 1,6, or 1,8 Elimination***

Some self-immolative spacers are based on an electronic cascade for the disassembly of an aromatic structure bearing a hydroxyl,<sup>51,52</sup> an amino, or a thiol, group.<sup>53</sup> As long as they are protected (or masked), these groups are not enough nucleophiles to activate the electronic delocalization and trigger the cascade process. Both positive entropy and the formation of stable products (for example, CO<sub>2</sub>) play a fundamental role in this process, making it irreversible and spontaneous. To date, most reported self-immolative spacers in this series rely on 1,4- or 1,6- eliminations. 1,8-elimination was shown to be possible in para-amino(or hydroxy)cinnamyl alcohol or coumaryl alcohol spacers, summarized schematically in Figure 1.11. However, deletion 1,8 and 1,10 cannot free the starting group, as the energy would be too high to break the system's aromaticity.

---

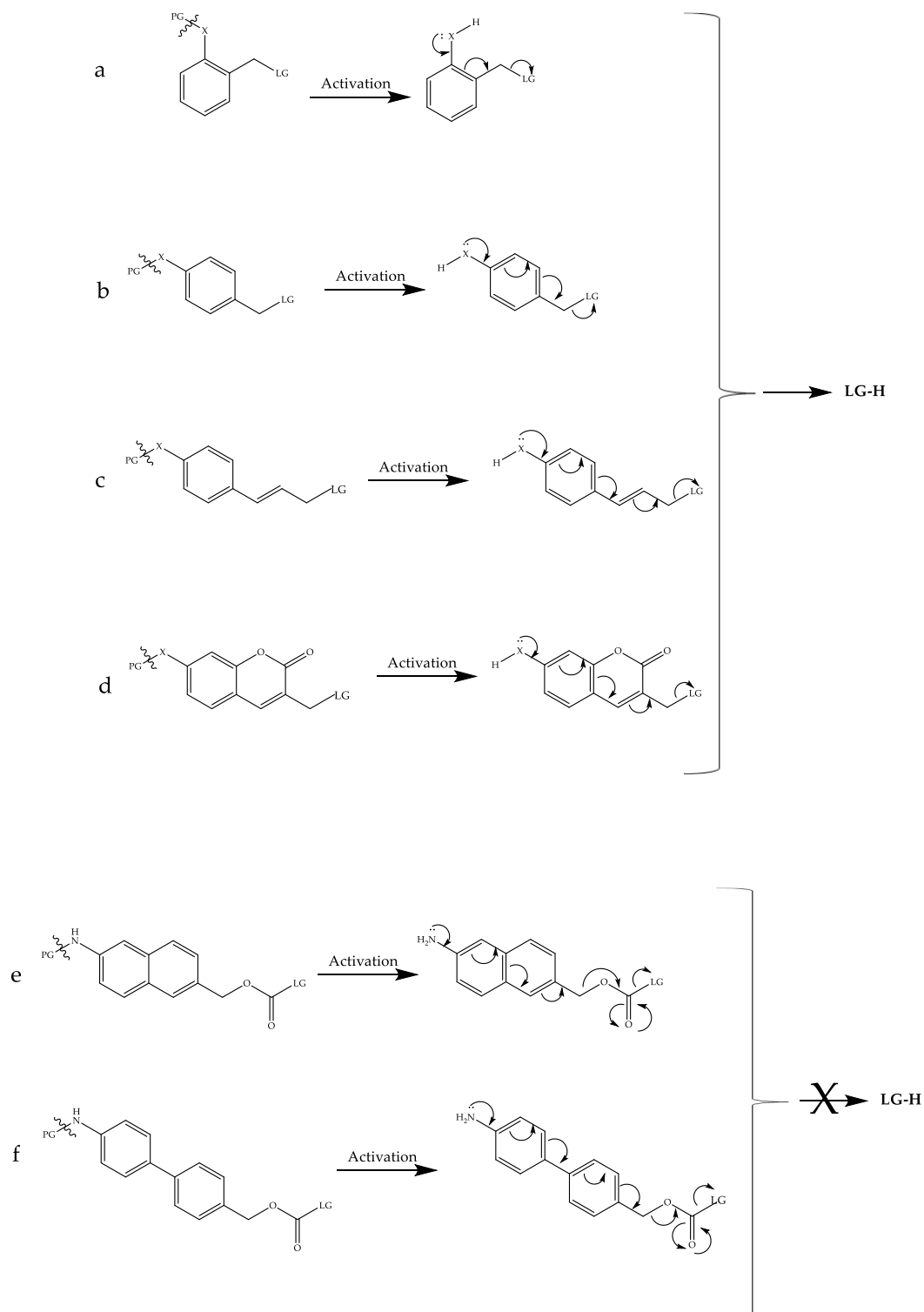


**Figure 1.11. Schematic representation of self-immolative fragmenting by 1,4, 1,6, or 1,8 elimination.**

In some cases, the activator group's nucleophilic character can result from a change in its oxidation state. Hydroxylamine and amine can be formed by

reducing the nitro group in prodrugs and is used as the trigger for fragmentation of many self-immolative prodrugs.<sup>54</sup> The hydroxy trigger can be formed by hydrolysis of an ester, a carbamate,<sup>55</sup> or a glycosyl ether (by  $\beta$ -glucuronidase,  $\beta$ -galactosidase, and  $\alpha$ -galactosidase,<sup>56</sup> or by oxidation of the unsubstituted 4-position of the linker.

The amine is not a good outgoing group, and it can not activate the self-immolative process by simple alkyl connection. In fact, the most common strategy involves the use of the carbamate group. The process is irreversible due to the decomposition into carbamic acid, amine, and carbon dioxide. Examples of amino-containing drugs that have been deactivated as autoimmolative carbamates the prodrugs include aniline mustards,<sup>57</sup> anthracyclines, analogs of duocarmycin, and enediyne.<sup>58</sup>

### ***1.9.2 Self-Immolative Prodrugs Fragmenting Following Cyclization***

After activation, the autoimmolative prodrugs activated by cyclization have an available nucleophilic group. The nucleophile (such as hydroxylamino, hydroxy and amino) is entropically and sterically favorable with respect to the carboxylic group derived from the drug. Nucleophile attachment to the carbonyl core generates a thermodynamically stable five- or six-membered ring. The cycling rate can be increased by designing sterically clogged linkers. These factors drive the reaction irreversibly, allowing the drug to be released (Figure 1.12).

---

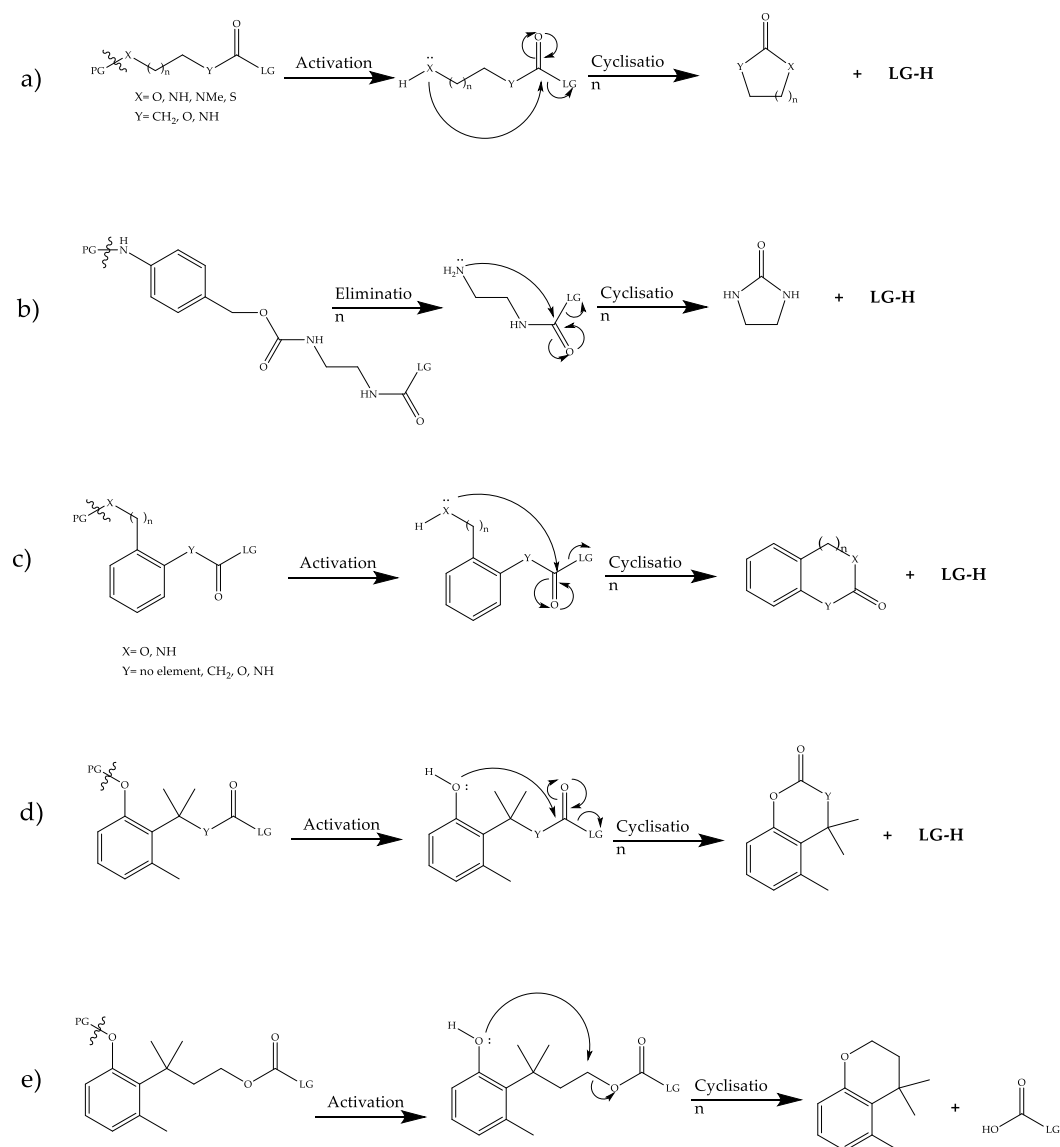


**Figure 1.12.** Schematic representation of self-immolative fragmenting by cyclization.

In most cases, cyclization occurs more slowly than elimination. In some cases, the elimination can be coupled to the cyclization to facilitate the enzymatic activation by lowering the steric hindrance. In the design of cyclization-based prodrugs, conformational aspects must be taken into account.

In 2015 the FDA approved a new antifungal prodrug, isavuconazonium sulfate (trade name Cresemba, Figure 1.13). Isavuconazonium sulfate is an acyloxy alkyl triazolium salt-based prodrug of the broad-spectrum antifungal agent isavuconazole. Although the parent prodrug has

considerable water solubility, the latter has still been improved for parental administration. After intravenous administration, isavuconazonium sulfate is rapidly activated by hydrolysis from plasma esterases, principally from butyrylcholinesterase, into benzyl alcohol, which subsequently undergoes an intramolecular cyclization that triggers *N*-dealkylation to release isavuconazole, and harmless by-products, i.e., acetaldehyde and BAL8728 (1-methyl-1,4-dihydro-2*H*-pyrido-[2,3-*d*]-[1,3]-oxazin-2-one).<sup>59</sup>

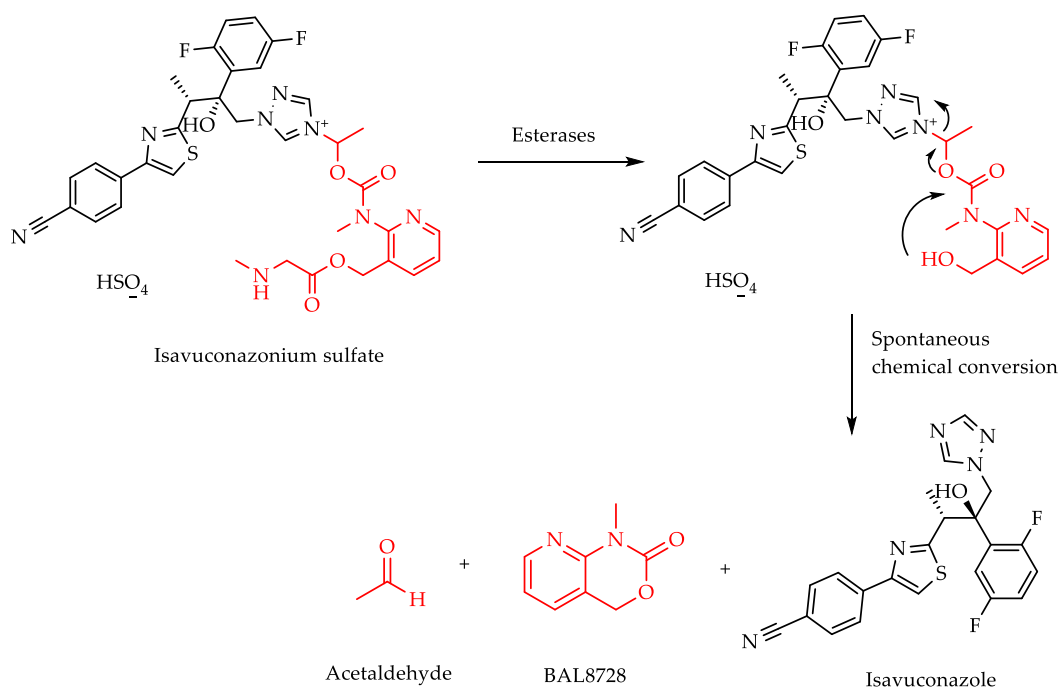


**Figure 1.13.** Bioconversion mechanism of Isavuconazonium sulfate.

### 1.9.3 Kinetic analysis of self-immolative drugs

Most experiments measure the total disassembly kinetics, which measures the temporal evolution of the compound's concentration after enzymatic or chemical activation. The mechanism concerns a series of irreversible unimolecular reactions. When their rate constants are different, the concentration of the precursor, the intermediates and the concentration of the released compound evolve in a multi-exponential way with relaxation times as many as the rate constants  $k_i$  (with  $t_i = 1/k_i$ ).<sup>60</sup> So, to analyze self-immolative kinetic, a key parameter is the temporal resolution. In fact, a

photoactivable compound requires much shorter times than stirring activation. The other key factor during the kinetic experiment and the frequency of data acquisition. Disregarding the value of  $k_3$ , since the  $\text{CO}_2$  cation occurs on the millisecond scale,  $k_1$  and  $k_2$  influence the system's kinetics. In most cases,  $k_1$  mainly influences the reaction rate when the activation is enzymatic (Figure 1.14).

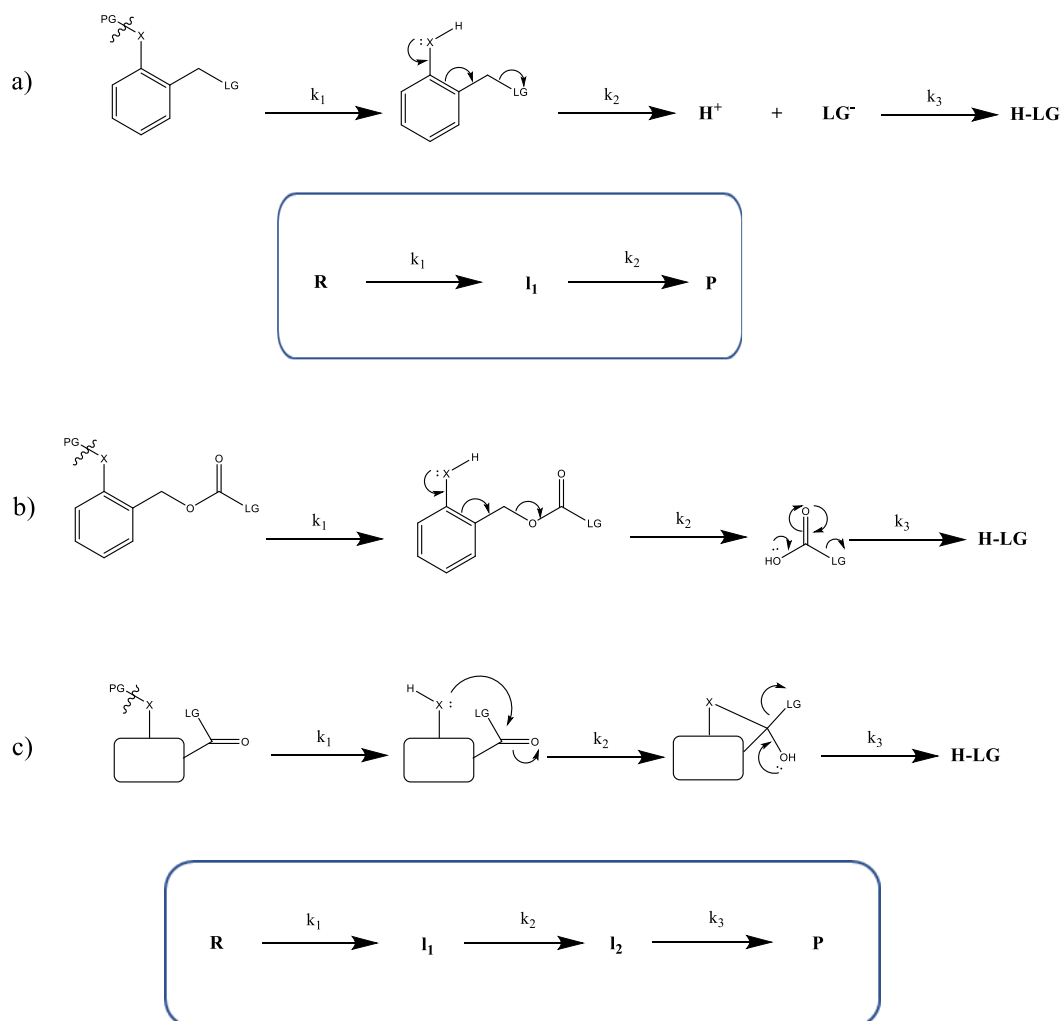


**Figure 1.14.** Schematic representation of enzymatic activation kinetics.

#### 1.9.4 Structure-Property relationships

The aromatic functionality of the spacer plays an important role in the design of a self-immolating spacer. The kinetics of autoimmolation were first studied with the benzene ring by analyzing the difference between eliminations involving the ortho (1,4-elimination) or para (1,6-elimination)

benzyl position with respect to the nucleophilic atom. Disassembly times were similar for both elimination mechanisms. In a double-release system, the leaving group located in the para position (1,6-elimination) was released faster than the ortho (1,4-elimination).

The elimination based on electronic delocalization involves forming a quinone or azaquinone methide intermediate and results in loss of electron density at the benzylic position associated with the release of a leaving group. Therefore the resonance energy of the aromatic ring can be altered by the substituents. Furthermore, other parameters, such as solvent, pH, and temperature, play a fundamental role. Increasing the aromatic ring's electronic density should facilitate the dearomatization and stabilize the transient positive charge in the benzyl position during the elimination leading to the quinone methide intermediate. In fact, activating groups (*e.g.*, OMe) should increase the HOMO energy of the aromatic ring and correspondingly strengthen the HOMO-LUMO interaction between the bonding and  $\pi$  ring molecular orbital and the non-bonding  $\sigma^*$  C-LG orbital (LG = leaving group). This interaction should lead to the strengthening of the C-C benzyl bond (which becomes shorter) and the weakening of the C-LG bond, facilitating the release of the outgoing group. Indeed, self-immolative rate is significantly accelerated by the graft electron donor groups (such as OMe and NHMe). In contrast, electron-withdrawing substituents induce a drop in electron density on the aromatic ring, which destabilizes the partial positive charge at the benzylic position in the spacer disassembly transition state, thus increasing the kinetic stability of the activated spacer.<sup>61-64</sup>

The disassembly rate was also evaluated among different heterocycles. After activation, the arm ring loses its aromatics, so it should speed up the process for a system with low resonant energy. In fact, the phenanthrene spacer's disassembly is five times faster than that of the naphthalene spacer

---



23, which is itself 10-times faster than that of the benzene spacer 20. Pyridine and pyrimidine have lower resonance energy (142 and 132 kJ/mol) than benzene (about 150 kJ/mol); therefore, it should favor the construction of fast self-immolative spacers. This has been observed in a spacer containing the pyridine nucleus. After enzymatic activation, the self-immolative degradation was complete after 30 minutes, compared to more than 4 hours for the benzene analogue.<sup>65</sup>

---

---

## CHAPTER 2 NEW SELF-IMMOLATIVE PRODRUG OF TIMOLOL

### 2.1 INTRODUCTION

Glaucoma is one of the primary diseases of vision loss worldwide and is associated with damage to the optic nerve due to retinal ganglion cell degeneration (RGC). The main risk factor is intraocular pressure (IOP). In the world, 60 million people are affected by glaucoma, and 8.4 million are blind. An estimate indicates that in 2040 this number will increase to 111.8 million.<sup>66</sup> The formal definition of clinical glaucoma as suggested by Casson et al. is:<sup>67</sup>

*“a group of ocular disorders of multifactorial etiology united by a clinically characteristic optic neuropathy with potentially progressive, clinically visible changes at the optic nerve head (ONH), comprising focal or generalized thinning of the neuroretinal rim with excavation and enlargement of the optic cup, representing neurodegeneration of retinal ganglion cell axons and deformation of the lamina cribrosa; corresponding diffuse and localized nerve-fibre-bundle pattern visual field loss may not be detectable in early stages; while visual acuity is initially spared, progression can lead to complete loss of vision; the constellation of clinical features is diagnostic.”*

Glaucoma is classified into two subtypes, with an open angle and a closed angle. Angular closure is defined by the presence of a specific irido-trabecular or synechial contact that obstructs the trabecular network and elevated IOP.

Currently, glaucoma diagnosis is made using a combination of functional and structural assessments. Standard automated perimetry is used to assess possible functional deficits in glaucoma patients, while diagnostic tools are primarily based on quantifying changes in retinal nerve thickness (RNFL) using optical coherence tomography (OCT) and disc tomography.

---

Confocal laser scanning tomography is used to assess morphological changes at the optic nerve head (ONH) site. IOP, currently the only risk factor in which it is possible to intervene for glaucoma, is evaluated using tonometry devices. The major limitation of measuring IOP by tonometry is that a thicker central cornea, measured by ultrasound pachymetry, leads to a measured IOP higher than the real one, while a thinner central cornea underestimates the true IOP..

## **2.2 THERAPY FOR GLAUCOMA**

Therapy for glaucoma treatment can be pharmacological or surgical. In the first case, it is possible if glaucoma is diagnosed in time, while surgical therapy (usually used later) serves to avoid total loss of vision when the disease is in an advanced stage.

Medical, laser, or surgical therapy aims to prevent glaucomatous damage to the optic nerve and the visual field, stabilizing the IOP. The sight lost due to glaucoma cannot be recovered. Surgical therapy for normal pressure glaucoma includes laser trabeculoplasty or a filtering procedure and possibly the use of draining devices. Trabeculoplasty using argon laser can be performed as an initial treatment in cases where medical therapy fails or in patients who do not tolerate the medication.<sup>68</sup>

Drug therapy of glaucoma reduces IOP by decreasing the rate of water inflow and / or by increasing the rate of water outflow. There are five main classes of drugs (given as eye drops) approved by the FDA to decrease IOP in glaucoma. Cholinergic agents work by increasing outflow through the trabecular reticulum, through action on the muscarinic receptors located on the ciliated muscle. Although the most used drug is pilocarpine, it has considerable side effects (causing miosis, myopia, and darkening eyes). Prostaglandin F receptor (PTGFR) analogs are generally administered to lower the IOP by increasing the aqueous outflow by altering the

---

composition of the extracellular matrix of the ciliary muscle and the trabecular meshwork. These are the most efficient of the IOP-reducing fractions and a single daily dose, reducing IOP throughout the day. PTGFR analogs cause the elongation and thickening of the hazel and blue irises with brown spots to become diffusely brown. Inhibitors of the  $\beta$ -adrenergic receptor dramatically reduce IOP by inhibiting  $\beta$ -adrenergic activity. However, they are only useful during the day and not during the night. A more recent approach sees the use of carbonic anhydrase inhibitors in the non-pigmented ciliary epithelium, thus reducing the formation of aqueous humor. These drugs have the ability to reduce IOP during the day and night.  $\alpha$ -adrenergic receptor agonists lower IOP mainly through stimulation of the  $\alpha_2$ -adrenergic receptors in the eye. Like beta blockers, they lower IOP during the day, except at night.<sup>69</sup>

### 2.3 OPHTHALMIC PRODRUGS

The corneal barrier is the main obstacle for the permeation of ophthalmic drugs in topical administration. In fact, only a small percentage is absorbed by the corneal tissue, while the majority (50–99%) enter the systemic circulation. The prodrugs were introduced in ophthalmology about 30 years ago when the ocular adrenaline was improved using its prodrug, dipivalil adrenaine (Dipivefrina). Dipivefrin, a dipivalic acid diester of adrenaline, penetrates the human cornea 17 times more rapidly than adrenaline (increase of lipophilicity of 600 times) is consequently much more effective while also reducing the side effects.

The prostaglandin analogs latanoprost (Xalatan; Pfizer), bimatoprost (Lumigan; Allergan), travoprost (Travatan; Alcon) represent the class of ocular hypotensive active ingredients for the treatment of glaucoma. They are lipophilic isopropyl ester (latanoprost, travoprost, unoprostone) or ethanolamine amide (bimatoprost) prodrugs that are rapidly hydrolyzed

---

inside the eyepiece biologically active prostaglandin tissue.<sup>70,71</sup> The parent drugs are poorly permeable and cause eye irritation, while the lipophilic prodrugs have a mile of ocular absorption and safety. Recently the FDA has approved in the USA the marketing of Latanoprostene bunod (commercial name Vyzulta) has been used in trials the treatment of Glaucoma, Open-Angle Glaucoma, Open Angle Glaucoma, Ocular Hypertension, and Intraocular Pressure. Latanoprostene bunod is the first prostaglandin analog synthesized, capable of releasing nitric oxide (NO). The acid metabolite latanoprost (F2-alpha analogue) and its ability to donate NO relax tissues / cells. Both latanoprost and latanoprostene bunod share a latanoprost acid backbone. In contrast, latanoprostene bunod integrates a donor fraction of NO instead of the isopropyl ester found in latanoprost.<sup>43</sup>

#### 2.4 TIMOLOL PRODRUGS: STATE OF THE ART

Timolol  $\{(S)\text{-}1\text{-}(tert\text{-butylamino})\text{-}3\text{-}[(4\text{-morpholin-}4\text{-yl-}1,2,5\text{-thiadiazol-}3\text{-yl)oxy]propan-2-ol}\}$ <sup>72</sup> is a non-selective beta-adrenergic receptor antagonist drug used orally or eye drops. It is used, in the form of eye drops, to treat increased pressure within the eye, such as glaucoma and ocular hypertension. It is also often used to treat hypertension, to prevent further complications after a heart attack and to prevent migraines, and for chest pain due to insufficient blood flow to the heart. In fact, it has been estimated that only 1–2% (or less) of an instilled dose penetrates the inner eye, the remaining dose reaching the systemic circulation causing various undesirable effects such as asthenia, fatigue, dizziness, headache, bradycardia, gastrointestinal disorders and metabolic alterations such as hypoglycaemia.<sup>73</sup>

The drug is basic, having a pK<sub>a</sub> of 9.2. Therefore, at pH 7.4, 98% of the drug is in ionized form. Log P for this drug is very low (–0.04; pH 7.4), and thus the drug exhibited very poor permeability across the lipoidal corneal

---

membrane. Prodrugs of timolol were developed to facilitate corneal absorption and lower systemic exposure to avoid cardiovascular and respiratory-related side effects.

Bundgaard et al. synthesized lipophilic ester prodrugs of timolol and studied lipophilicity and stability of these prodrugs. All synthesized prodrugs were more lipophilic than the parent drug and regenerated timolol into ocular tissue after administration. From this, it can be inferred that esterases' activity at the corneal level is very high. Among all the new synthesized prodrugs, *O*-butyric timolol showed the highest absorption rate. Nevertheless, none of the compounds reduced systemic absorption of timolol. Systemic absorption was reduced from 15 to 3.75 mM, leading to a lowering of aqueous humor and a reduction of drug in plasma levels.<sup>74</sup>

A few years after Pech et al. synthesized palmitoyl timolol malonate (PTM) (Figure 2.1) to the point of increasing cornea permeability. Despite the permeability of PTM was not good ( $0.42 \times 10^{-6}$  for PTM and  $2.2 \times 10^{-6}$  cm/s for timolol), it was able to reduce ocular hypertension. The authors hypothesized that the effect is due to a prolonged release of the drug from the corneal epithelium, where the compound has remained adsorbed. In this case, PTM was more stable in solution, probably due to the length of the chain.<sup>75</sup>

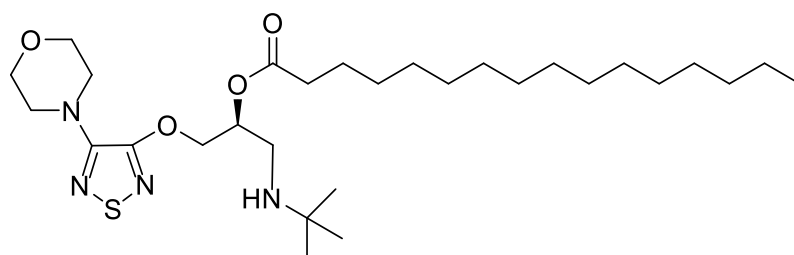


**Figure 2.1.** Chemical structure of Palmitoyl Timolol Malonate (PTM).

In order to increase the stability of timolol prodrugs, new carbamates were synthesized. A priori carbamates have the following advantages: (a) carbamylated amines do not ionize and are more compatible with biological

systems, (b) the modification, practically regardless of basicity, is applicable to primary and secondary amines, (c) they have a high potential for chemical selectivity in the presence of other groups functional such as hydroxyl and (d) are chemically stable. The secondary amine of timolol was an *N*-alkoxy derivative. This new prodrug has a hydrolysis 100–500 times greater in plasma than the buffer solution at 37 °C and high stability at pH 4. The ocular tissue esterases catalyze this hemiacetal prodrug's hydrolysis, which spontaneously converts to timolol via the formation of a carbamic acid intermediate liberating CO<sub>2</sub><sup>76</sup> (Figure 2.2).

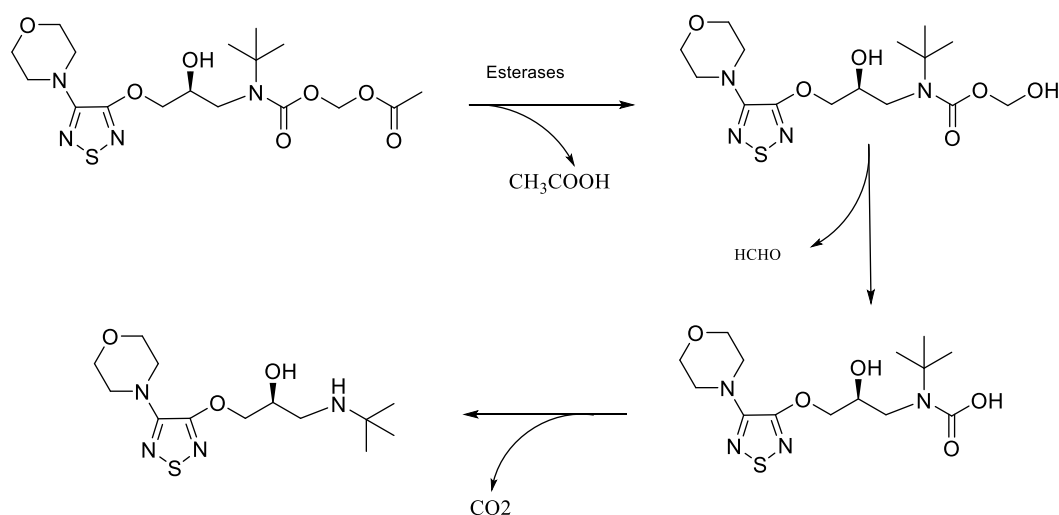


**Figure 2.2.** Bioconversion of Timolol derivate.

Although timolol is one of the most widely used drugs for lowering intraocular pressure in the eye, all approaches to realizing new timolol prodrugs have a negative outcome, and the main reason is due to poor stability in ophthalmic solutions. In fact, the high rate of hydrolysis in the timolol-derived ester is due to the nearby position of the amino group, which favors hydrolysis at physiological pH (Figure 2.3 a, b). In the case of acyloxy alkyl carbamate, the low physiological pH stability is due to intramolecular, entropically stable cyclization, which liberates oxazolidone and spontaneously and irreversibly formaldehyde and acetic acid (Figure 2.3 c, d).

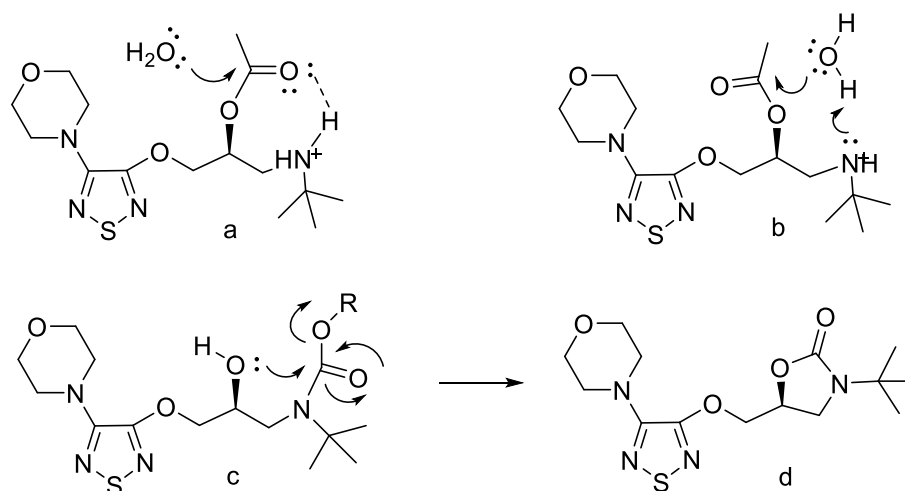


**Figure 2.3.** Schematic representation of spontaneous and irreversible hydrolysis of the Timolol derivative ester.

## 2.5 DESIGN OF NEW BIOTINYLATED DERIVATIVES OF TIMOLOL

In order to increase timolol permeability in the ocular tissue and reduce the undesirable effects of the drug, a new tripartite prodrug of timolol (BST, Figure 2.4) has been designed. Given the recent results on ophthalmic transporters, it was decided to covalently bind the biotin via a self-immolative spacer at the timolol. In this work, we wish to exploit biotin's dual effect, capable of increasing molecular recognition for some receptors, favor permeability and conferring greater lipophilicity to the molecular structure.

This approach, never used for an ophthalmic drug, has some advantages:

1. Increases the lipophilic character of the drug by favor corneal permeability.
2. Increases the degree of specific receptor molecular recognition.
3. After enzymatic activation in the ocular tissue, the drug is released spontaneously and irreversibly.
4. The self-immolative spacer is non-toxic and does not cause undesirable effects.



5. The possibility of combining different types of conveyors suitable for ocular tissue.
6. It is possible to act on some characteristics of the spacer (length, steric effects, electronic effects, reactivity disassembling).

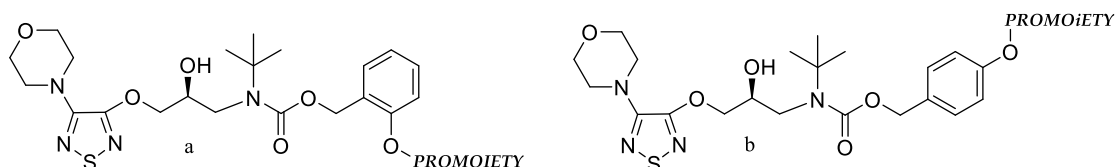


**Figure 2.4.** Different position of the promoiety.

Considering 1,4- or 1,6- eliminations can be hypothesized that the aromatic ring's *para*-substitution (Figure 2.4) is preferred due to the lower steric impediment during the enzymatic activation process. Preliminary molecular docking studies have suggested that ortho-substitution results in a significant decrease in the ligands' affinity with the transporter binding site.

There are two potential derivable sites in the timolol, the hydroxyl group and the amino group. The choice is based mainly on the stability of acyl derivatives. In fact, the formation of a carbamate bond is the most appropriate choice since the carbamate group shows greater chemical stability than the ester.

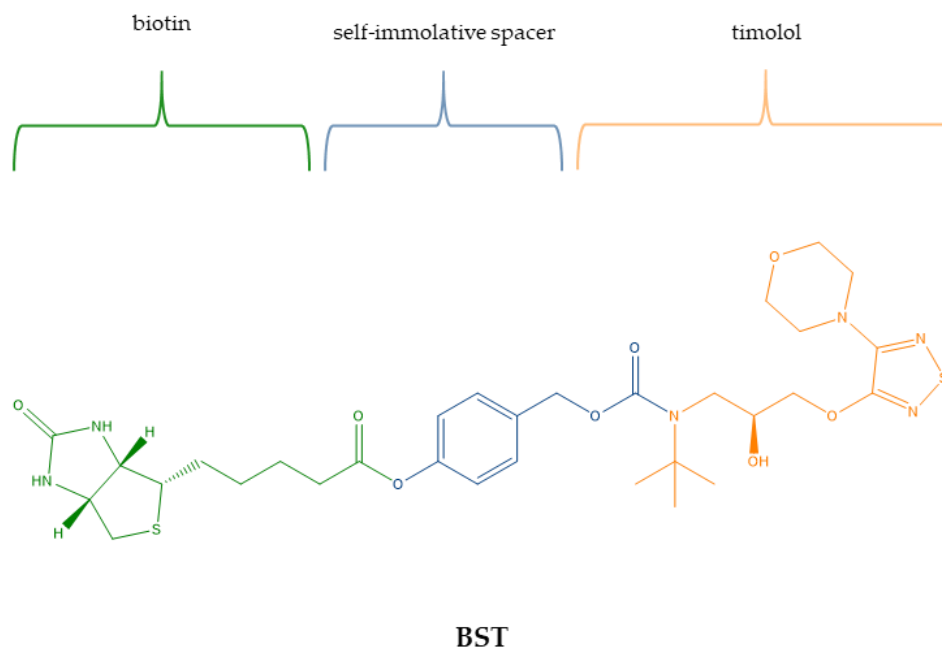


**Figure 2.5.** Structure of novel self-immolative prodrug of Timolol.

Esterases appear to be concentrated in the iris-ciliary body, corneal epithelium, retina, and optic nerve. Different classes of esterases, acetylcholine esterase, pseudocholine esterase, butyrylcholine esterase, and carboxylesterases are responsible for the facile conversion of the ester prodrugs to parent drugs.

The spacer is a substituted 1,4 aromatic system that allows spontaneous elimination after esterase activation of the ester group (Figure 2.6).

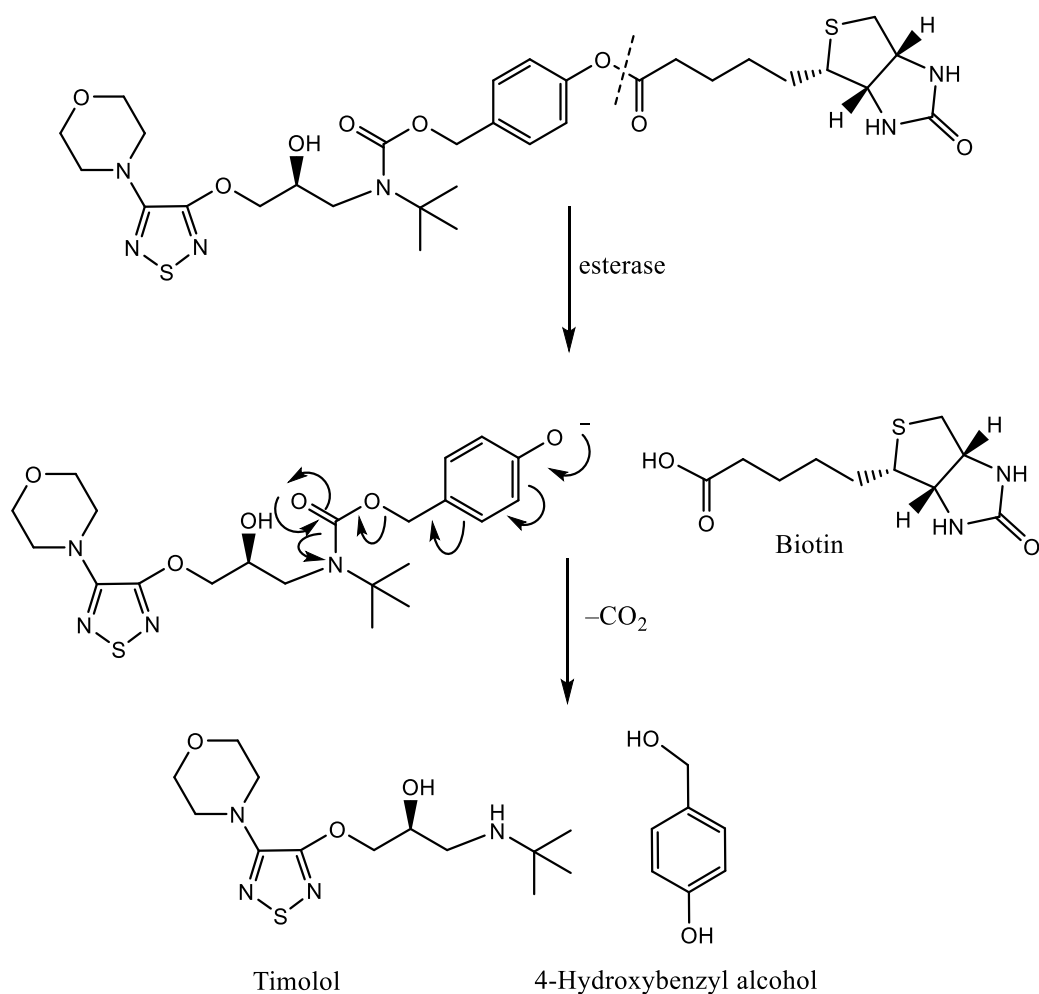


**Figure 2.6.** Schematic representation of the bioconversion of BST.

In fact, after hydrolysis, 4-hydroxy benzyl alcohol, CO<sub>2</sub> and timolol will be released spontaneously. The spacer should ensure a sufficient distance for the esterase to catalyze the hydrolysis reaction without steric hindrance.

Benzyl alcohol is metabolized to benzoic acid, which reacts with glycine and is excreted as hippuric acid in the human body. Acceptable daily intakes were established by the World Health Organization at 5 mg/kg for benzyl alcohol. No adverse effects of benzyl alcohol have been seen in chronic exposure animal studies using rats and mice.<sup>77</sup>

Biotin is part of the B-complex vitamins used in cell growth, the production of fatty acids, metabolism of fats, and amino acids. It plays a role in the Krieb

cycle, which is when energy is released from food. It is not toxic to the ocular system.<sup>78</sup>

To evaluate the spacer's effect on biotin's molecular recognition and to evaluate biotin's ability to be absorbed by active transport systems, two other derivatives of timolol were synthesized: ST and BT (Figure 2.7).

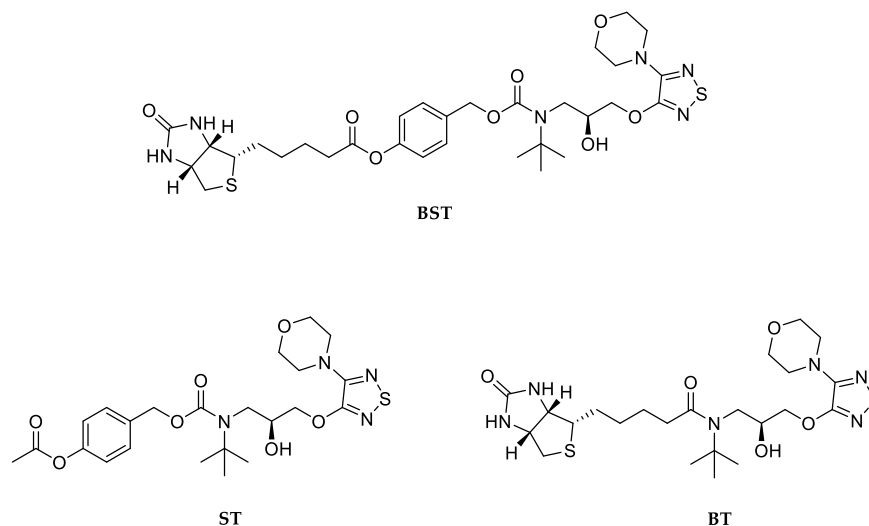


**Figure 2.7.** Structure of the newly designed prodrugs: BST, ST, and BT.

## 2.6 PHYSIOLOGICAL PROPERTIES AND FUNCTIONS OF SODIUM DEPENDENT MULTIVITAMIN TRANSPORTER (SMVT)

Sodium-dependent multivitamin transporter (SMVT; expressed by the SLC5A6 gene) is a vital transmembrane protein responsible for transporting vitamins and other essential cofactors as biotin, pantothenic acid, and lipoic acid. SMVT is expressed in many tissues such as the cornea, placenta, brain, liver, intestines, lungs, kidneys, heart, and retina. SMVT is a carrier-mediated, highly sodium-dependent generator system. The hydropathy plot (Kyte-Doolittle algorithm) revealed that the human SMVT protein is composed of 635 amino acids and 12 transmembrane domains (TMD) with both amino and carboxy ends oriented towards the cytoplasmic environment.<sup>79</sup> Despite the current knowledge of cell biology, molecular identity, and regulation of the SMVT backbone system, structure-function,

and structure-regulation relationships are not fully known. Said et al. investigated the biology and functional role of SMVT in biotin regulation. Nine histidine residues have been identified in the primary amino acid sequence of SMVT, of which seven (His46, His54, His115, His125, His238, His254, and His 533) are conserved across species (human, mouse, rat, and rabbit).

The mutagenesis approach allowed them to understand the role of His in biotin regulation by SMVT. Indeed, the conserved His residues such as His46 and His533 have been reported to be expressed at the membrane-aqueous interface while His54 and its 125 residues are located in the extracellular domains. The third TMD constitutes its 115 residues, and the large intracellular domain between the sixth and seventh TMD constitutes His238 and His254. His residues resulted in changes in the membrane expression of hSMVT and significantly decreased biotin uptake, indicating an important role of His115 and His254 residues in regulating the SMVT system. Mutations in Asn138 and Asn489 significantly reduced the ability of the transporter without altering its affinity.<sup>80</sup> The topological prediction analysis showed that Cys68 and Cys144 hSMVT proteins are extracellular, Cys294, and Cys450 are cytoplasmic, and Cys104, Cys186, Cys309, Cys358, Cys410, and Cys443 are present in the hydrophobic. Overall, these results suggest that the hSMVT protein is glycosylated, and this enzymatic process is important for its function.

## **2.7 COMPUTATIONAL APPROACH TO THE TRANSPORT OF BIOTINYLATED DRUGS**

Computer-aided molecular design (CAMD) and computational chemistry are important aspects of drug design and have been used to follow atom-by-atom reactivity and interaction.<sup>81</sup> From hit identification to lead optimization and beyond, approaches such as structure-based, ligand-based, and virtual screening are commonly used to support drug

---

discovery.<sup>82</sup> Generally, these methods can be divided into two categories: structure-based and ligand-based drug design. In the first category, using available 3D-structural and other relevant biological information concerning the target protein, the binding energy of small molecule inhibitors is calculated, and the chemical structures are modified accordingly with the target information. The 3D-structural information is obtained either from the experiment (X-ray or NMR determination of the protein structure) or from reliable computational methods (*i.e.*, homology modeling). Molecular mechanical (MM) as well as quantum mechanical (QM) approaches may be used to identify small molecules with binding affinity and then to refine the structure of these small molecules toward higher binding affinity ones. Often, the 3D-structural information of the target protein is not available and/or there is no good template for homology modeling; In this case, the ligand-based methods such as QSAR are preferentially used. From the dataset obtained from a series of lead compounds, 2D or 3D descriptors are calculated. QSAR equations are derived based on the 2D descriptors, and, usually, a pharmacophore model is created from the 3D descriptors. The QSAR equation and the pharmacophore model are used to suggest new compounds with improved activity.<sup>83</sup> In some other cases, the two different structure and ligand-based methodologies can be joined simultaneously to filter a significant number of compounds.<sup>84</sup>

## **2.8 HOMOLOGY MODEL AND COMPUTATIONAL STUDY OF SMVT**

However, despite the increasingly evident scientific importance of SMVT, its biological role has been hampered as the transporter's crystal structure has never been released. For the new prodrugs' rational design, it was decided to build a homology model of hSMVT, using the software implemented in YASARA. By exploiting the gentle identification of the

---

hSMVT transporter as SLC5A6, we constructed its 3D molecular structure using the homology modeling approach, starting from the sequence Q9Y289 (SC5A6\_HUMAN) deposited in UniProt Knowledgebase (<https://www.uniprot.org/uniprot/>).

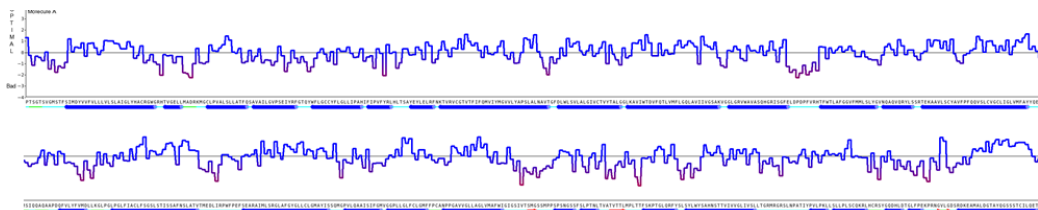
Indeed, this task was developed by mixing the first three classical steps (i. finding homologous model proteins of the known structure, ii. selecting the best model or set of models, and iii. optimizing the alignment of multiple sequences between the queries and model protein sequences)<sup>85</sup> with evolutionary coupling analysis.<sup>86</sup>

As the last step, we performed the typical fourth step, which consisted of creating the homology model for the query sequence that closely resembles the model structures, adapting the query residual deletions and inserts relative to the model structures, in order to obtain a series of hybrid models ordered according to their overall Z-score.<sup>87</sup>

The hybrid model (Z-score of -0.768) was chosen for further computational studies (Table 2.1).

**Table 2.1.** *The resulting hybrid model obtained the following quality Z-scores and quality model.*

Check type	Quality Z-score	Comment
Dihedrals	-0.468	Good
Packing 1D	-0.308	Good
Packing 3D	-1.247	Satisfactory
Overall	-0.768	Good



A genetic sequence alignment *via* the SwissProt database shows that SMVT exhibits substantial homology with some known sodium-dependent nutrient transporters. Of these, the pantothenate permease from *E. coli* and *Hemophilus influenzae* and the mammalian iodide transporter, glucose transporters, and myo-inositol transporter show maximal homology with SMVT

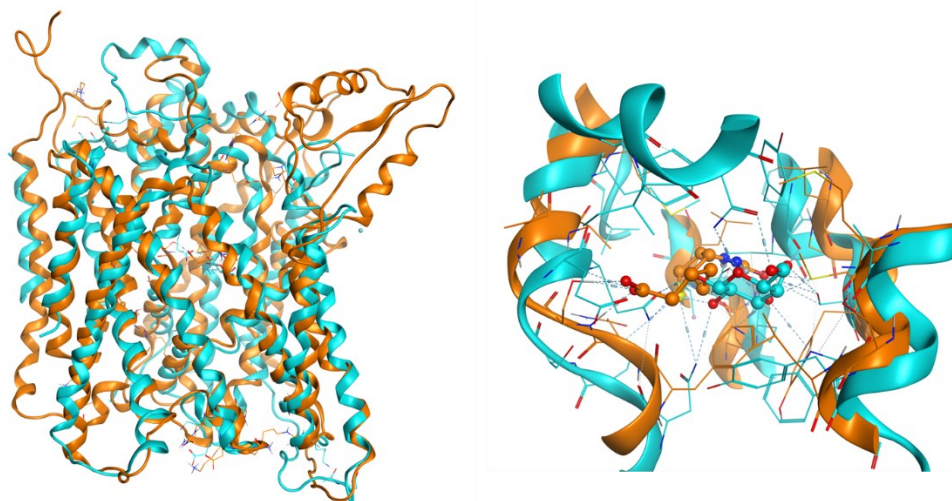


**Figure 2.8.** (a) Aligned structure and (b) detailed view of the binding site of hSMVT(orange) and vSGLT (cyan).

The alignment of hSMVTs with the crystal structure of sodium/sugar symporter with bound galactose (PDB ID: 3DH4), shown in Figure 2.8, demonstrates the high similarity of the protein structures. Both substrates (biotin and galactose) bind in the same area as the transporters. Secondary membrane transporters couple “uphill” translocation of substrate across the membrane to the energetically favorable flow of ions down their concentration gradient. Both the substrates they transport, ranging from ions, sugars, and lipophilic drugs. Although the transport mechanism



needs to be elucidated experimentally, SMVT is likely to adopt the same mechanisms as *Vibrio parahaemolyticus* sodium/galactose symporter (vSGLT). In vSGLT, the transporter has two main alternating conformations, facing the cytoplasmic side and the extracellular side. Interconversion between the two conformations facilitates the substrate translocation across the membrane. This translocation mechanism can be achieved through appropriate conformational changes.

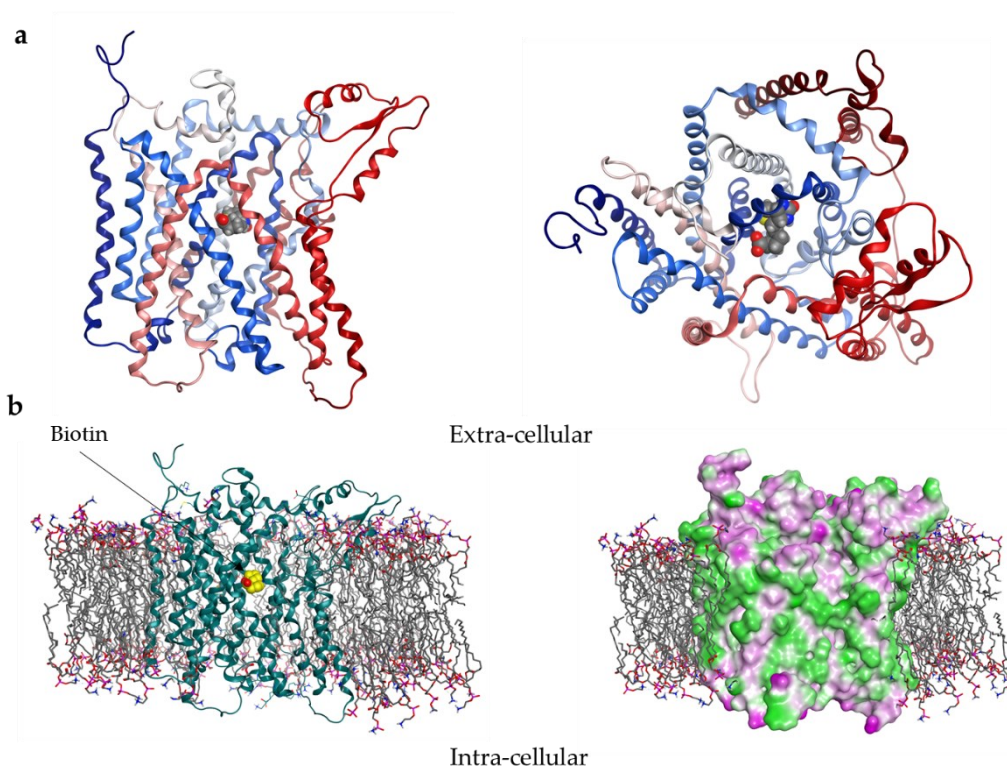


**Figure 2.9.** (a) Side and extracellular views of the cartoon representation of the different domains of hSMVT. (b) Structure of the domains of the transporter buried in the membrane with the relative hydrophobic surface.

The functional center of SMVT consists of two symmetrical and inverted halves (Figure 2.9a). The natural substrate (biotin together with the  $\text{Na}^+$  ion) is bound to the center of the central helices in the center of the membrane. (Figure 2.9b). The substrate is closed with respect to the extramembrane space by hydrophobic residues. The cytoplasmic gate is much smaller,

consisting of a few side chains, and a large cavity is located on the outside of this gate.

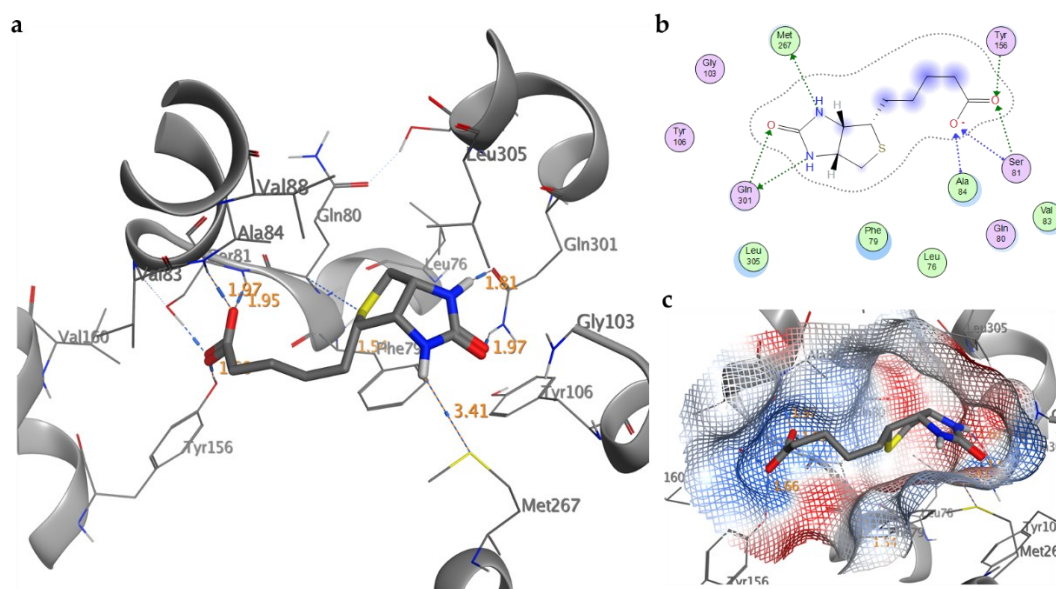


**Figure 2.10.** Biotin. **(a)** Interaction profile of the best-docked poses (stick model). **(b)** Binding site interactions in 2D representation. **(c)** View of biotin inside binding pocket in electrostatic potential surface representation.

Figure 2.10 shows the docked and minimized biotin laying. The biotin-binding site is near the center of the protein, lined with residues of four helices. Two helices adopt a distorted helical structure within the membrane bilayer at the point of contact with the substrate, which likely has implications for how the bond drives the alternating access mechanism.

Ala84, Ser81, and Thr156 are involved in hydrogen bonding with the negatively charged carboxylate group of biotin at a distance of 1.95 Å, 1.97 Å, and 1.72 Å, respectively (Figure 2.10a). While the aliphatic portion establishes weak hydrophobic interactions with the Ala84 side chain, the thiophene portion establishes an H-bond with Met267, the imidazole fraction two H-bonds with Gln301 at 1.81 Å and 1.97 Å.

To verify the docking results' reliability, Molecular Dynamic (MD) Simulations were performed, based on the molecular docking results. This initial analysis allowed to verify the stability of the protein structure and the biotin binding inside the cavity, especially the ligand's interactions with the key residues. A 100 ns MD Simulation was performed to analyze in greater detail any changes in the protein-ligand complex. All hydrogen bonds of the bond pocket were maintained throughout the simulation. Both the protein structure and the ligand reached equilibrium after 10 ns and a very similar average RMSD, 1.7 Å and 2.2 Å for ligand and protein, respectively (Figure 5.1). The flexibility of the different residues of hSMVT, by calculating the root mean square oscillations (RMSFs) of C $\alpha$ -atoms, was analyzed. A relatively higher RMSF value is obtained around residues 20-40 (Figure 5.5), probably due to the side chain's increased flexibility near the extracellular site. Furthermore, to understand the effect of biotin-binding on the internal dynamics of hSMVT, the dynamic cross-correlation matrix (DCCM) was calculated by using the coordinates of C $\alpha$  atoms from the trajectories. While all domains show areas of high structural correlation, only the membrane domain shows anti-correlation relationships (Figure 5.4).

**Table 2.1.** Calculated binding energies (kcal/mol),  $K_i$  (nM) calculated, and  $K_i$  (nM) experimental for the binding sites of hSMVT transporter for  $\alpha$ -Lipoic Acid, Pantothenic acid, Gabapentin enacarbil, Biotin, BST, and BS.

Ligand	Calcd $\Delta G$	Calcd $K_i$ (nM)	Exp $K_i$ ( $\mu$ M)
$\alpha$ -Lipoic Acid	-7.0	7.4	7.4
Pantothenic acid	-6.7	12.2	—
Gabapentin enacarbil	-8.2	1.0	—
Biotin	-8.1	1.1	—
BST	-8.3	0.8	—

BT	-7.9	1.6	—
----	------	-----	---

To evaluate the 3D structure and reproducibility of the affinity towards the physiological ligands of hSMVT were docked. Compounds ( $\alpha$ -Lipoic Acid, Pantothenic acid, Gabapentin enacarbil, Biotin, BST, and BS) were evaluated using AutoDock4, showing excellent results by comparing the calculated  $K_i$  with the experimental  $K_i$ , as shown in Table 2.1. Molecular docking was performed using the three-dimensional homology structures of hSMVT. AutoDock 4.2.6 software implemented in YASARA (v. 19.5.5, YASARA Biosciences GmbH, Vienna, Austria) was used for all docking experiments.

The calculated binding energy of  $\alpha$ -Lipoic Acid, with the respective calculated  $K_i$  values is identical to the experimental  $K_i$ , while for BST, the affinity is slightly better ( $-8.3$  kcal / mol). For BT, the affinity decreases ( $-7.9$  kcal/mol), suggesting a lower affinity within the binding site.

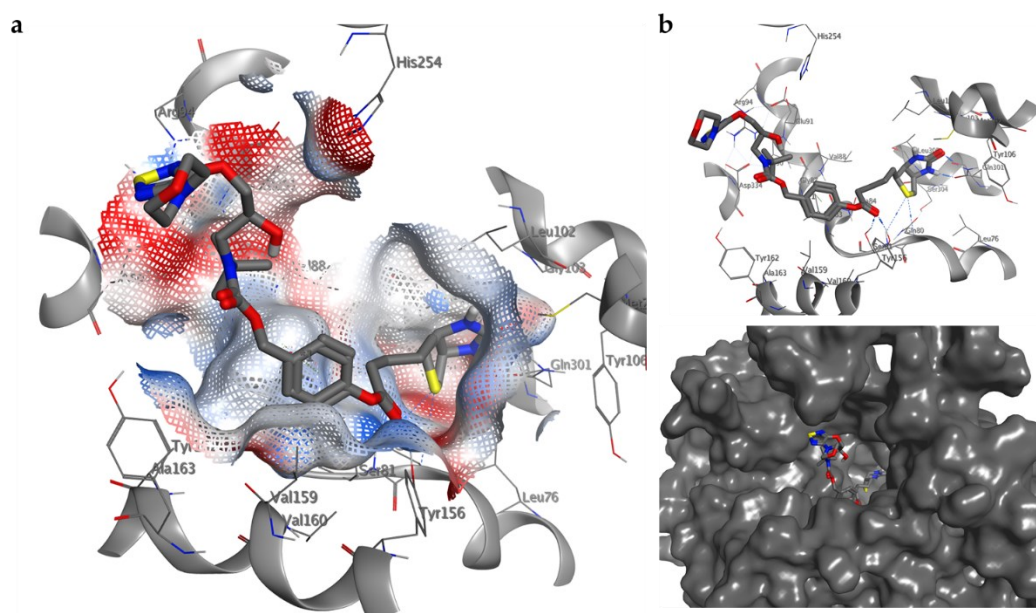


**Figure 2.11.** BST (a) View of the inside binding pocket in electrostatic potential surface representation (ligand in stick model). (b) Binding site interactions in 2D representation. (c) View of BST inside binding pocket in surface representation.

By visualizing in detail the docked pose of BST inside hSMVT pocket (Figure 2.11), it can be seen that the entire fraction of biotin adopts a pose similar to the docked pose, keeping all the H-bonds in the lower part of the pocket, *i.e.*, NH-Gln301 (2.03 Å), CO-Gln301 (2.15 Å) and S-Gln80 (3.06 Å). In the tunnel's upper zone, the ester group is stabilized by two H-bonds with Tyr186 (2.65 Å) and Ser81 (2.38 Å). It is interesting to note that the self-immolative spacer and timolol do not interact with any residues of hSMVT, apart from the weak hydrophobic interactions with Val83 (Figure 2.11).

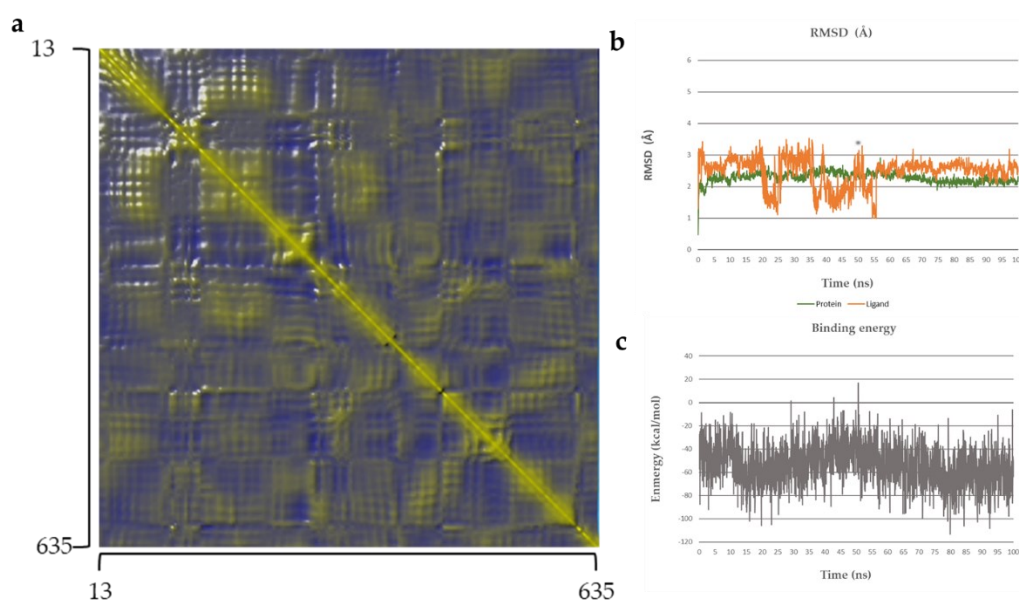


**Figure 2.12.** BST. **(a)** Dynamic cross-correlation matrix. The DCCM is visualized with colors ranging from blue (-1, fully anti-correlated) to yellow (+1, fully correlated). **(b)** RMSDs ligand and protein during MD simulation. **(c)** . Binding energy variation during MD simulation.

A detailed analysis of the trajectories developed by MD Simulation highlights the good stability of the protein-ligand complex. RMSD analysis shows that BST has notable fluctuations reaching an equilibrium at 60 ns (Figure 2.12b). These oscillations of the ligand are due to the fraction of timolol that at first of the MD simulation fails to stabilize in the upper edge of the pocket, while the protein structure seems to reach a slight flexion at

5 ns, remaining at low RMSD levels. The DCCM plots (Figure 2.12a) of the BST-hSMVT complex show a high correlation in all domains, resulting in even more stability than the hSMVT-biotin complex. The obtained binding energy values include solvation events according to the Poisson-Boltzmann approach (PBS), implemented in the Yasara software package; they show a slight decline at 50 ns to return to the previous values, with a minimum of  $-113.04$  kcal/mol at 80 ns (Figure 2.12c). A relatively higher RMSF value is obtained around residues 460-635 (Figure 5.5), in an incredibly flexible zone of the protein due to the cell membrane's interactions.

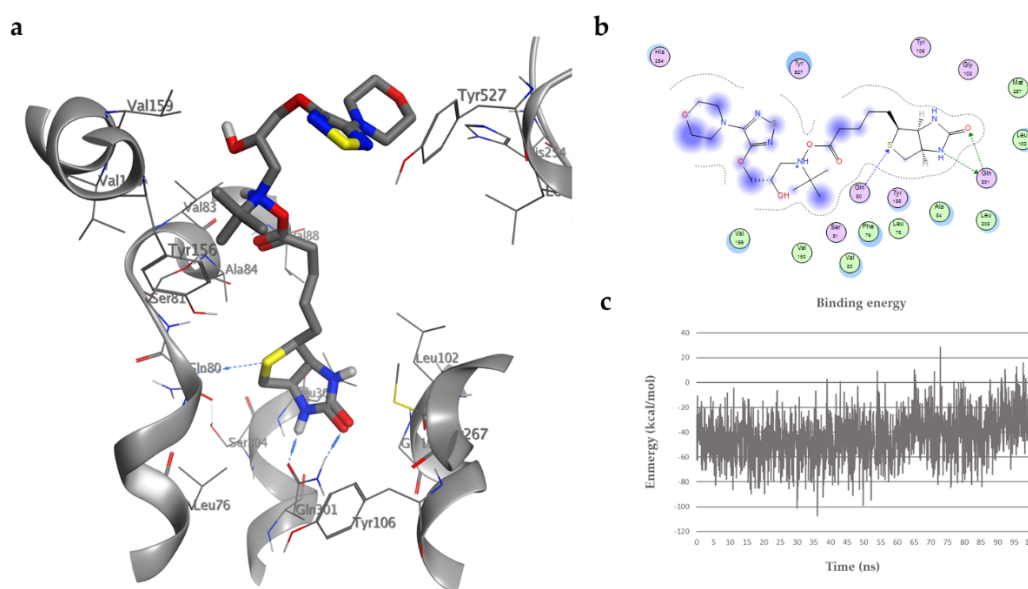


**Figure 2.13.** BT (a) Interaction profile of the best-docked poses (ligand in stick model). (b) Binding site interactions in 2D representation. (c) Binding energy variation during MD simulation.

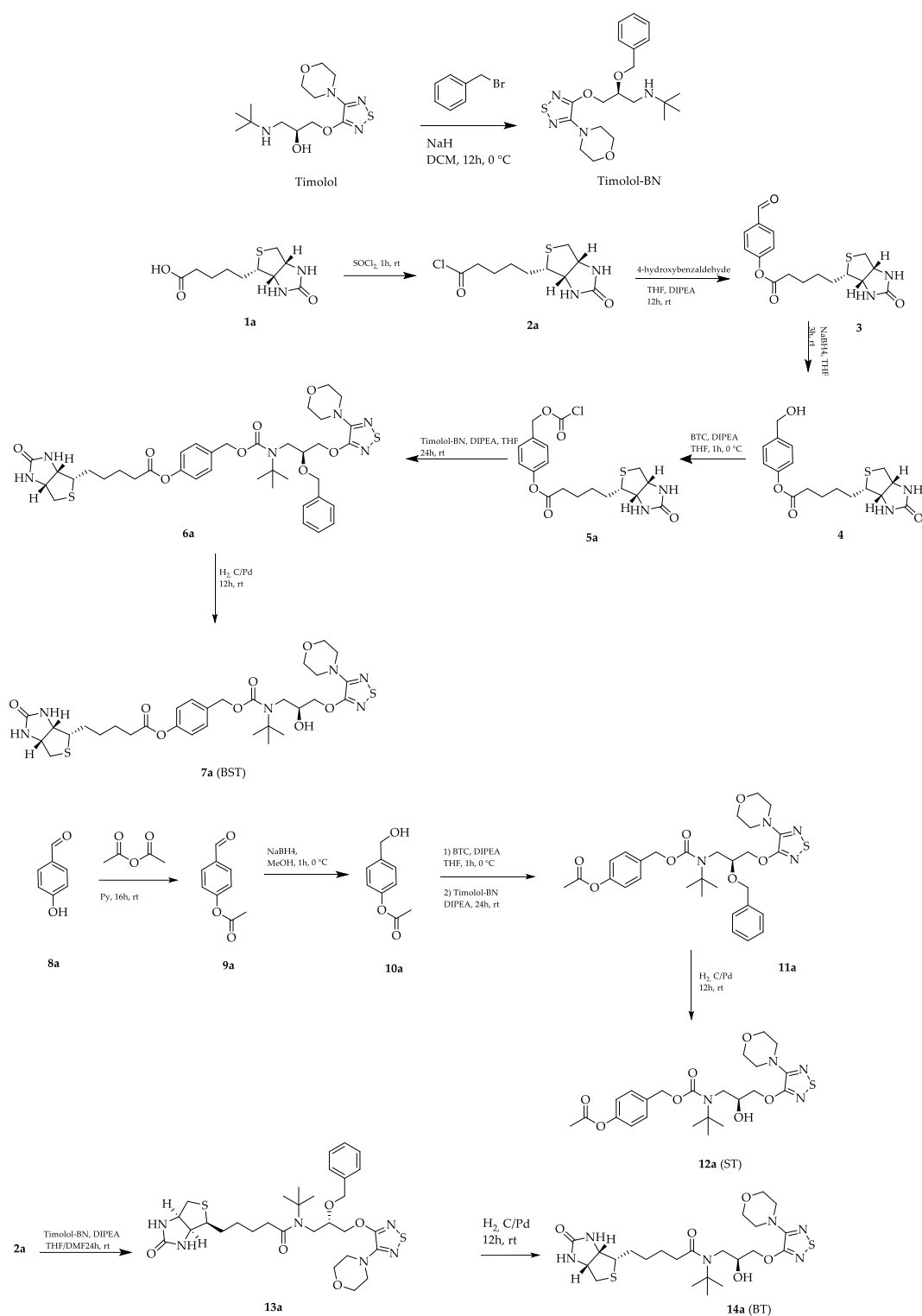
BT prodrug's computational analysis shows essential information useful for future drug design approaches if confirmed by the experimental data. In fact, BT maintains the interactions of the hydrophilic zone of the hSMVT pocket but with an average increase in the length of the H-bonds of  $0.1 \text{ \AA}$ . This results in a loss of binding energy of  $0.4$  kcal/mol. The timolol fraction exits the pocket establishing weak hydrophobic interactions with His254 and Tyr527. As shown in Figure 5.3, the binding energy of BT decreases

during the MD simulation. This is probably due to the displacement of the side chains, leading to an increase in the internal hydrophobic channel volume. These data are supported by the DCCM graphs (Figure 5.5), which show the areas of anti-correlation in the main domain.

This detailed computational analysis demonstrates that the correct choice of spacer and parent drug modifications can influence the protein-drug complex's stability, hence the correct molecular recognition.

---

## 2.9 SYNTHESIS OF THE NEW TIMOLOL PRODRUGS



**Scheme 2.1.** Synthetic scheme for the molecules BST, ST, and BT.

The synthesis of the three prodrugs of timolol was performed according to the following synthetic path shown in Scheme 2.1. The biotin was reacted



with thionyl chloride to obtain derivative acyl chloride 2. Without any purification, the acyl chloride was reacted with 4-hydroxybenzaldehyde to obtain ester 3. After reducing the aldehyde functionality with NaBH<sub>4</sub>, alcohol 4 was reacted with triphosgene to obtain the carbon chloride derivative 5a. Without any purification, timolol, previously benzylated in the alcoholic functionality (timolol-BN), was added to obtain derivative 6a. The final structure (BST) was obtained by debenzylation with H<sub>2</sub> catalyzed by Pd/C in high yields. To verify biotin's effective efficacy as a transporter with high molecular reconstitution, the TS derivative was synthesized starting from the acetylation of 4-hydroxybenzaldehyde. Intermediate 10a was obtained by subsequent reduction with NaBH<sub>4</sub> in methanol. The reaction with triphosgene leads to the formation of the carbon chloride intermediate, which by subsequent reaction with timolol-BN leads to the synthesis of carbamate 11a with moderate yields. Deprotection of the hydroxyl group described above.

Finally, to evaluate the parent drug release and the effect of the self-immolative spacer, prodrug BT was synthesized by reaction of biotin acyclic chloride 2a and timolol-BN. The subsequent debenzylation leads to the prodrug 12a (ST).

## **2.10 DETERMINATION OF PARTITION COEFFICIENT (LOG P) CHEMICAL (NON-ENZYMATIC) STABILITY**

The synthesized compounds were evaluated to establish their stability in an aqueous solution at pH 5.7. A lower pH improves ester stability for the eye drop formulation. Although in BST, the carbonate bond between spacer and timolol is very stable, the BT prodrug is more stable in solution. The hydrolysis of the ester bond spontaneously releases the spacer and timolol. ST is the least stable prodrug, probably due to facilitated ester hydrolysis.

---

**Table 2.3. Experimental partition coefficient (log P) and chemical stability in solution.**<sup>a</sup>Ratio = (Area% tx/Area% t0)% by HPLC

Ligands	Partition coefficient log P	Chemical stability				
		1d	1w	4w	8w	12w
Timolol	0.05	–	–	–	–	–
Biotin	0.55	–	–	–	–	–
BST	2.59	99.2	98.5	98.0	97.7	97.4
ST	2.29	99.1	97.4	94.5	93.4	90.1
BT	1.27	99.6	98.9	98.6	98.4	98.1

Evaluation of log P is associated with the physico-chemical and physiological properties of the compound such as its membrane permeability. Compounds with lower log P (<0) are more polar and have poor membrane permeability, however compounds with log P higher (> 3) they are more apolar and have poor water solubility. BST shows the highest value among the synthesized derivatives (Table 2.3). The trend clearly indicates an increase in LogP as the number of acceptors and donors of H-bonds decreases. Furthermore, the self-immolative spacer clearly affects the lipophilicity of the derivatives.

## 2.11 CONCLUSIONS AND PERSPECTIVE

Glaucoma is a degenerative eye disease that leads to increased intraocular pressure (IOP), which could progress, causing irreversible damage to the optic nerve, leading to blindness. Therapy for glaucoma treatment can be pharmacological or surgical. Timolol is a non-selective  $\beta$ -adrenergic receptor blocker used for the treatment of glaucoma. Its therapeutic effects

are due to the reduction of the secretion of aqueous humor at the ciliary process level, therefore of the intraocular pressure. A significant disadvantage of timolol eye drops is the relatively high incidence of cardiovascular and respiratory side effects since 1–2% of the instilled dose enters the eye, while the majority reaches the systemic circulation. To overcome these problems, new biotinylated self-immolative prodrugs of timolol have been designed and synthesized. Prodrugs that can take advantage of carrier-mediated transport mechanisms offer intriguing targets in drug design. In this case, the new derivatives were designed using a molecular modeling approach for recognition by the hSMVT transporter. The protein structure was reconstructed using a homology modeling approach. This approach made it possible to evaluate *in silico* the stability and the quality of recognition of the new prodrugs designed.

Furthermore, this methodology allows making appropriate modifications to the structure to improve the affinity of the transporter. This study highlights the probable binding site of biotin and other physiological ligands for the hSMVT transporter for the first time. The key residues in the interaction with the ligands were shown in detail, and MD simulation was performed for the first time on this protein, highlighting the correlations between the various domains. This approach could be applied to improve the molecular recognition of drugs in the future.

Unfortunately, the COVID-19 pandemic has slowed down *in vivo* studies to evaluate the transport of new biotinylated derivatives of timolol.

---

---

## CHAPTER 3 CNT TRANSPORTERS FOR NEW PRODRUG OF ACYCLOVIR

### 3.1 INTRODRUCTION

Specific transporters mediate the transcellular flux of nucleosides and exogenous nucleoside drugs in mammalian cells. Nucleoside transporters I can be classified as Na<sup>+</sup>-independent equilibrative nucleoside transporter (ENTs) and Na<sup>+</sup>-dependent concentrative nucleoside transporter (CNT).<sup>88-90</sup>

This last comprises five subtypes, N1 to N5, which are defined based on their respective substrate selectivity.<sup>91</sup> N1 is selective for uridine and purine nucleosides, N2 is selective for adenosine and pyrimidine nucleosides, N3 has a broad specificity for both pyrimidine and purine nucleosides while N4 has a broad selectivity for pyrimidine but is capable of carrying also adenosine and guanosine, except inosine. The N5 prefers guanosine as the substrate.<sup>92,93</sup>

Vickers et al. showed that ENT1 and ENT2 tolerate modifications in the 5 positions of the nitrogenous base and in the 2' and 5' positions of the uridine ribose, while the removal of the hydroxyl group in the 3' position of the ribose portion of the uridine cancels the transport of the substrate for lack of interaction of the binding site with both transporters. Compared to ENT1, ENT2 showed lower affinity for cytidine and cytidine analogs, suggesting a lower tolerance for the presence of the base amino group at position 4.<sup>92</sup>

Equilibrative nucleoside transporters can also transport substrates bidirectionally. In the absence of sodium, sodium-dependent nucleoside transporters are also efficient of nucleoside efflux from inside the cells. Furthermore, in the absence of an inwardly directed Na<sup>+</sup> gradient, Na<sup>+</sup>-dependent nucleoside transporters can release nucleosides.<sup>94</sup> An example of

---

a nucleoside transporter's role in drug delivery is the movement of the anti-human immunodeficiency virus drug, 2',3'-dideoxyinosine (ddI), across the blood-brain barrier.<sup>95</sup> Other examples of drugs whose cellular uptake is associated with ENT include S-adenosylmethionine (SAME),<sup>96</sup> fludarabine,<sup>97</sup> arabinosylcytosine (araC),<sup>98</sup> and azidothymidine (AZT).<sup>20</sup>

Hosoya et al.<sup>99</sup> have demonstrated, for first, that in pigmented conjunctiva of rabbit systems exist Na<sup>+</sup>-dependent for the transporter of nucleosides. In particular, systems type N3 would be more responsible for uridine transport, without excluding systems N2 and N4. In 2003 Mujumdar et al.<sup>100</sup> showed a nucleoside transporter sodium-dependent on rabbit cornea. These results were confirmed in a recent study (2018)<sup>101</sup> that highlights the presence of equilibrative nucleoside transporters (ENT) type ent1, ent2, and ent3. The knowledge regarding the presence and functional importance of these NTs could be an essential aspect to be considered for the transcorneal permeation of antimicrobial and anticancer agents used in ocular therapeutics.

### **3.2 HERPES ZOSTER OPHTHALMICUS**

Herpetic keratitis from herpes simplex (HSV) causes a broad spectrum of diseases that include primary infections and recurrent, such as gingivostomatitis, labial herpes, and genital infections, neonatal and congenital eczema in patients with atopic dermatitis, pateruccio, the visceral infections in immunocompromised patients, the encephalitis and erythema. Patients undergoing bone marrow transplantation or organ chemotherapy and HIV-positive patients may develop multiple lesions and be extended by HSV with possible interest visceral. The clinical manifestations of ocular infection by HSV can affect the eyelids, the conjunctiva, cornea, uvea, and retina. Keratitis represents the event more common of herpetic infection.<sup>102</sup>

---

Clinical studies underestimate the incidence and prevalence of infection because more than two-thirds of infections are asymptomatic. Some works have shown that primary infections are clinically manifest in 1–6% of cases. In 33% of cases, the HSV infection manifests as a relapsing infection. The HSV-1 and 2 can be transmitted from asymptomatic patients, causing primary infections or applicants. Ocular infections primarily occur with the conjunctiva and/or surface layers corneal involvement. The study of the Moorfields Hospital shows moderate or severe conjunctivitis in 84%, blepharitis in 38%, a dendritic ulcer in 15%, and stromal keratitis in 2% of cases. About 21% of all acute conjunctivitis recognize a herpetic etiology. The recurrence is mainly interested in the conjunctiva and eyelids, less the cornea (31%). Of patients with primary keratitis, 40% develop an episode of relapse of epithelial keratitis within 5 years; 21% more than one. The 25% has stromal keratitis and 5% an increase of the intraocular pressure.<sup>103,104</sup>

The initial phase of herpes zoster ophthalmic is very specific and differs very little from a common syndrome influenza type. Includes signs and general symptoms such as fatigue, fatigue and general indisposition. These symptoms persist in general for about a week. Although at this stage the herpes zoster ophthalmic produces more often a rash fever, with a unilateral rash on the forehead, the upper eyelid, and involving the nose, a minority of patients may have only ophthalmic signs, limited mainly to the cornea. About 60% of patients feel pain in the dermatome concerned before the classic rash.<sup>105</sup>

- *Ocular manifestations of herpes zoster ophthalmic*

In ocular manifestations of herpes zoster ophthalmic, the cutaneous manifestations of herpes zoster ophthalmic strictly comply with the median line and involve one or more branches of the ophthalmic branch of the trigeminal (V) nerve, *i.e.*, the branches supraciliary, lacrimal, and

---

nasociliary. Since the branch's nasociliary innervates the ocular globe, the ophthalmic involvement more serious develops in the case of this branch's involvement. The involvement of the tip of the nose (sign of the Hutchinson) was used as a clinical sign the predictor of ocular involvement.<sup>106</sup> It should be borne in mind that up to one-third of patients with the sign of the Hutchinson negative develop anyway ocular manifestations.<sup>107</sup>

- *Blepharitis and conjunctivitis*

The eyelid involvement in herpes zoster ophthalmic is widespread. Patients develop blepharitis and often have secondary ptosis at edema and the inflammatory process. The majority of patients present on the eyelids the classical vesicular lesions that evolve subsequently in minimum scars.<sup>108</sup>

- *Corneal Involvement*

Involvement of the cornea in the course of herpes zoster ophthalmic can lead to a significant loss of sight. The cornea undergoes direct damage from viral replication and damage by antigen-antibody reaction and hypersensitivity reactions cell-mediated.<sup>109</sup> Patients with corneal involvement have various degrees of vision decrease, pain, and hypersensitivity to light. The corneal complications occur in 40% of cases of ophthalmic herpes zoster.<sup>110</sup> In the case of epithelial keratitis, the first corneal injuries consist of keratitis epithelial episode.

### **3.3 PHARMACOLOGICAL THERAPY AND OPHTHALMIC PRODRUGS OF ACYCLOVIR**

The emergency treatment of ophthalmic herpes zoster involves adequate analgesia, local treatment of skin lesions, the use of antiviral agents, and, if the secondary bacterial infection is present, the use of antibiotics. In the

---

event of impairment of the blink reflex and/or eyelid ptosis, an eye lubricant may be indicated to avoid corneal injury.

Aciclovir or acyclovir, chemically acycloguanosine and often abbreviated ACV, is an antiviral medicine, a similar acyclic of guanosine. The molecule is one of the antiviral drugs most commonly used, particularly in the treatment of infection by herpes simplex virus types 1 and 2 and in the treatment of varicella-zoster (chickenpox) and herpes zoster. Acyclovir orally, 800 mg 5 times per day, can reduce the duration of signs and symptoms as well as incidence and severity of the complications of herpes zoster ophthalmic ACV can reduce the pain during the acute phase but does not seem to have any effect on the reduction of incidence or severity of postherpetic neuralgia.<sup>111</sup> The ACV is of more significant benefit to the patient if the therapy is initiated within 72 hours after the onset of skin lesions. Similarly, the complications are more frequent in patients in whom the treatment was delayed. Both famciclovir (500 mg/day) that valaciclovir (1 g/day) have proved to be useful as ACV (800 mg 5 times a day) in the treatment of herpes zoster and reduction of complications.<sup>112,113</sup> Famciclovir and valaciclovir have schemes of administration simpler than ACV, increasing patient compliance.

To the inside of the cell, ACV is monophosphorylated thanks to the enzyme thymidine kinase's action, coded only from herpesviruses and not from the organism. It is for this reason that the drug acts mainly on infected cells and not on healthy ones. Subsequently, ACV monophosphate is phosphorylated in biphosphate and, finally, triphosphate by the host cell kinases. The ACV triphosphate acts as a competitive inhibitor with deoxyguanosine triphosphate for the viral DNA polymerases, blocking action through training an irreversible complex with the nascent viral DNA chain. The ACV in the form of triphosphate can also be incorporated into

---



the viral DNA in growth causing the premature termination due to the lack of the hydroxyl group (OH) in position 3'.<sup>114</sup>

Unfortunately, ACV transport is scarce due to its low aqueous solubility (1.4 mg / mL) and moderate lipophilicity (logP -1.47).<sup>115</sup> Despite this, ACV can be administered as eye drops, which would be the formulation more practical for treating ocular infection. The effectiveness of ointment for eyes of ACV 3% has been reported in the treatment of epithelial keratitis.<sup>116</sup> ACV ointment is not effective when deeper tissues are involved and against stromal keratitis.<sup>117</sup> Prodrug strategies have been applied to improve ACV delivery properties by increasing water solubility or by improving membrane permeability through increased lipophilicity or by targeting the oligopeptide transporter on the cornea.

Some water-soluble ester derivatives of ACV, including glyceryl esters, alanine and succinate, have been synthesized and biologically tested for their antiviral activity. These prodrugs were less active than ACV itself against HSV-1 and HSV-2 rabbits in primary renal cell cultures. The hydrophilic nature of ACV negatively contributes to ocular bioavailability. Therefore, lipophilic 2'-aliphatic esters of ACV were synthesized.<sup>118</sup> These esters were more lipophilic (up to 140 times) and exhibited lower aqueous solubility than ACV. The esters readily hydrolyzed to ACV in ocular tissue homogenates and showed increased corneal permeation.<sup>119</sup> Anand et al. have prepared the dipeptide prodrugs of ACV conveyor of oligopeptides to improve the ocular bioavailability of ACV.<sup>120</sup> The presence of an oligopeptide transporter on the cornea has been supported by the results obtained in permeability studies of valacyclovir using excised rabbit cornea. The permeabilities of dipeptide prodrugs were 1.7-2.9 times higher than for ACV through the rabbit cornea. Valaciclovir was inhibited by dipeptide prodrugs, suggesting that valaciclovir was recognized by the oligopeptide

---

transporter and can be actively transported. This is also supported by Caco-2 permeation experiments, in which the transport of Gly-Val-acyclovir was inhibited in the presence of glycylsarcosin.

Valprudi et al. have developed synthesized derivatives biomethylated ACV to increase the bioavailability of the drug (ACV) to make it both more lipophilic and, at the same time, site-specific.

### **3.4 Structure And The Transport Mechanism Of The Concentrative Nucleoside Transporter CNT**

Humans have three isoforms of CNT. The substrate specificities and tissue distributions of these isoforms are different<sup>14,121</sup> The crystal structure of a *Vibrio cholerae* CNT (vcCNT) represents the first opportunity to study the recognition of nucleosides from a structural perspective. vcCNT is an excellent model for studying CNTs: it shares a high sequence identity (36-39%) with hCNT and uses a Na<sup>+</sup> gradient for nucleoside transport. In addition, they have a very high sequence identity for the nucleoside binding site (64% with CNT1, 73% with hCNT2, 91% with CNT3). CNT has been crystallized as a homotrimer-shaped-like, an inverted triangular basin with its mouth facing the intracellular side and a knob-like structure facing the extracellular side (Figure 3.1b). The three-fold axis coincides with the crystallographic six-fold axis and is perpendicular to the membrane. When viewed from the intracellular side, each side of the triangle formed by the trimer is about 92 Å, and when viewed parallel to the membrane, the trimer is about 57 Å in height (Figure 4.1).

---

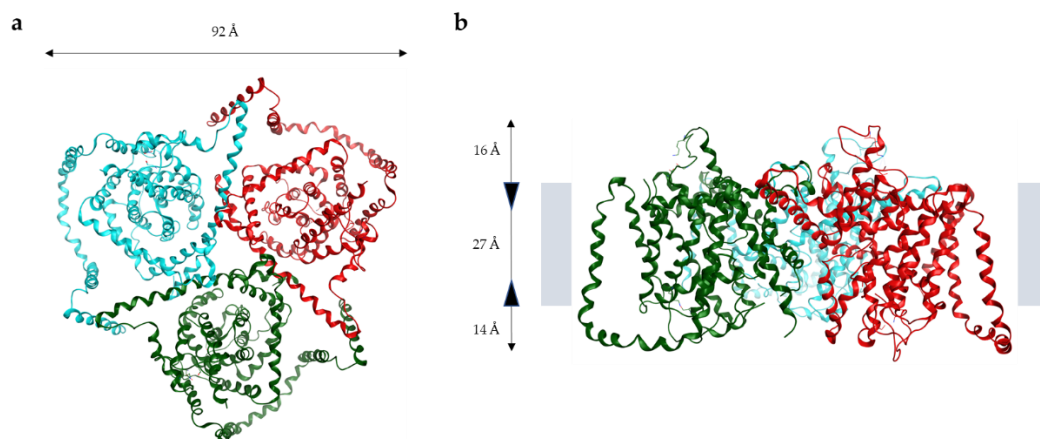
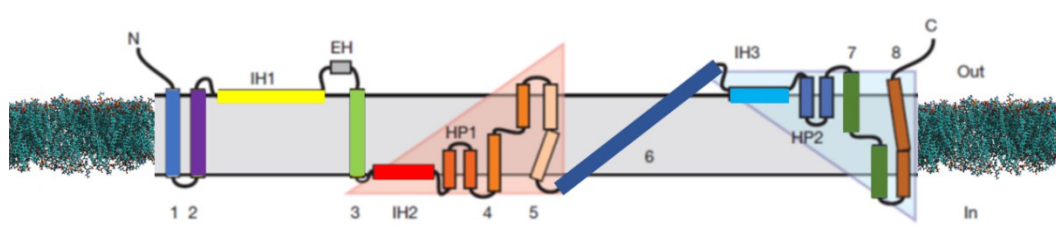


**Figure 3.1** (a) Cartoon representation of the vcCNT trimer viewed from the cytoplasm. Individual protomers are colored cyan, red and green. (b) Cartoon representation for the vcCNT trimer viewed parallel to the membrane. The putative membrane bilayer is indicated in grey boxes. The dimensions of the putative membrane bilayer, extracellular region, and intracellular region are shown.

The membrane-embedded area lies roughly in the middle of the transporter, judging from three hydrophobic helices' positions on each protomer. The predicted location of the lipid bilayer of the membrane suggests that the pelvis's mouth penetrates the plane of the membrane. The presence of polar amino acids on the basin's surface probably allows the aqueous solution to reach deep into the membrane's bilayer and access the transporter's surface.

The crystal structure revealed that each protomer has eight transmembrane helices (TM1-TM8), two reentrant helix-turn-helix hairpins (HP1 and HP2) with opposite orientations within the membrane, and three interfacial helices (IH1-IH3) parallel to the membrane (Figure 3.2).



---

**Figure 3.2.** Schematic representation of vcCNT topology. The group of helices under the orange triangular background is related to the helices group under the cyan triangular background by two-fold pseudo-symmetry, with the symmetry axis parallel to the membrane.

All protomers can be grouped into two subdomains based on their positions (in the outer and inner regions) with respect to the centroid of the crystal. TM1, TM2, IH1, EH (a short stretch of extracellular helices), TM3, and TM6 are found in the outer part of CNT and appear to be important in maintaining transporter stability. These helices in the outer region form a scaffold for the conveyor. The trimerization contacts unfold from one part of the scaffold domain: IH1, EH, TM3, and TM6 (Figure 3.2). IH1 is a 40 Å long amphipathic helix, most likely located at the water/membrane interface, while TM6 is approximately 60 Å long and inclined almost 60° to the membrane. The EH protrudes into the extracellular solution and is approximately 16 Å long. Since IH1 is involved in trimerization, it is limited to the membrane/water interface and interacts with many TMs (TM2–TM5), which is essential for maintaining the overall structure of vcCNT. The crystal structure suggests that vcCNT adopts a trimeric configuration. The structure contains three deep slits (one per subunit) on the intracellular side facing the trimer's center. The uridine bound in the fissure is directed towards the transporter's intracellular basin; however, it is not free to be released into the intracellular solution because TM6 and TM7b partially cover the binding site. The nucleoside binding site is positioned in the centre of the double internal symmetry and coated by the tips of HP1 and HP2 and the unwound regions of TM4 and TM7 (Figure 4.2). The interactions between uridine and the binding site show that many polar or HP1, HP2, TM4, and TM7-laden amino acids interact with uracil base and ribose. HP1 and TM4b are responsible for the interaction with the uracil base (Figure 3.3).

---

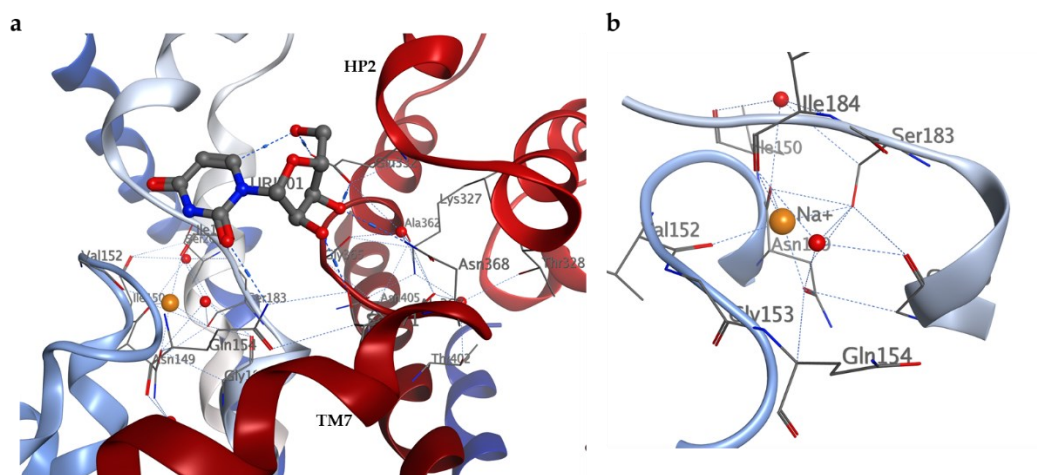


**Figure 3.3 (a)** The nucleoside-binding site, showing HP2 and TM7b. Hydrogen bonds are shown as blue dashed lines. **(b)** The Na<sup>+</sup>-binding site is located between HP1 and the unwound region of TM4.

HP2 and TM7 are responsible for the interactions with ribose with the side chains of Glu332 (HP2), Asn368 (TM7), and Ser 71 (TM7) interact with ribose directly (Glu332, Asn368 and Ser 371) or indirectly through a molecule of water (Asn 368). The Glu332 residue mutation in CNT has been shown to have significant functional effects on both nucleoside binding and transport rate.<sup>122</sup>

For CNT to be a Na<sup>+</sup> coupled transporter, it must contain at least one Na<sup>+</sup> binding site. Further inspection reveals that this site is octahedrally coordinated by three backbone carbonyl groups, two side-chain hydroxyl groups, and a water molecule with typical distances (approximately 2.4 Å) for Na<sup>+</sup> coordination by protein (Figure 3.3a).<sup>123</sup>

The Na<sup>+</sup> binding site is close to the nucleoside binding site, but Na<sup>+</sup> does not directly interact with the nucleoside (Figure 3.3a). Since the key amino acid residues for nucleoside base interactions are located on HP1 and TM4b, it is likely that the role of Na<sup>+</sup> binding is to bring HP1 closer to TM4 to complete nucleoside binding site formation.<sup>124</sup>

LEE et al.<sup>125</sup> presented CNT structures in conformations towards the interior-substrate, towards the interior, multiple intermediate, and open towards the outside. The results provide many structural and mechanistic insights into the conformational path of this secondary active transporter's elevating transition.

The proposed intermediate structures provide a new perspective on the lifting mechanism, suggesting that the lifting passes through intermediates rather than a single movement. The overall fold of the structure consists of two domains: a transport domain, containing transmembrane helices (TM1, TM2, TM5 and TM8), helical hairpins (HP1 and HP2), a scaffold domain, consisting of TM6 and TM3, involved in open state of trimerization and finally partially unwound propellers (TM4 and TM7). TM6 is hypothesized to serve as a hydrophobic barrier to the transport of nucleosides. The nucleoside binding site is located under the TM6 domain, where the upper part of the transport domain (TM4b and HP2b) interacts with the scaffold domain (TM3 and TM6), hindering access to the extracellular environment.

In the outward-facing conformation, the transport domain's translocation involves an upward movement of about 12 Å and a tilt of about 18° with respect to the plane of the membrane. Movement makes both sites accessible from the extracellular side, showing the sodium and nucleoside binding sites above TM6.

However, the transport domain in protomer C takes a different position from both inward and outward facing states (Figure 3.4).

---

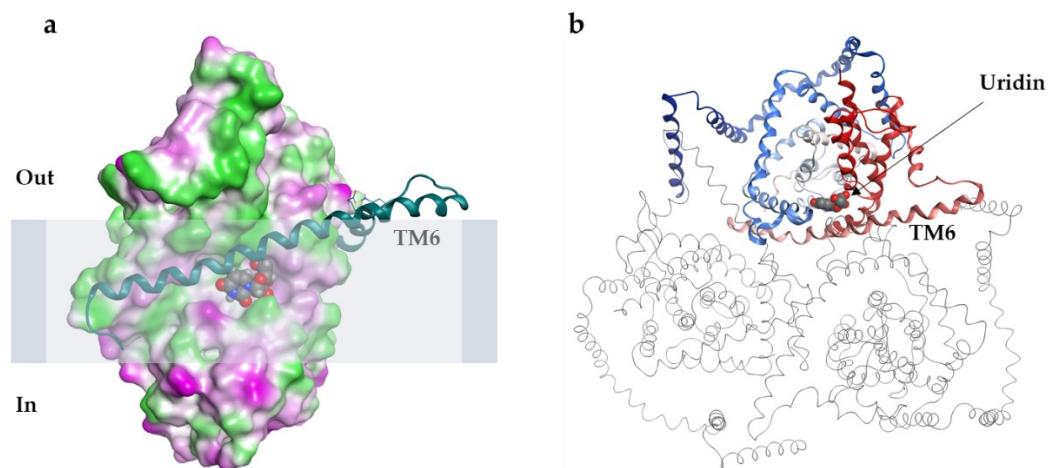


**Figure 3.4** (a) In hydrophobic surface representations (hydrophobic in green, hydrophilic in fuchsia), the transport domain resides midway between the inward and outward-facing states, with the substrate-binding sites (uridine) behind TM6. (b) View from the cytoplasmic side of the TM6 domain facing inward of the trimerization interface.

The scaffold domain, in elevator-like motion, changes interactions with the transport domain. The interface dominido is composed of HP1b, HP2b, TM4b and TM7b in the transport domain and TM3 and TM6 in the scaffold domain. TM4b and HP2b interact with the scaffold region to close binding sites on the extracellular site in the inward-facing state. In the intermediate states, HP1b, HP2b, TM4b and TM7b make both substrate binding sites inaccessible to the membrane sides through interaction with the scaffold domain. Hence, more interface is formed in these intermediates ( $\sim 1,800 \text{ \AA}^2$ ) than in internal ( $\sim 1,400 \text{ \AA}^2$ ) or external ( $\sim 1,700 \text{ \AA}^2$ ) states. The hydrophobic amino acid residues mainly constitute HP1. In the outward-facing conformation, HP1b and TM7b interact with the scaffold domain to hinder binding sites on the cytoplasmic side. The substrate binding sites are occluded on both sides of the membrane, leaving no room for ion loss during the intermediate states. In particular, the size of the nucleoside binding site decreases during the transition to the intermediate state, suggesting that the transport domain becomes more compact in the intermediate states during the transition and expands in the final states..

### 3.5 STATE OF THE ART

Hydrophobic prodrugs have usually been developed to increase membrane permeability. The same strategy has also been used to improve topical administration of drugs absorbed through the eye, as the corneal barrier hinders the permeation of topically administered ophthalmic active ingredients. As a result, only a low percentage of the instilled dose is absorbed, while the majority (50-99%) of which enters the systemic circulation.<sup>126</sup>

Develop a lipophilic prodrug is not always the appropriate strategy for ophthalmic use. In fact, after crossing the corneal epithelium, the drug must be able to reach systems at the deepest of the eye. Often the failure of an ophthalmic drug derives from its low permeation in deep tissues. A strategy very common would be a transporter-targeted modification of the drug. Transporters play a vital role in the influx of nutrients across biological membranes. The presence of active transporters has been demonstrated on ocular tissues. These include carriers of peptides, amino acids, glucose, vitamins, nucleosides / nitrogenous bases and lactate. Prodrugs that target the transporter offer many advantages in the active transport of drugs. Prodrugs designed to target influx transporters may increase the absorption of hardly permeating parent drugs. In addition, some physicochemical properties of the drug, such as solubility and stability, can be improved compared to the parent drug.<sup>127</sup>

Up to now, the pharmaceutical chemists have focused mainly on conveyors of amino acids and vitamins, demonstrating that the prodrugs are actively transported in the eye.

Vidarabine, trifluridine, idoxuridine and ACV are used in the treatment of epithelial keratitis. Although ACV is less toxic than the other agents, its

---



therapeutic utility is limited to superficial corneal keratitis, due to poor corneal permeability. Oral ACV has been shown to be useful in the treatment of systemic and ocular HSV infections. Due to their increased hydrophobicity, these drugs are poorly soluble in water and therefore their 1–3% eye drop formulation is not easily achievable.<sup>128</sup>

ACV has been derivatized in many ways to increase its transportability into the eye. In particular, many amino acid esters from ACV have been prepared.<sup>129</sup>

### 3.6 RATIONAL DESIGN OF ACV PRODRUGS

In order to increase ACV permeability in the ocular tissue and reduce the undesirable effects of the drug, a new prodrug of ACV has been designed. ACV, however, it is not substrate for CNT and ENT transporters but instead permeate the cornea primarily by passive diffusion.<sup>100</sup>

To increase ACV recognition, we have prepared ACV prodrugs conjugated with uridine (Urd), with promoiety properties. In fact, uridine is actively transported by all nucleoside transport systems (CNT and ENT).<sup>130</sup> This approach has never been considered for substrate/receptor recognition to promote cellular absorption. Currently, the only crystallized transporter available is the hCNT1. For this reason, we have focused our attention on the derivatization to be carried out depending on the data present in the literature. Zhang J. et al. showed that human hCNT1, hCNT2 and hCNT3 have different characteristics for the study and development of nucleoside analogues. The regions of the sugar fraction most critical for the interaction with hCNT2 were the C (3') and C (5') - OH groups, necessary for high affinity interactions with hCNT2, as all changes in C (3') and C (5') decreased the ability of hCNT2 to bind Urd analogs. The critical position of the Urd base for the bond was identified as (3) -H. When the 3'- or 5'-

---

hydroxyl groups and the N (3')-H were removed or modified the loss of more than 10.5 and 6.7 kJ / mol in Gibbs free energy, respectively, has suggested that these sites were involved in hydrogen bonding with hCNT2. Positions C (2') and C (5) were important regions for the interaction of hCNT2. Furthermore, hCNT2 tolerated removal of the 2-hydroxyl group but not its configuration inversion or substitution with an O-methyl or azide group. Positions C (2') and C (5) are the second most important regions for hCNT2-Urd interactions, while they were relatively less important for hCNT1 or hCNT3 binding than Urd. N (3') methylation reduced interactions with hCNT1, due to the reduced transportability of 3MeUrd. C (2') - OH was not fundamental for hCNT1-Urd interactions (Figure 3.5a) because Urd analogs with modifications in this position were both good inhibitors and permeating hCNT1. The 5'-hydroxyl group, which was previously identified as a potential H-bond donor for high affinity<sup>131</sup>, was not important for transport by hCNT1, because 5'-dUrd and 5'-Cl-dUrd remained good permeants. The C (3'), C (5), and N (3') regions of Urd affected hCNT3 to different degrees. A potential hydrogen bond interaction at C (3') of Urd was important for high-affinity binding and transport because removal or modification of the 3'-hydroxyl group drastically reduced bonding of the analog.

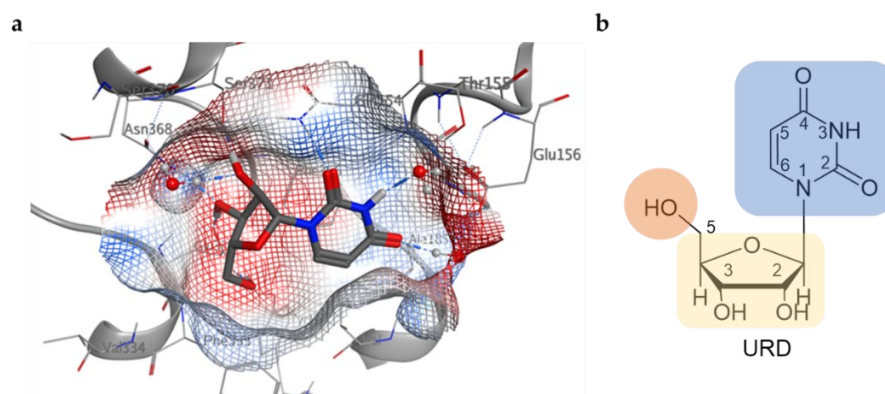


**Figure 3.5.** (a) View of uridine inside binding pocket in electrostatic potential surface representation. (b) 2D structure of uridine.

These data suggest that the optimal position to make changes to the uridine is the glycosidic hydroxyl in C (5'). In fact, both for steric hindrances (Figure 3.5 a) and for molecular recognition, a modification in C (5') is the only solution for the synthesis of prodrugs conjugated to uridine. Moreover, the possibility of rotation around the C–O bond would allow a smaller steric hindrance of the conjugated drug.

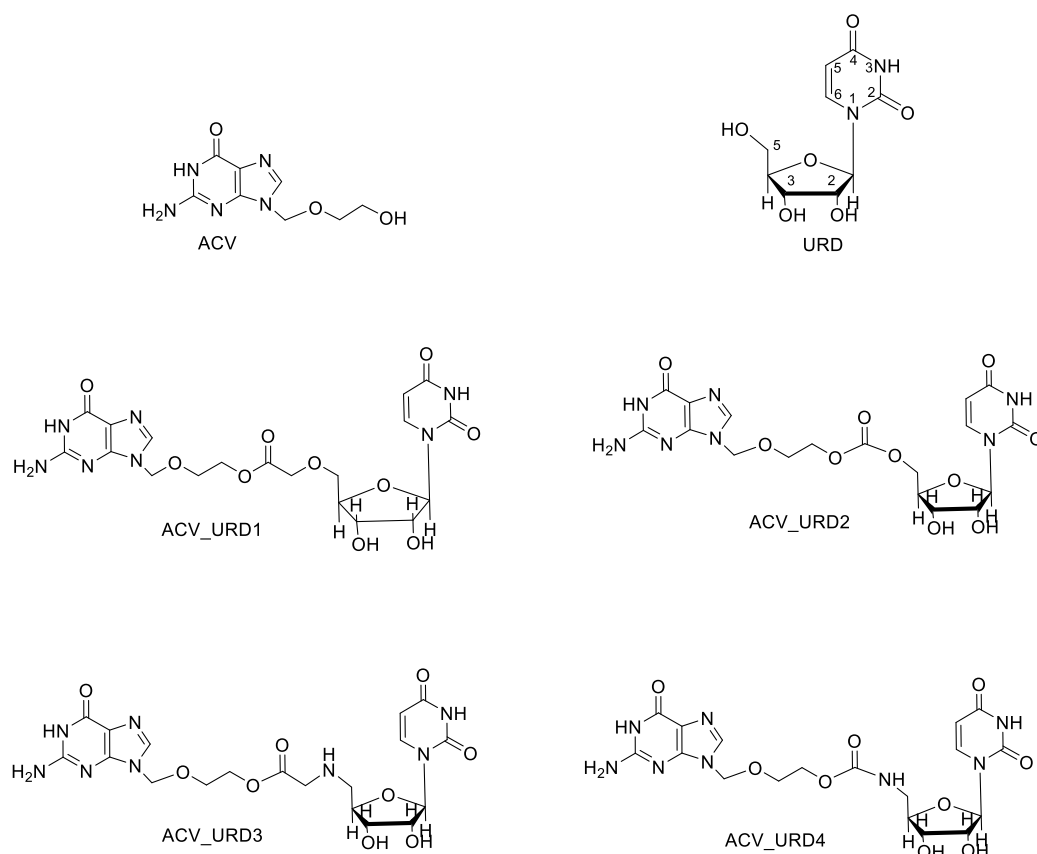


**Figure 3.6.** Structures of novel designed ACV prodrugs.

To avoid that ACV could interact with the vcCNT binding site's external area, we used small spacers, one and two carbon atoms. To prepare a prodrug containing both ACV and URD, the two reference prodrugs ACV\_URD1 and ACV\_URD3 were designed (Figure 3.6). The functional groups to bind drug and promoiety are ester in the first case and carbonate in ACV\_URD3. Both functional groups should resume the parent drug ACV from the esterases and carboxylesterases present in the ocular tissues.

The different functional groups used to combine drug and promoiety will be used to evaluate the stability of the prodrugs both in the cellular environment and in ophthalmic formulations. Furthermore, the different lengths of the spacer could provide useful suggestions in the interaction between the prodrug-transporter.

The logP calculated for the ACV\_URD1 and ACV\_URD3 derivatives with respect to ACV are very similar; therefore, to increase the lipophilicity of the carbamate derivative, the hydroxyl groups in positions C (2') and C (3') have been acetylated. Increased logP for ACV\_URD3 should promote better corneal permeability. In the ideal case, the ester functional group should be more susceptible to hydrolysis than the carbonate, restoring the essential hydroxyl functionalities of the interactions with the nucleoside binding site.

The hydrogen bonds between the -OH group in C (5') and the residue Glu332 is fundamental for the transportability of the nucleoside substrates in CNT2 with respect to CNT1 and CNT3. To restore this interaction, we decided to convert the hydroxyl group to C (5') into amine. In this case, as it is possible to see from the laying of the molecular docking, the hydrogen bond with the residue Glu332 has been reprinted. We believe it is interesting to study the interactions between Urd derivatives and the binding site of the CNT family.

Consequently, derivatives ACV\_URD2, ACV\_URD4, and ACV\_URD6 were prepared (Figure 3.6).

This approach, never used for an ophthalmic drug, has some advantages:

1. Increases the lipophilic character of the drug by favor corneal permeability.
  2. Increases the degree of specific receptor molecular recognition.
-

3. After enzymatic activation in the ocular tissue, the drug is released spontaneously and irreversibly.
4. Possibility of combining different types of transporter suitable for ocular tissue.
5. Possibility of changing the lipophilicity of the final prodrug, derivatizing the glycosidic hydroxyls.
6. Understanding the interactions between nucleoside derivatives and binding site of vcCNT transporters.

### 3.7 COMPUTATIONAL APPROACH FOR DRUG-CNT TRANSPORTER SYSTEMS

Computer-aided molecular design is an important aspect of drug design and discovery. Computational studies were performed with vcCNT from *Vibrio cholerae* (ID PDB: 4PD6).<sup>124</sup> This approach has allowed us to evaluate the stability of the interactions between the reference prodrug (ACV\_URD1) and the recognition site of the transporter vcCNT.

The AutoDock 4.2.5.1 software (v. 1.1.2, Molecular Graphics Lab at The Scripps Research Institute, La Jolla, California)<sup>132</sup> was used for all docking studies.

**Table 3.1.** Calculated binding energies (kcal/mol) and  $K_D$  (nM) calculated for the binding sites of vcCNT transporter for uridin, BST and BS ACV\_URD 1-4

Ligand	Calcd $\Delta G$	Calcd $K_d$ ( $\mu M$ )
URD	-7.8	1.9
ACV_URD1	-8.1	1.2
ACV_URD2	-8.1	1.2
ACV_URD3	-8.3	0.8
ACV_URD4	-8.2	1.0

Aligning the lower energy docked pose with the crystallized ligand pose of the crystallized ligand for the 4PD6 X-ray structure (RMSD = 0.11 Å) confirmed the accuracy of the docking algorithm. The values of the binding energies of prodrugs are very similar to uridine; ACV\_URD3 and ACV\_URD4 have slightly lower energies,  $-8.3$  kcal/mol and  $-8.2$  kcal/mol, respectively (Table 3.1), due to the hydrogen bond between the amine and amide nitrogen with Glu332.

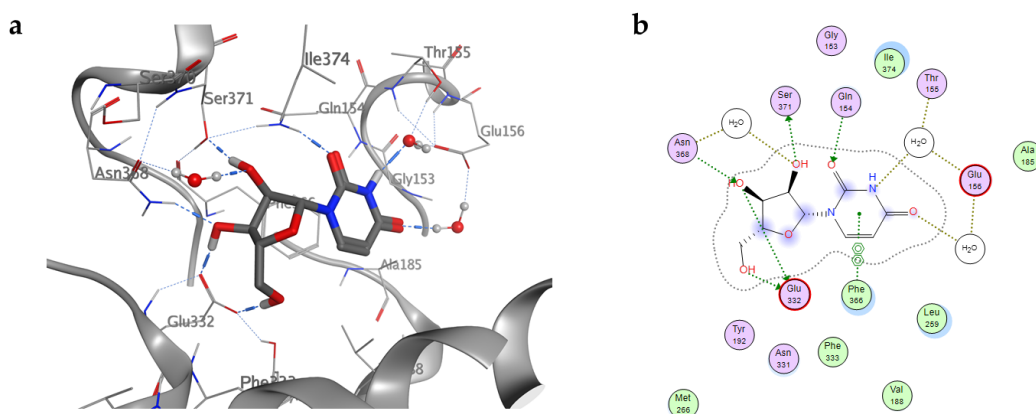


**Figure 3.7.** (a) 3D interaction profile of uridine in the crystallized structure. (b) 2D profile of interaction.

The good energy binding value obtained from molecular Docking ( $-7.8$  kcal/mol) is mainly due to the interaction between the uridine and the binding site (Figure 6.4 a, b). The nucleoside-binding site is located at the center of the internal two-fold symmetry and lined by the tips of HP1 and HP2 and the unwound regions of TM4 and TM7 (Figure 3.7). Inspection of the interactions between uridine and the binding site shows that many polar or charged amino acids from HP1, HP2, TM4 and TM7 interact with the uracil base and ribose. HP1 and TM4b are responsible for interacting with the uracil base. Infact, the side chains of Gln154, Thr155, and Glu156 from HP1 interact with the uracil base either directly (Gln154) or indirectly through a water molecule (Thr155 and Glu156; Figure 6.4 b). Val188 from

TM4b interacts with the uracil base employing van der Waals interactions. The residue corresponding to Gln154, together with that corresponding to Val 188, is essential for CNT's nucleoside specificity; Glu156 is critical for Na<sup>+</sup>-nucleoside coupled transport. HP2 and TM7 are responsible for the interactions with ribose. The side chains of Glu332 (HP2), Asn368 (TM7) and Ser 371 (TM7) interact with the ribose either directly (Glu 332, Asn 368 and Ser 371) or indirectly through a water molecule (Asn 368).

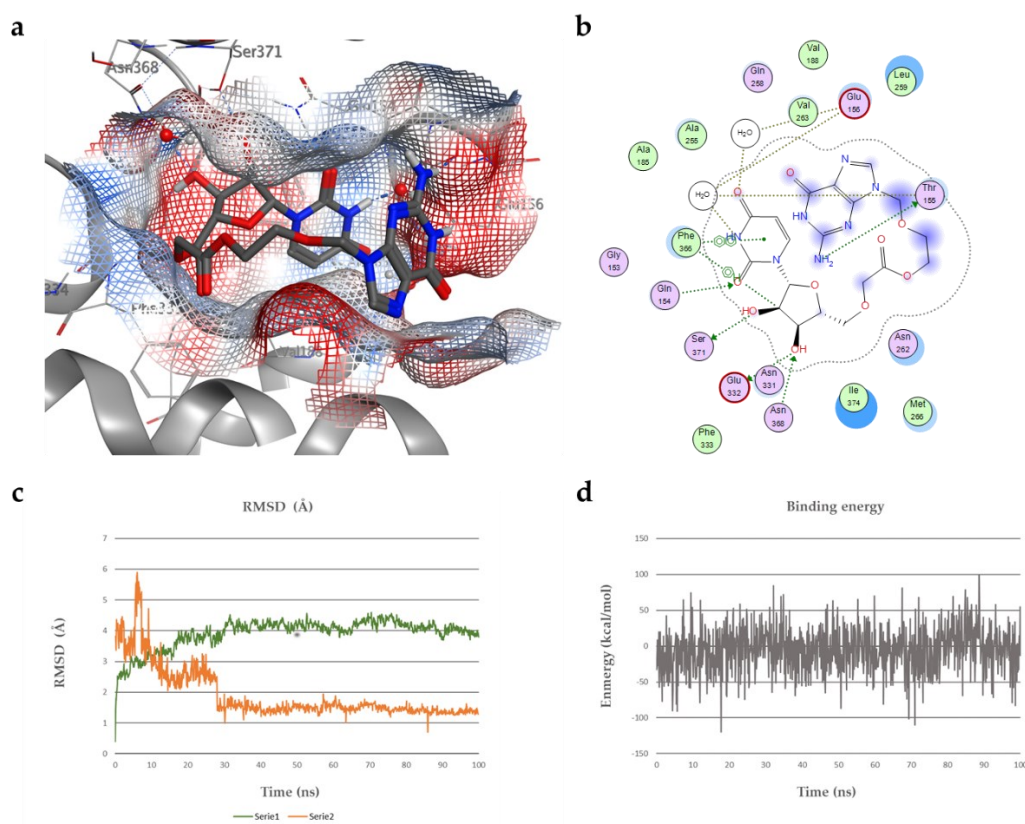


**Figure 3.8.** Docking binding pose (a) and Interaction (b) inside the binding pocket of the protein. RMSDs (c) and energy of binding (d) and protein and its complexes with ACV\_URD1 ligand.

A docked analysis of ACV\_URD1 shows that the uridine portion fits inside the binding pocket, maintaining interactions with all key residues for molecular recognition. The small spacer that allows uridine-ACV conjugation shows weak hydrophobic interactions with the Leu259 residue.

Fortunately, the nucleoside region of ACV is positioned outside the nucleoside-binding cavity, showing only an electrostatic interaction with the residue Gln258.

Trajectory analysis shows that the hydrogen bonds between the uridine and the polar residues of the binding site (Gln154, Glu156, Glu332) are stable for all 100 ns of MD simulation, with a mean binding value of 1.87 Å.

RMSD of the protein (Figure 3.8c) increases up to 30 ns, reaching stability throughout the MD simulation, demonstrating that the prodrug ACV\_URD1 does not influence the interactions between the protein residues, keeping the tertiary structure of the protein itself and the quaternary of the entire trimeric system stable. The ligand stabilizes after 30 ns maintaining an average RMSD of 1.6 Å redocking (-8.2 kcal/mol) performed after the 100 ns of MD simulation highlights the protein-substrate complex stability. The acylguanosine portion shows a slight fluctuation outside the cavity, probably due to the lack of interactions with the TM6 portion of vCNT. Furthermore, the binding energy also does not show significant fluctuations during the simulation (Figure 3.8c). The DCCM plots of ACV\_URD1 and the protein show an overall slight increase in anti-correlated motions around the TM6 domain (Figure 5.10), probably caused by the interaction with the acyclovir fraction. The lower flexibility of the spacer in ACV\_URD2 slightly reduced anti-correlated movements in TM6. The docked pose is very similar to ACV\_URD1, with the drug exposed at the top of the binding pocket. Both prodrugs show a folding to form a sort of horseshoe (Figure 3.7a). This conformation remains stable throughout the dynamics, allowing a lower fluctuation of the RMSD of ACV\_URD2 during the simulation.

---



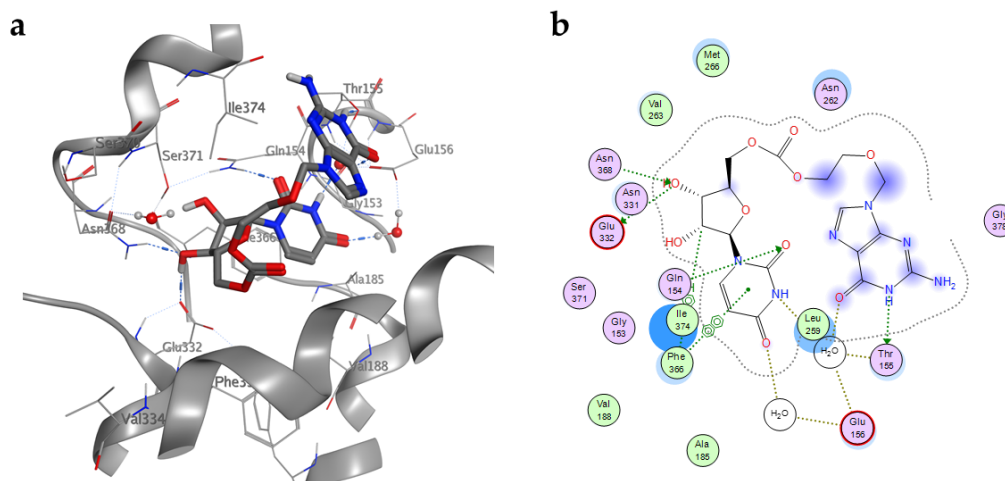
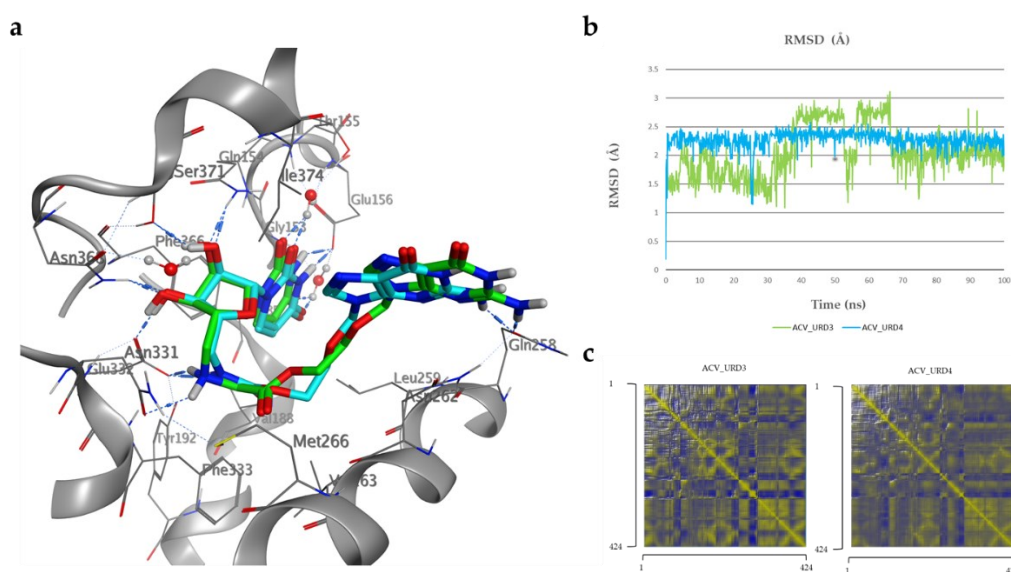


**Figure 3.9** (a) Interaction profile of the best-docked poses for compound ACV\_URD2 (stick model) and (b) binding site interactions.

ACV\_URD3 and ACV\_URD4, amino and amide derivatives in C5 'of the ribose ring, restored the hydrogen bond with Glu335 at 1.73 and 1.81 Å, respectively (Figure 3.9). Docked laying is similar between the two prodrugs. The purine fraction of ACV interacts via H-bond with Gln258 at 1.9 and 2.0 Å, ACV\_URD3 and ACV\_URD4, respectively. The amino acid residues that interact with the nitrogenous base in the vcCNT structure (Gln154, Glu156, Glu 332, Asn 368, and Ser 371) mirror the same interactions as uridine, suggesting good recognition within the binding site.



---

**Figure 3.10** (a) Interaction profile of the best-docked poses for compounds ACV\_URD3 (green stick model) and ACV\_URD4 (cyan stick model). (b) RMSD ligands during MD simulation. (c) . Dynamic cross-correlation matrix of ligands 1–4. The DCCM is visualized with colors ranging from blue (-1, fully anti-correlated) to yellow (+1, fully correlated).

The average RMSD value of ACV\_URD4 reaches a plateau in the first ns of simulation and remains stable for the entire duration, while ACV\_URD3, despite a lower average RMSD in constant values, undergoes moderate fluctuations, especially from 30 to 70 ns (Figure 3.10b). Correlation analysis in both prodrugs revealed that several residues moved in a concerted fashion, except that negative correlations were recorded in some domains. In particular, the domain of TM6 records anti-correlated movements, especially for ACV\_URD3 (Figure 3.10c). The RMSF graphs also confirm a lower residual fluctuation between 70–100, while high values are recorded between 270–300, *i.e.*, in the TM6 region.

Although all prodrugs had good stability within the uridine binding site, some derivatives moderately influenced some vcCNT transporter domains. Comparing the RMSF and DCCC data of all four prodrugs reveals that the changes in IH1 and TM6 in vcCNT are coupled to fundamental structural changes in the trimerization contacts.

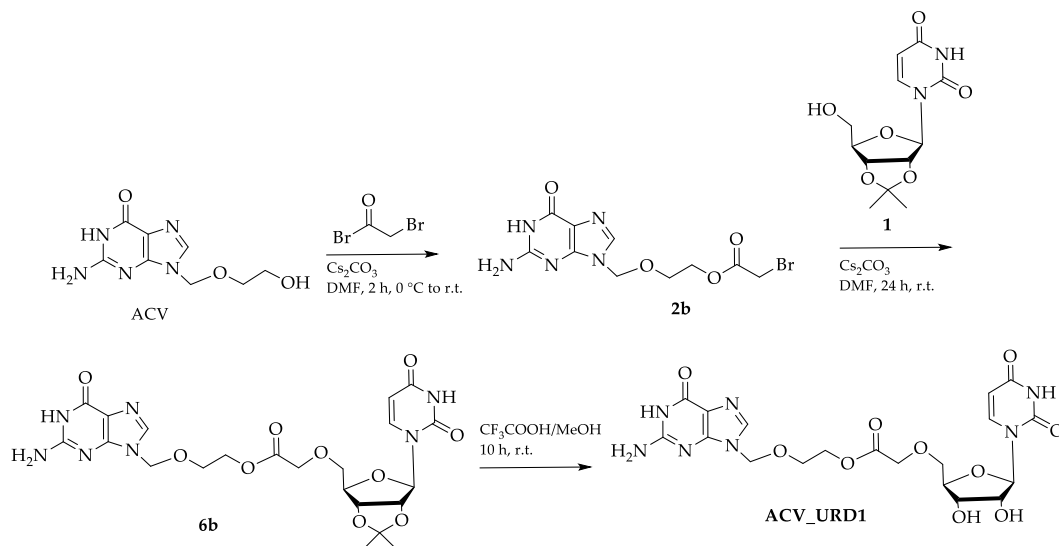
While IH1 is a 40 Å long amphipathic helix that is most likely located at the water/membrane interface, TM6 is about 60 Å long and almost 60° inclined with respect to the membrane responsible for contacts with prodrugs. Likely, TM6-prodrug interactions cause structural changes in the 247–250 and 268–298 traits that result in negative correlations in IH1.

This complex analysis of the trajectory of the MD simulation demonstrates good general stability of the vcCNT-ACV\_URD4 complex, with a low anti-

---

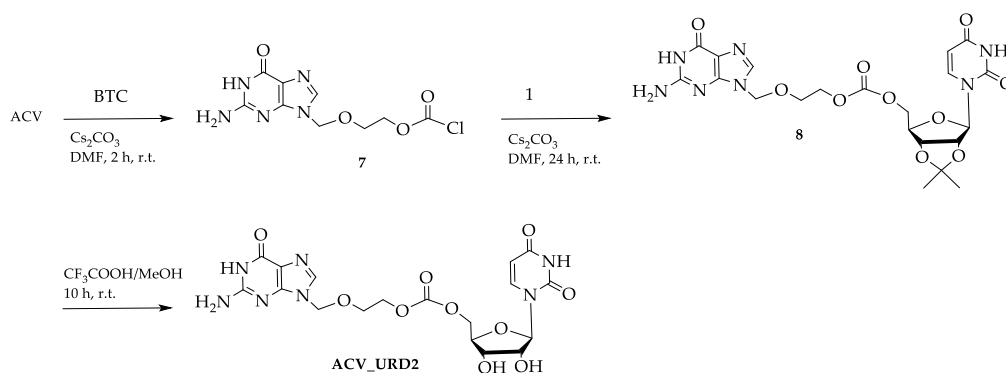
correlation between the domains responsible for extracellular contact and the domain of the substrate-binding site (HP1 and TM4b).

### 3.8 SYNTHESIS OF THE NEW ACYCLOVIR PRODRUGS



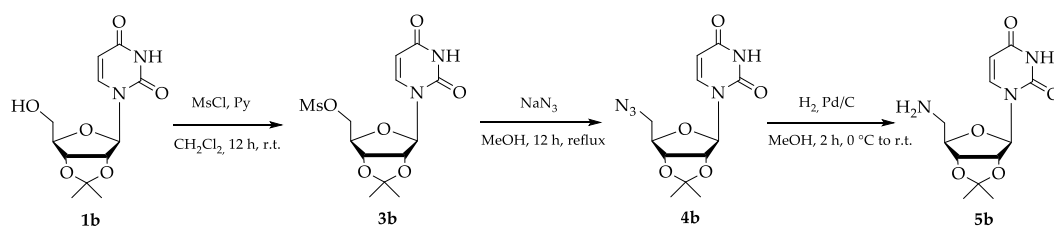
**Scheme 3.1**

2-Bromoacetate derivate **2b** is prepared by acetylation starting from ACV by reaction with 2-bromoacetyl bromide in the presence of cesium carbonate. Compound **2b** by nucleophilic substitution with intermediate **1** leads to the formation of compound **6b**. Deprotection of the acetal group of compound **6b** in the presence of trifluoroacetic acid generates the final prodrug ACV\_URD1.



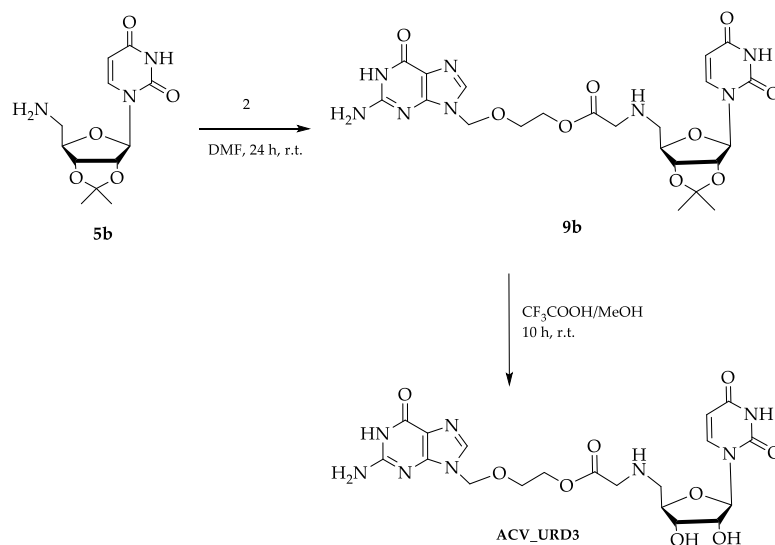
**Scheme 3.2**

ACV by reaction with triphosgene in a basic environment leads to the synthesis of carbonochloridate **7**, which is reacted with compound **1** to give carbonate **8**. The deprotection of the hydroxyl groups in positions C (2') and C (3') respectively, in an acid environment, leads to the prodrug ACV\_URD2.



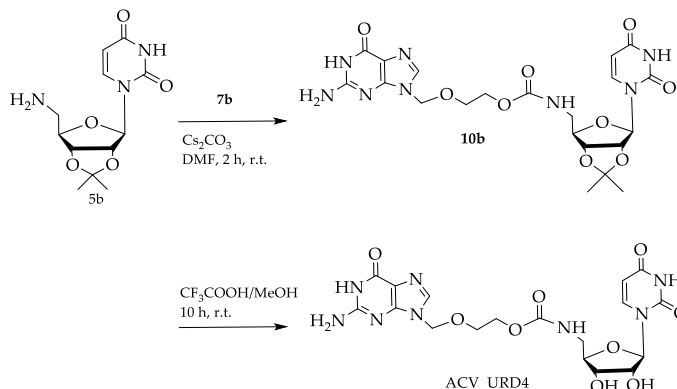
**Scheme 3.3**

For the obtaining of the final prodrugs, for simplicity, we report the synthesis of intermediates. Compound **1** is mesylated in position 5 by reaction with the mesyl chloride in the presence of pyridine. Subsequently, intermediate **4** is generated by nucleophilic substitution with sodium azide in MeOH. By reduction with  $\text{H}_2$  in the presence of  $\text{Pd/C}$ , the latter leads to the formation of the amino group in position 5 of the compound **5**.



**Scheme 3.4**

By the reaction of the amino derivative **5** with the derivative 2-bromoacetate **2** the compound **9** is obtained. Subsequently, deprotection leads to the formation of the final prodrug **ACV\_URD3**.



**Scheme 3.5**

The amine derivative **5** reacts with the carbonochloridate **7** to form the carbamate **10**. The latter by deprotection of hydroxyl groups leads to the formation of the prodrug **ACV\_URD4**.

### 3.9 CONCLUSIONS AND OBJECTIVES

Nucleosides play essential roles in cell homeostasis, functioning as signaling molecules and nucleotide precursors. Although in mammals, nucleosides can be synthesized *de novo* or *via* a salvage pathway, many human cells cannot synthesize them *via* the *de novo* biosynthetic pathway. Therefore, to achieve nucleoside homeostasis, the nucleoside transporter facilitated nucleoside salvage pathway is of great importance.<sup>133</sup>

To date, nucleoside transporters have not been considered for the transport of drug-nucleotide conjugates into cells. Despite the high selectivity of CNT and ENT it has been shown that dependent  $\text{Na}^+$  systems can transport molecules structurally very different from nucleosides, such as anthracycline pirarubicin<sup>134</sup>. Furthermore, it has been shown that in both

systems (CNT and ETN) there are considerable differences in transportability in nucleoside derivatives. The new prodrugs synthesized represents a valid alternative to the drugs currently present in the ophthalmic field. This project identifies in transporter CNTs a targeted strategy for delivering drugs inside cells and in targeted organs. In-depth computational studies have highlighted exciting ideas for the rational design of prodrugs recognized by CNTs, providing mechanistic insights into uridine-drug reuptake. Indeed, this is the first molecular modeling study applied to family CNTs. Unfortunately, the COVID-19 pandemic has slowed down both the in vivo experiments on cell lines to prove the new synthesized prodrugs' uptake and the ophthalmic formulation tests.

---

---

## CHAPTER 4 SIGMA-1 RECEPTORS IN OCULAR PATHOLOGIES

### 4.1 INTRODUCTION

Initially mistaken for a subtype of opioid receptors, sigma receptors ( $\sigma$ ) are now considered enigmatic and distinct receptor classes. Despite its increasing importance in human physiology and disease, the molecular architecture of the  $\sigma_1$  receptor and mechanisms of action remain, in some aspects, unanswered.<sup>135,136</sup> Widely distributed in the central nervous system, and also found in peripheral tissues including liver, kidney, heart, eye, and endocrine, immune and reproductive tissue;<sup>137,138</sup> furthermore,  $\sigma$  receptors were over-expressed in several tumor cell lines.<sup>139,140</sup> They consist of two subtypes, the sigma 1 ( $\sigma_1$ ) and the sigma 2 ( $\sigma_2$ ) receptor, which can be distinguished by molecular weight, tissue distribution, and ligand binding profile, pharmacology, and activation mechanisms.<sup>141</sup> The  $\sigma_1$  receptor is an enigmatic mammalian transmembrane protein implicated in drug addiction, depression, neuropathic pain, and neurological disorders, including Alzheimer's and Parkinson's diseases, and recently, amyotrophic lateral sclerosis. Generally defined as a chaperone protein, residing specifically at the endoplasmic reticulum (ER) mitochondrion interface called the MAM (mitochondrion-associated ER membrane),<sup>142</sup> the cloning of the  $\sigma_1$  receptor in the 1990s established that it is an evolutionary separate with no appreciable similarity to any other. Lately, the matter was settled by its crystallization.

Macular degeneration, glaucoma, retinitis pigmentosa diabetic senile and retinopathy are characterized by the progressive loss of retinal neurons that could lead to blindness.  $\sigma_1$  receptors were detected in different cell types in the eye using RT-PCR and immunoblotting, with supporting

---

immunohistochemical data from retinal pigment epithelium (RPE) cells, retinal ganglion cells (RGCs),<sup>143</sup> and segments internal photoreceptors.<sup>144</sup> Furthermore, common mechanistic defects in retinal degeneration include oxidative stress, increased inflammation, and activation of apoptotic signaling pathways. Glial cells play an important role and are sensitive to the intervention of  $\sigma_1$  receptor agonists.<sup>145</sup>

Many studies have shown that  $\sigma_1$  receptor agonists can decrease RGC apoptosis in some clinically important in vitro and in vivo models. The selective  $\sigma_1$  (+) - pentazocine receptor has been most commonly used and has been shown to slow homocysteine and glutamate-induced excitotoxic cell death,<sup>146,147</sup> and stress apoptosis oxidative in primary RGCs and RGC-5 cells. In addition to (+)-pentazocine, other  $\sigma_1$  receptor agonists such as (+)-SKF10,047 and SA4503 can also confer protection to retinal cells.<sup>148</sup> Consistent with the specific biological and physiological functions of the  $\sigma_1$  receptor in these processes,  $\sigma_1$  receptor antagonists such as NE-100 and BD1047 attenuated the agonists' protective effects.<sup>149</sup> The mechanisms by which agonists can decrease apoptosis in these in vitro models include modulation of some molecular targets, including caspase-3, intracellular calcium, caspase-9, modification of the expression levels of FasL, Bax and TRAIL and stress response proteins (IRE1, ATF4, ATF6, CHOP, PERK).

The  $\sigma_1$  receptor agonist PRE084 was administered intraperitoneally to rats just before ischemia and also immediately after reperfusion.<sup>1</sup> Pretreatment with the  $\sigma_1$  receptor antagonist BD1047 prevented the protective effects of these sigma agonists.<sup>150</sup> Intravitreal administration of PRE084 before A $\beta$  injection reduced retinal damage by increasing the level of Bax and phosphorylated JNK, all attenuated by co-administration of the antagonist BD1047.<sup>151</sup>

---



Effects of (+) - pentazocine were observed on retinal microglia isolated from rat pups, as well as effects on retinal neurons. Inflammation, induced using lipopolysaccharide (LPS) in order to alter cell morphology without affecting the expression of the  $\sigma_1$  receptor and cell viability.<sup>152</sup> (+) - Pentazocine mitigated intracellular and LPS-induced ROS and NO formation, as well as release of pro-inflammatory cytokines, including tumor necrosis factor- $\alpha$ , IL-10 and MCP-1.<sup>152</sup> (+)-Pentazocine also inhibited LPS-induced ERK and JNK phosphorylation, suggesting that it may confer these protective effects through modulation of the mitogen-activated protein kinase (MAPK) signaling pathway. The  $\sigma_1$  receptor antagonist BD1063 prevented the protective effects conferred by (+)-pentazocine,<sup>152</sup> confirming the  $\sigma_1$  receptor specificity of these effects. These results suggest that the protective effects of  $\sigma_1$  receptor agonists in the retina may involve modulation of glial responses in addition to effects on neurons.

#### 4.2 CRYSTAL STRUCTURE AND BINDING SITE

Schmidt et al. published for the first time the crystal structure of the human  $\sigma_1$  receptor complexed with two chemically different ligands (a high-affinity antagonist PD144418 and either agonist or inverse agonist 4-IBP).<sup>153</sup> The receptor crystallized as a trimer, and each protomer, including four  $\alpha$ -helices each, exhibits a fold including a single transmembrane domain (Figure 4a), divergent from the main models of a two-pass transmembrane architecture. Each of the three promoters' cytosolic domain shows  $\beta$ -barrel fold with the ligand-binding site buried at its center. This large, hydrophobic ligand-binding cavity shows remarkable plasticity in ligand recognition.<sup>154</sup>

---

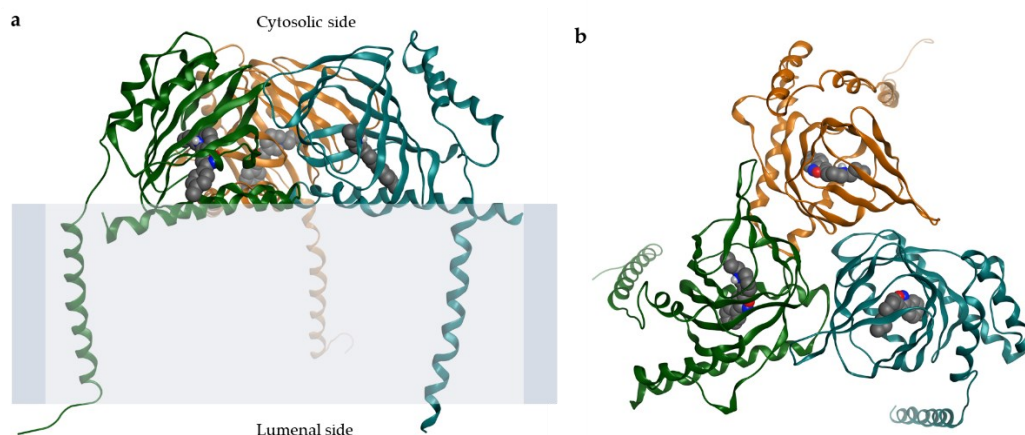


**Figure 4.1.** (a) Cartoon representation for the  $\sigma_1$  receptor trimer (ID PDB: 5HK1) viewed parallel to the membrane. The putative membrane bilayer is indicated with grey boxes. (b) Cartoon representation of the  $\sigma_1$  receptor trimer viewed from the cytosolic side. Individual protomers are colored cyan, orange, and green.

The carboxy (C)-terminal domains adjacent to the membrane mediate the receptor's trimeric structure, packing tightly together with an interface of  $\sim 9,300 \text{ \AA}^2$  between each adjacent pair of protomers. In contrast, the three transmembrane helices are widely separated from each other, located at each corner of the triangular trimer, where they mediate the lattice contacts (Figure 4b). The cytosolic domain of each of the three protomers shows a  $\beta$ -barrel fold with the ligand in the center, flanked by four  $\alpha$ -helices. The ligand-binding domain is highly conserved in sequence between species, as is the intermolecular interface between the three protomers. The proximal side of the membrane of the cytosolic domains is a too flat hydrophobic surface, which is probably embedded in the plane of the membrane.

#### 4.3 NITRIC OXIDE (NO): A POTENTIAL ENEMY AGAINST GLAUCOMA

NO is an endogenous messenger synthesized from nitric oxide synthase (NAS). It is a potent vasodilator and physiologically regulates blood pressure. In vascular beds throughout the body, NO mediates the vasodilation caused by the autonomic nervous system's parasympathetic

component. Besides, many vascular beds are innervated by nitrergic nerves that release NO to cause vasodilation, for example, in the choroid.<sup>155</sup>

NO mediates IOP maintenance and controls basal ocular vascular tone by activating the sGC signaling pathway. Due to this, a hybrid drug design strategy was used to design scaffolds via the fusion of antiglaucoma scaffolds with NO donor fractions. The hybrid drug design in this context has been widely used to design the NO donor derivative of the prostaglandin analogs (PGF $2\alpha$ ), which are most frequently used for IOP lowering. These hybrid scaffolds induce a significant reduction in IOP through the concomitant activation of two independent mechanisms: prostaglandin F (FP) receptor activation and sGC/cGMP stimulation in target tissues. The increased NO-induced vasodilation, antiplatelet activity, and anti-inflammatory effects are critical to the success of this class of drugs.<sup>156</sup> In addition to the NO-donor derivative of prostaglandin analogs (PGF $2\alpha$ ), research has also begun to develop a NO donor derivative of phosphodiesterase-5 (PDE5) inhibitor as future generation NO donors.<sup>156</sup> This section will discuss updates on the FDA-approved NO donor analog PGF $2\alpha$  and hybrid scaffolds submitted to clinical and preclinical investigations.

Vyzulta (latanoprostene bunod ophthalmic solution, 0.024%, LBN) is the most recent example of an analog of NO donor PGF $2\alpha$  (Figure 9), which exemplifies the success of this hybrid drug design strategy. Vyzulta was discovered by Nicox and later licensed by Bausch&Lomb. The FDA approved the ophthalmic solution in November 2017 for lowering IOP in patients with OAG and OHTN. This antiglaucoma drug is one of the first new glaucoma drops to hit the market in 20 years with a dual-action approach. LBN undergoes rapid in situ metabolism by esterases and releases latanoprost acid and butanediol mononitrate, which further

---

metabolizes to 1,4-butanediol and NO, leading to simultaneous activation of FP receptors and the NO / soluble GC / cGMP signaling pathway

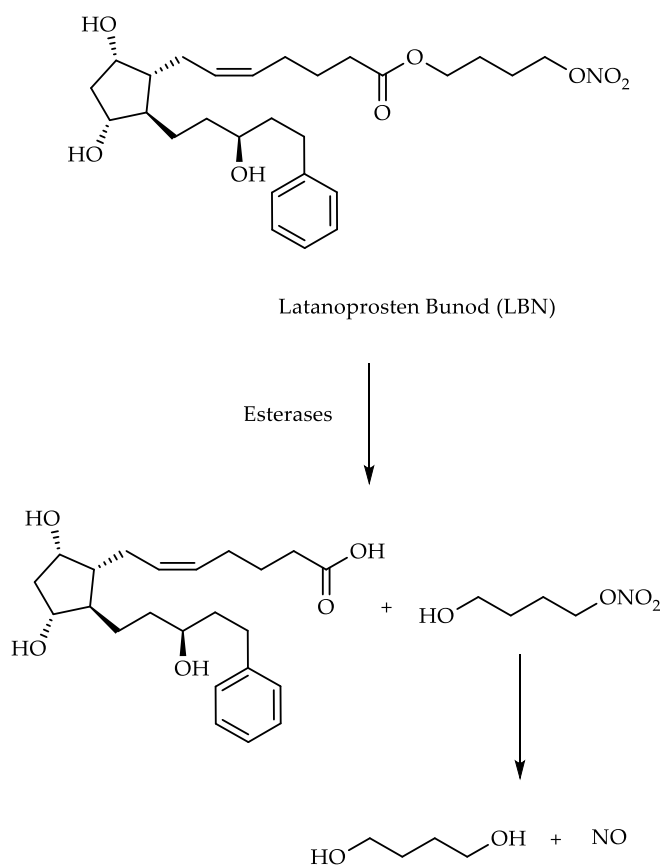


**Figure 4.2.** Latanoprost Bunod bioactivation mechanism.

This increases both uveoscleral and conventional outflow, causing a significant lowering of the IOP. Initial preclinical studies by Krauss et al. revealed that LBN demonstrated effective control of IOP in laser-induced OHTN cynomolgus monkeys and attenuated the hypertensive response to intravitreal injection of hypertonic saline in a rabbit model of transient OHTN along with a rapid decrease in IOP. LBN also exerted potent stimulation of the sGC signaling pathway in human PC12 cells and HEK293 cells. Overall, the results indicated that LBN possessed more significant IOP-lowering activity than latanoprost, possibly due to concomitant NO and latanoprost acid contribution. The results were further supported by

the favorable outcome of several clinical studies that demonstrated a greater IOP reduction potential of LBN than latanoprost.

Other PGF<sub>2</sub> $\alpha$  analog NO donors were synthesized. In 2010 Borghi et al. designed NCX-125 (Figure 4.3), an analog of NO donor latanoprost. The double-acting compound was synthesized using EDC-mediated amide coupling between 2-hydroxypropan-1,3-diyl dinitrate and latanoprost free acid. NCX-125 demonstrated significantly higher IOP reduction potential in rabbit, dog, and non-human primate models compared to latanoprost. It induced inhibition of NO-dependent iNOS ( $IC_{50} = 55 \pm 11 \mu\text{M}$ ) in RAW macrophages. Furthermore, anti-inflammatory activity was also exhibited by NCX-125, indicating its therapeutic utility in glaucoma.

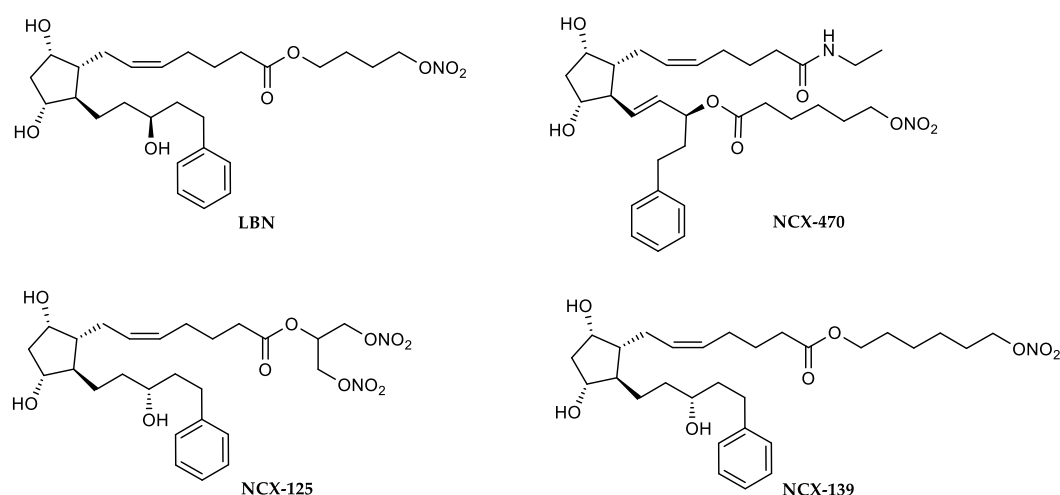


**Figure 4.3.** LBN and NO derivatives of prostaglandins.

Studies were also conducted on NCX-139 (Figure 9), another analog consisting of latanoprost amide and a NO donor fraction. The result of the study demonstrated the remarkable IOP lowering activity of NCX-139 in glaucomatous dogs and OHTN rabbits. Furthermore, NCX-139 showed a NO-mediated vascular relaxant effect, together with the shift of 3H-PGF<sub>2</sub> $\alpha$  binding on recombinant human FP receptors, demonstrating a double action: NO/cGMP signaling and FP receptor.

NCX 470, an analog of the NO donor bimatoprost (Figure 4.3), is currently in clinical development by NICOX. The chemical architecture of NCX-470 consists of an esterified hydroxyl group (position 15) with a donor fraction of NO [6-(nitroso)hexanoic acid]. In preclinical studies, NCX-470 demonstrated IOP-lowering activity in transient OHTN rabbits and exerted a more significant reduction in IOP (NCX 470, 0.042%) than bimatoprost (0.03%) in normotensive ocular dogs (ONT) and laser-induced OHTN in non-human primates. Overall, NCX-470 demonstrated more significant IOP reduction (up to 3.5 mmHg) than bimatoprost in head-to-head comparisons, as evidenced by the results of non-clinical drug studies conducted on animal models of glaucoma and OHTN. Recently, Nicox announced enrolment in the Phase 2 study of NCX-470 to determine the appropriate dose for the transition to Phase 3 studies.

#### 4.4 SIGMA RECEPTOR LIGANDS DONATING NITRIC OXIDE

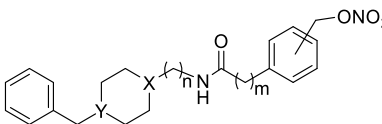
Recent developments on NO donor drugs and the discovery of the physiological role of SR1 have been designed and synthesized SR1 ligands capable of releasing NO.

The design and development of new potent and selective  $\sigma_1$  ligands are essential for medicinal chemistry.<sup>157</sup> They enclose few standard features for the selective binding with  $\sigma_1$  receptor: (i) the two aromatic rings, involved in hydrophobic interactions, (ii) the amide oxygen atom, which can accept a hydrogen bond from a donor residue of the receptor, and (iii) the piperidine nitrogen atom, which coordinates the positive ionizable residue in the binding site. Moreover, it was shown that Glu172, hydrogen-bonded by the protonated ligand's amine group, and Asp126, which produces an intramolecular hydrogen bond with Glu172 instead of interacting with the ligand, are essential for the ligand binding.

---

In the 4-benzylpiperidine compound series (**9–16**), the meta-substituted compound **9** showed an affinity for the  $\sigma_1$  receptor with a  $K_i$  value of 49 nM and 330 nM for the  $\sigma_2$  receptor. Elongation to the three-carbon aliphatic chain (**10**) increased the affinity of the  $\sigma_2$  receptor by more than 3 times with a  $K_i \sigma_1$  value of 64 nM and  $K_i \sigma_2$  of 93 nM. A good affinity for the  $\sigma_2$  receptor was also maintained in compound **11** with a  $K_i$  value of 75 nM, although in the chain of four carbon atoms, the affinity of the  $\sigma_1$  receptor (148 nM) is reduced. Further elongation of the five-carbon chain restores the preferential affinity of the  $\sigma_1$  receptor with a  $K_i$  value of 50 nM with respect to the  $\sigma_2$  receptor ( $K_i$  value of 142 nM).

**Table 4.1.**  $\sigma_1$  and  $\sigma_2$  Binding Assays for Compounds 9–20.



Compound	X	Y	n	m	Substitution	$K_i$ (nM) $\pm$ SD <sup>a</sup>	
						$\sigma_1$	$\sigma_2$
<b>9</b>	N	CH	2	0	meta	49 $\pm$ 1	330 $\pm$ 9
<b>10</b>	N	CH	3	0	meta	64 $\pm$ 0.7	93 $\pm$ 3
<b>11</b>	N	CH	4	0	meta	148 $\pm$ 1	75 $\pm$ 2
<b>12</b>	N	CH	5	0	meta	50 $\pm$ 0.9	142 $\pm$ 13
<b>13</b>	N	CH	2	0	para	89 $\pm$ 2	2,673 $\pm$ 44
<b>14</b>	N	CH	3	0	para	145 $\pm$ 12	230 $\pm$ 18
<b>15</b>	N	CH	4	0	para	250 $\pm$ 9	89 $\pm$ 2
<b>16</b>	N	CH	5	0	para	93 $\pm$ 2	70 $\pm$ 3
<b>17</b>	CH	N	0	0	Meta	24 $\pm$ 0.6	19 $\pm$ 0.2
<b>18</b>	CH	N	0	1	Meta	19 $\pm$ 1	320 $\pm$ 4
<b>19</b>	CH	N	0	0	Para	22 $\pm$ 0.8	270 $\pm$ 5
<b>20</b>	CH	N	0	1	Para	170 $\pm$ 6	2,514 $\pm$ 24
Haloperidol						2.5 $\pm$ 0.4	16 $\pm$ 2
(+)-Pentazocine						4.7 $\pm$ 0.7	1,465 $\pm$ 224
DTG						ND <sup>b</sup>	18 $\pm$ 1

Para substitution of the nitrate group yields compounds with generally lower affinities than both receptor subtypes. An improvement in the affinity of the  $\sigma_2$  receptor is observed with the elongation of the aliphatic linker. Indeed, compound **13** has  $K_i \sigma_2$  of 2673 nM, while compound **16** has  $K_i \sigma_2$  of 70 nM. Compounds **9–16** show fluctuating behavior with affinities ranging

from 89 nM for compound **13** to 249 nM for derivative **15**. Compounds with 1-benzylpiperidine-4-amine fraction (**17–20**) have good affinities towards  $\sigma_1$  receptor and a lower general affinity to the  $\sigma_2$  receptor. Compounds **17–19** have a  $\sigma_1$  receptor affinity in low two nM digits ( $K_i \sigma_1$  of 24, 19, and 22 nM, respectively). The other compounds show a lower affinity with  $\sigma_2$  receptor, leading to >10-fold selectivity with respect to the  $\sigma_1$  receptor. A docking study was conducted to identify and study the key molecular interactions involved in receptor/ligand recognition. The crystal structure of the  $\sigma_1$  receptor PD144418 (PDB code 5HK1) has an occluded and elongated binding cavity similar to a  $\beta$ -barrel, with the highly conserved Glu172 amino acid residue located near the center of the cavity, forming a salt bridge with ligands. Since all compounds have a tertiary amine, we performed the study considering the *N*-protonated structures (pH = 7.4). Therefore, the salt bridge formation was used as a filter to identify and choose docking poses. The calculated free energies of binding ( $\Delta G$ ) and  $K_i$  values at the catalytic site of the  $\sigma_1$  receptor for compounds **9–20** and haloperidol are shown in Table 4.2.

**Table 4.2.** Calculated Binding Energies (kcal/mol) and Binding Constants  $K_i$  (nM) for the Binding Sites of  $\sigma_1$  and  $\sigma_2$  Receptors for Compounds **9–20**.

Compound	Calcd $\Delta G \sigma_1$	Calcd $K_i \sigma_1$	Exp $K_i \sigma_1$	Calcd $\Delta G \sigma_2$	Calcd $K_i \sigma_2$	Exp $K_i \sigma_2$
<b>9</b>	-9.96	49.61	49.3	-8.81	345.91	330.4
<b>10</b>	-9.83	61.79	63.8	-9.68	79.60	93.0
<b>11</b>	-9.20	179.20	148.1	-9.49	109.71	75.5
<b>12</b>	-10.27	29.39	50.4	-9.19	182.08	142.2
<b>13</b>	-9.77	68.38	89.0	-7.58	2760.6	2,673
<b>14</b>	-9.13	201.50	145.2	-8.89	302.20	230.3
<b>15</b>	-9.03	238.57	249.6	-9.33	143.75	89.5
<b>16</b>	-10.18	34.22	93.1	-9.69	78.30	70.1
<b>17</b>	-10.34	26.11	24.0	-11.74	2.46	18.6
<b>18</b>	-11.23	5.81	19.1	-8.75	382.79	319.8
<b>19</b>	-10.73	13.52	21.8	-9.03	238.57	269.7
<b>20</b>	-9.14	198.13	170.5	-7.68	2,331.71	2,514
Haloperidol	-10.9	10.14	2.5	-10.34	30.92	16.0



Detailed analysis of the binding site showed that the orientation changes according to the protonated *N*-position and the length of the ligands. Furthermore, the protonated piperidine ring's position is quite characteristic, close to the carboxylic function of Glu172. The docking studies conducted on the  $\sigma_2$  receptor were performed using a homology model.<sup>158</sup> In this case, the salt bridge interactions between ligands and Asp29 and Asp56 residues were considered. In series 4-benzylpiperidines with the nitrate group in the meta position (**9–12**), compound **9** showed a preferential affinity for the  $\sigma_1$  receptor with a  $K_i$  value of 49 nM.

Compound **9** is placed within the receptor site with the piperidinium proton engaged in a salt bridging interaction with Glu172 and a hydrogen bond with N-H amide at 2.1 and 2.8 Å, respectively (Figure 4.3). The nitrate group is positioned on the cytosolic side of the membrane, showing polar interactions with the Asp126 and His154 residues. The optimal position of the piperidine ring favors the  $\pi$ - $\pi$  stacking of the hydrogen in position 4 of the piperidine system with the Tyr103 residue. The benzyl group faces the side near the cell membrane near the  $\alpha_4$  and  $\alpha_5$  chains establishing hydrophobic interactions with the Leu182 and Met93 residues. The elongation at the four-carbon chain (**11**) decreases the affinity for the  $\sigma_1$  receptor while increasing the affinity for the  $\sigma_2$  receptor. In fact, derivative **11** has an inverted orientation with respect to derivative **9**, with the nitrate group towards the  $\alpha_5$  helix to allow housing of the aliphatic chain inside the receptor pocket (Figure 4.4).

---

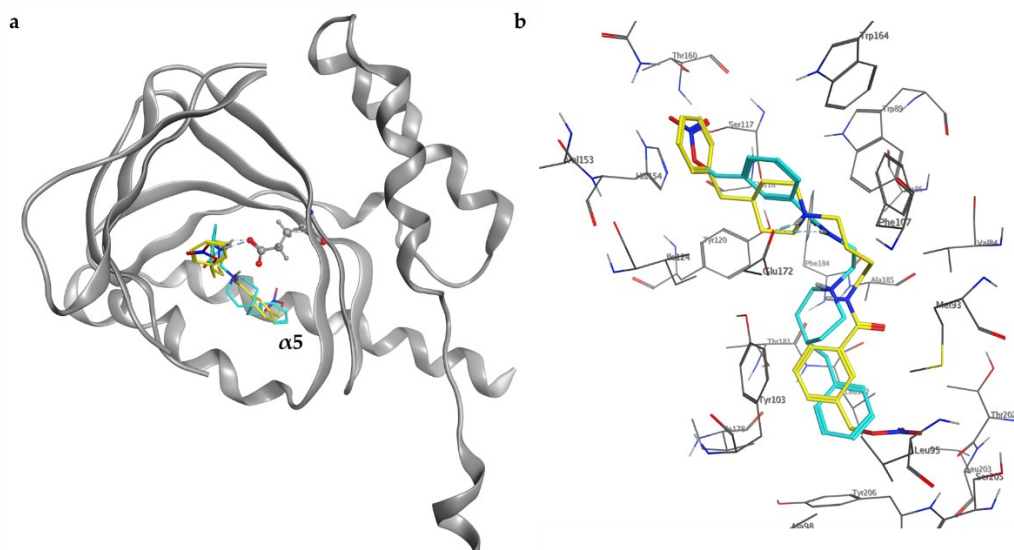


**Figure 4.4.** (a) 3D overlay of the best-anchored poses for **9** (blue) and **11** (yellow) linked to the orthosteric site of the  $\sigma_1$  receptor. The different lengths of the aliphatic linker reverse the orientation of the ligand within the receptor, (b) and a detailed view of docked poses with residues in evidence.

Para substitution of the nitrate group (**13–16**) decreases the affinity with respect to the substituted ligands in the meta position. This is probably due to a minor cationic interaction -  $\pi$  with the His154 residue. The most similar compounds of the series (**11** and **16**) show similar interactions within the  $\sigma_2$  receptor pocket. Both ligands form the saline bridge with the Asp56 residue, while the benzyl portion in position 4 at the piperidine ring shows aliphatic interactions with the Leu70, Met108, Pro113 and Val146 residues. The nitrate group establishes electrostatic interactions with the Arg36 residue, discriminating the different affinity between the different isomers.

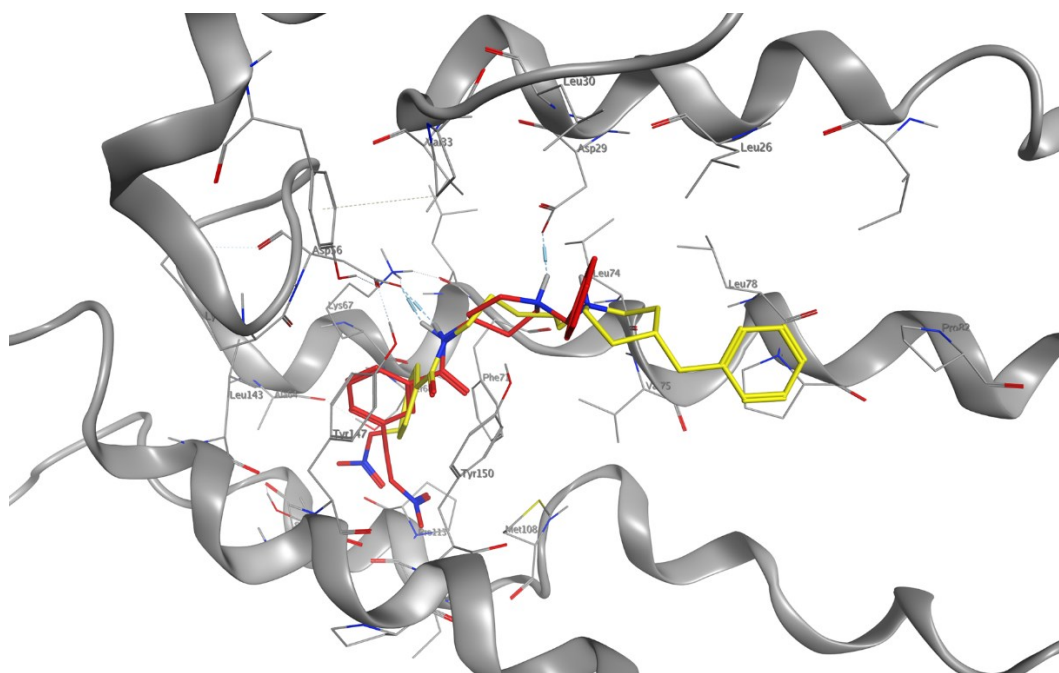


**Figure 4.5.** 3D structures of **16** (yellow) and **17** (red) bound to the  $\sigma_2$  receptor, showing the salt bridge and the cation- $\pi$  (green dotted line) interactions, and the hydrogen bonds with Asp29 and Asp56 (blue dotted line).

Compounds with similar aliphatic linker length in the series (**11** and **16**) show interactions comparable with that observed in the  $\sigma_1$  receptor pocket. In fact, compound **16**, the most active of the **9–16** series ( $K_i \sigma_2$  of 70 nM), forms a salt bridge with the Asp29 residue utilizing the pyridinium proton and a hydrogen bond with the Asp56, while the benzyl portion in position 4 to the piperidine ring shows hydrophobic interactions with the residues Val33, Leu26, Leu78, and  $\pi$ - $\pi$  interaction with Pro79 (Figure 4.5).

The good affinity of compound **17** with the  $\sigma_2$  receptor ( $K_i \sigma_2$  of 19 nM) is due to both the double hydrogen bond and the cation- $\pi$  interaction between receptor and ligand. In fact, the pyridinium proton forms a salt bridge with Asp29 while the amidic hydrogen forms a hydrogen bond with Asp56; the nitrate group is stabilized by the cation- $\pi$  interaction with the Phe71 and Pro113 residues (Figure 4.5).

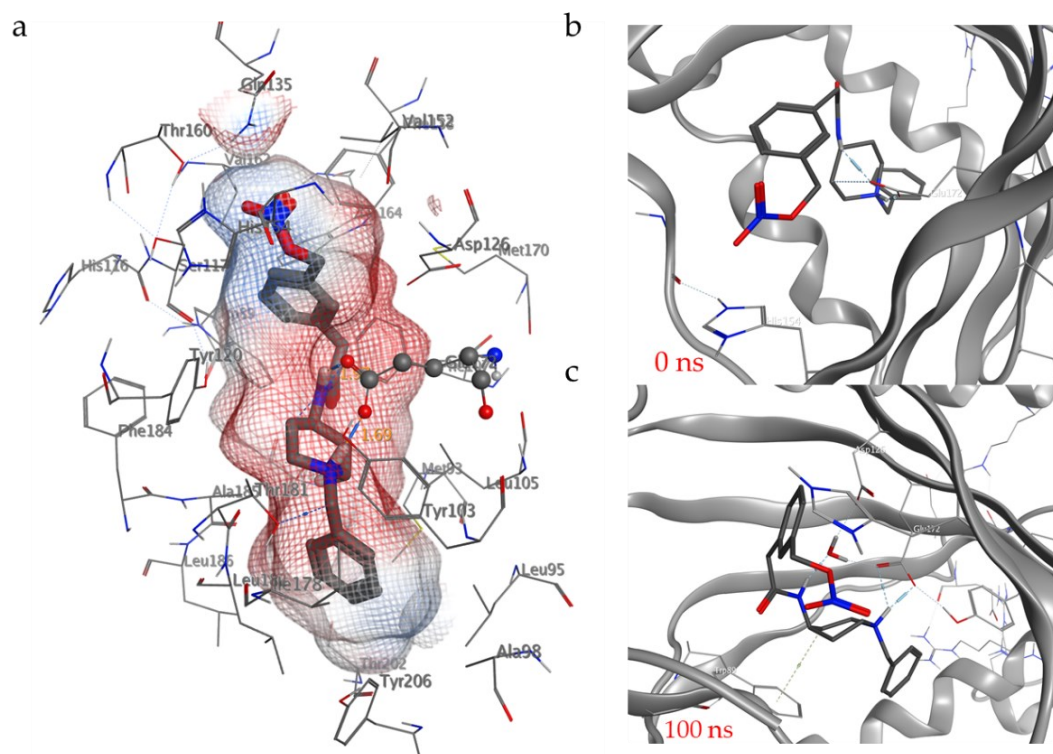


**Figure 4.6.** (a) View of **18** inside binding pocket in electrostatic potential surface representation. Poses of compound **18** bound to the  $\sigma_1$  receptor at 0 ns (a) and 100 ns (b) of MD simulation, showing salt bridge interaction with Glu172 (blue dotted line) and extensive hydrophobic contacts with other binding pocket residues.

Compound **18** showed a prominent affinity to the  $\sigma_1$  receptor. A short MD simulation was performed (10 ns) to identify the most stable pose. As shown in Figure 4.6a, ligand **18** shows a bidentate interaction between the piperidinium proton (due to the salt bridge formation) and the amide hydrogen with the Glu172 residue at 1.67 Å and 1.98 Å, respectively.

The ligand is placed inside the pocket by orienting the benzyl group along the side near the  $\alpha_5$  helix and the nitrate group towards the top of the receptor. After 100 ns of MD simulation, it is interesting to note that the ligand maintains the salt bridge with the Glu172 residue, and a new hydrogen bond bridge is established, favored by a water molecule between the Glu172 and Asp126 residues and the amide hydrogen ( Figure 4.6b,c). Furthermore, the His154 residue maintains a cationic- $\pi$  interaction with the

nitrate group, further stabilizing the conformation of the ligand within the binding site. After 100 ns of MD simulation, the distance between the nitrate group and the His154 residue decreases by 0.49 Å (from 3.80 Å to 3.31 Å) while the distance between the pyridinium and the Glu172 proton decreases by 0.88 Å (2.56 Å to 1.68 Å). The redocking of compound **18**, using the average pose in the last 5 ns of MD simulation, has a calculated  $K_i$  value of 15 nM, in agreement with the experimental one (19 nM).

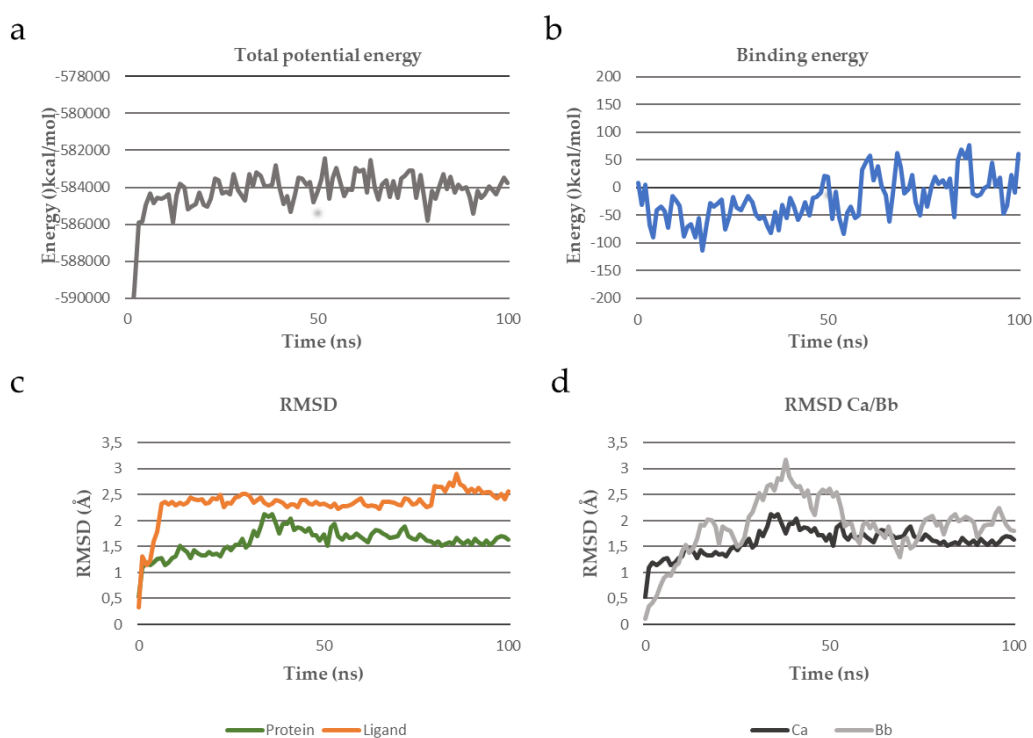


**Figure 4.7.** Total potential energy of the system (a), binding energy of the ligand (b), RMSD ligand after superposition on the receptor (c), and RMSDs from the starting protein structure (d) of  $\sigma_2$  receptor and its complex with compound **18**.

The system's potential energy is stable throughout the MD simulation, with a minimum at 17 ns (580877 kcal/mol). Overall, RMSD for the protein system appeared to have reached equilibrium after 13 ns with slight inflation at 36 ns, while ligand stabilization after 8 ns, while the ligand shows no fluctuations. The binding energy of the ligand undergoes a slight

increase after 58 ns, remaining stable throughout the MD simulation experiment. (Figure 4.7).

After experimentally measuring the affinity profiles of the compounds synthesized on the  $\sigma$  receptors, the ability of these compounds to release NO was evaluated. The nitrite content was measured with the Griess method by incubating the compounds (100  $\mu$ M), at 37  $^{\circ}$ C, in Tris-HCl buffer for 30 min.

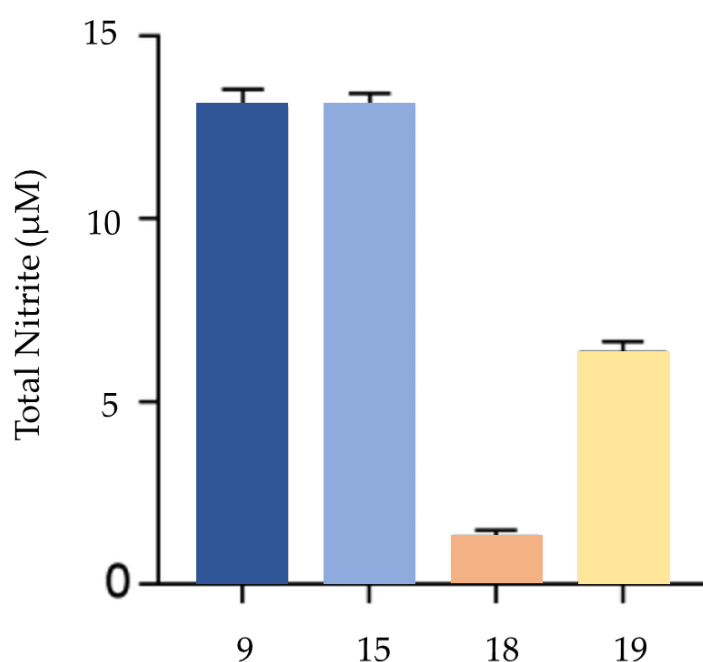


**Figure 4.8.** Total nitrite content measured using Griess reagent.

Compounds were selected based on their affinity profile against  $\sigma$  receptors. In particular, compounds **9**, **11**, **15**, and **17–19** were evaluated (Figure 4.8), having shown a good affinity for the receptors under examination. Compounds **9** and **15** were able to release a significant amount of NO in the  $\mu$ M range (**9**, 13.0  $\pm$  0.5  $\mu$ M; **15**, 13.0  $\pm$  0.4  $\mu$ M). The amount of NO released from compound **18** was 1.3  $\pm$  0.2  $\mu$ M, while compound **19** produced 6.3  $\pm$  0.3  $\mu$ M NO. Negligible amounts of NO were detected for compounds **11** and **17**.

---

#### 4.5 A COMPUTATIONAL MODEL TO PREDICT THE EFFECT OF LIGANDS ON SIGMA $\sigma_1$ RECEPTORS: PRELIMINARY RESULTS

The physiological classification of  $\sigma_1$  ligands as agonists and antagonists is based on the physiology of the animal under study, with agonists altering hyperlocomotion or other physiological responses through binding to  $\sigma_1$ , while antagonists attenuate this response.<sup>159,160</sup> Also, antagonists show similar functional effects to receptor knockdown, suggesting they indeed operate through blockade of  $\sigma_1$  activity.<sup>161</sup>

The different oligomeric states of  $\sigma_1$  receptors are significantly influenced by the different interactions with agonists and antagonists. In fact, it has been shown that the agonists decrease the oligomer state, while the antagonists increase the stability of the oligomer state.  $\sigma_1$  ligands significantly influence protein-protein interaction and stabilize higher molecular weight complexes (antagonist effect) or decrease protein-protein interactions by favoring low molecular weight oligomeric complexes (agonist effect).<sup>162</sup> The putative TM2 mutational study in the full-length receptor identified key residues (Gly87, Gly88, and Gly91) involved in oligomerization. Moreover, other essential residues for ligand binding in TM2 (Ser99, Tyr103, and Leu105-Leu106) are intimately related to the ability to form one or more oligomeric states. The oligomer can decay to an intermediate tetramer and monomer in the absence of ligands, although mutations of the GXXXG motif change the distribution of these species. However, it is intriguing to consider that protein-protein interactions may be involved in the reassembly of the functional receptor. In this regard, monomeric  $\sigma_1$ R has been reported to interact with ion channels such as Na 1.5 voltage-gated Na<sup>+</sup> channel, acid-sensing channels, and the dopamine D<sub>1</sub> receptor.<sup>163-165</sup> Interestingly, these interactions were disrupted in the presence of ligands such as haloperidol and/or (+)-pentazocine, so it is

---





First of all, an equal starting point was created for all the ligands, through an MD simulation of 100 ns of the  $\sigma_1R$  system without ligands. The second step involves an MD simulation of 200 ns for the antagonist PD144418 and the agonist PRE-084. In Figure 4.10 it is possible to see how the antagonist increases protein-protein interactions with an energy minimum at 200 ns and a second energetic minimum at 30 ns. PRE-084 shows an energetic maximum at 180 ns and 30 ns; according to experimental data, protein-protein interactions are disfavoured. For both cases, it is possible to estimate an average value at 50 ns.

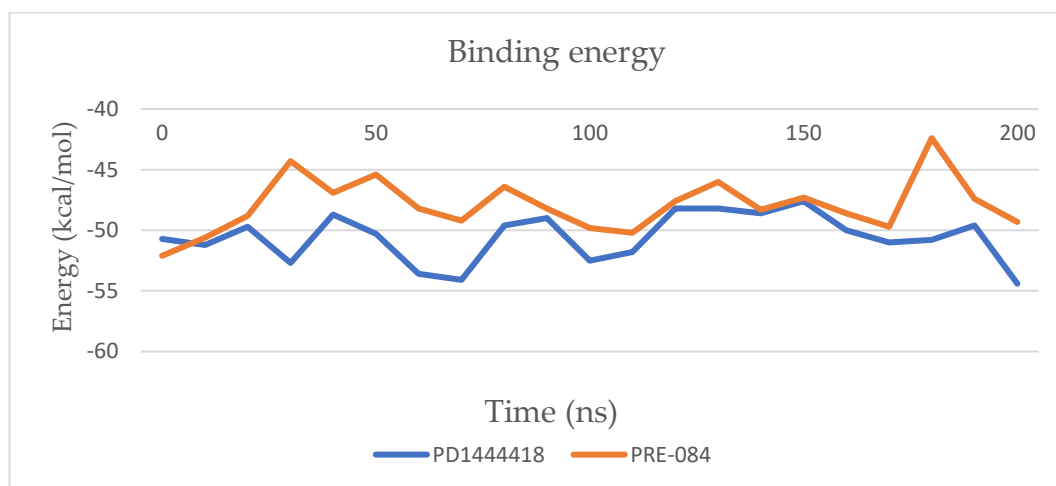


**Figure 4.10.** Free energy of binding protein-protein as a function of MD simulation.

The free energy of binding and the various energetic components of protein-protein interactions inside the homotrimer, calculated by Foldx, present unequivocal data on the protein complex's stability exerted by the ligands. In fact, in all cases, after 50 ns of MD simulation, the free energy of binding increases with the agonists, suggesting a destabilization of the protein system, while, with the antagonists, decrease, suggesting a better protein-protein interaction between the individual monomers of the complex.

	$\sigma$ IR	4IPB	COCAINE	PRE084	L-687,384	4-PPBP	CUTAMESINE	PD144418	E-52862	XD	HALOPERIDOL	BD1063	BD1047	BD1060
IntraclashesGroup1	34,00	36,23	39,39	33,28	28,03	32,53	36,30	25,34	32,59	32,62	31,89	43,90	34,54	
IntraclashesGroup2	34,00	36,23	30,02	33,28	28,03	32,53	36,30	25,34	32,59	32,62	31,89	43,90	34,54	
Interaction Energy	-32,83	-28,48	-27,69	-28,80	-26,05	-30,76	-30,08	-35,21	-38,93	-36,20	-34,80	-35,56	-37,65	
$\Delta\Delta G$	0,00	4,34	5,14	4,03	6,77	2,07	2,75	-2,38	-6,10	-3,37	-1,97	-2,73	-4,83	
Backbone Hbond	-2,00	-2,73	-3,12	-2,27	-2,27	-0,84	-3,16	-2,31	-3,59	-4,40	-4,89	-0,55	-2,18	
Sidechain Hbond	-8,89	-6,99	-10,55	-8,21	-7,17	-8,51	-9,07	-11,02	-11,65	-13,57	-12,69	-10,14	-12,40	
Van der Waals	-43,86	-46,89	-46,66	-42,44	-47,27	-49,77	-43,82	-36,69	-49,19	-52,06	-50,14	-50,90	-50,85	
Electrostatics	-6,88	-4,87	-7,75	-4,60	-5,63	-5,95	-4,57	-8,23	-5,41	-7,43	-4,28	-7,07	-7,72	
Solvation Polar	54,08	56,96	62,20	52,70	61,96	63,01	54,75	69,12	61,73	65,74	62,59	64,51	65,83	
Solvation Hydrophobic	-57,21	-61,90	-60,93	-55,45	-60,94	-63,94	-57,28	-67,17	-64,13	-67,63	-65,07	-66,23	-65,13	
Van der Waals clashes	2,89	3,34	4,79	0,82	4,75	3,40	1,49	1,48	3,34	4,88	4,44	13,43	2,86	
entropy sidechain	19,86	20,75	23,61	21,67	21,41	21,66	21,11	24,85	21,51	24,37	25,26	13,61	19,97	
entropy mainchain	8,16	12,58	10,15	8,77	8,28	10,24	9,81	8,50	5,78	13,05	10,10	9,33	7,52	
sloop_entropy	0,00	0,00	0,00	0,00	0,00	0,00	0,00	0,00	0,00	0,00	0,00	0,00	0,00	
mloop_entropy	0,00	0,00	0,00	0,00	0,00	0,00	0,00	0,00	0,00	0,00	0,00	0,00	0,00	
cis bond	0,00	0,00	0,00	0,00	0,00	0,00	0,00	0,00	0,00	0,00	0,00	0,00	0,00	
torsional clash	0,07	0,02	0,08	0,01	0,04	0,07	0,06	0,04	0,02	0,13	0,15	0,20	0,05	
backbone clash	6,15	7,03	7,49	6,28	8,81	8,19	6,47	8,96	8,56	8,49	8,35	4,93	7,77	
helix dipole	1,04	1,23	1,07	0,63	1,30	1,20	0,71	1,34	0,62	0,79	1,26	0,65	1,15	
water bndge	0,00	0,00	0,00	0,00	0,00	0,00	0,00	0,00	0,00	0,00	0,00	0,00	0,00	
disulfide	0,00	0,00	0,00	0,00	0,00	0,00	0,00	0,00	0,00	0,00	0,00	0,00	0,00	
electrostatic kon	-0,45	-0,38	-1,22	-0,65	-0,92	-0,45	-0,50	0,24	-0,59	-0,44	-0,49	-0,46	-0,36	
partial covalent bonds	0,00	0,00	0,00	0,00	0,00	0,00	0,00	0,00	0,00	0,00	0,00	0,00	0,00	
energy ionisation	0,36	0,39	0,61	0,24	0,49	0,26	0,41	0,35	0,30	0,37	0,41	0,35	0,40	
Entropy Complex	7,15	7,15	7,15	7,15	7,15	7,15	7,15	7,15	7,15	7,15	7,15	7,15	7,15	
Number of Residues	1950,00	1950,00	1950,00	1950,00	1950,00	1950,00	1950,00	1950,00	1950,00	1950,00	1950,00	1950,00	1950,00	
Interface Residues	128,00	135,00	132,00	124,00	121,00	132,00	118,00	130,00	138,00	132,00	134,00	134,00	134,00	
Interface Residues Clashing	0,00	0,00	0,00	0,00	0,00	0,00	0,00	0,00	0,00	0,00	0,00	0,00	0,00	
Interface Residues VdW Clashing	0,00	0,00	0,00	0,00	0,00	0,00	0,00	0,00	0,00	0,00	0,00	0,00	0,00	
Interface Residues BB Clashing	0,00	0,00	0,00	0,00	0,00	0,00	0,00	0,00	0,00	0,00	0,00	0,00	0,00	

**Figure 4.11.** Single empirical terms for each complex to calculate Gibbs free energy.

A detailed breakdown of different energy components reveals that the primary forces driving binding events are Hydrophobic Solvation ( $\Delta G_{\text{solvH}}$ ) and Van der Waals energy ( $\Delta G_{\text{vdw}}$ ). In contrast, Polar Solvation energy  $\Delta G_{\text{solvH}}$  negatively contributes to the free energy of binding (Figure 4.11).

The total number of interactions (Figure 4.12) is favorable to MD simulation with antagonists, justifying the ability to stabilize for contact surfaces protein-protein. A detailed analysis of the interactions highlights a favorable trend in forming hydrogen bonds in the backbone with an average increase of 19.7% and 29.30% in the sidechain.

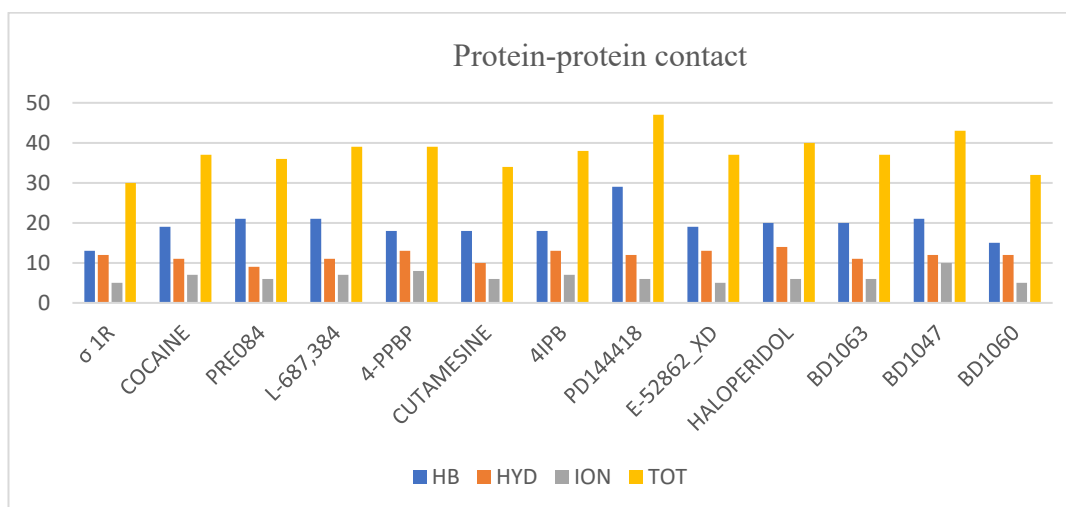


**Figure 4.12.** Protein-protein contact after 50 ns of MD simulation.

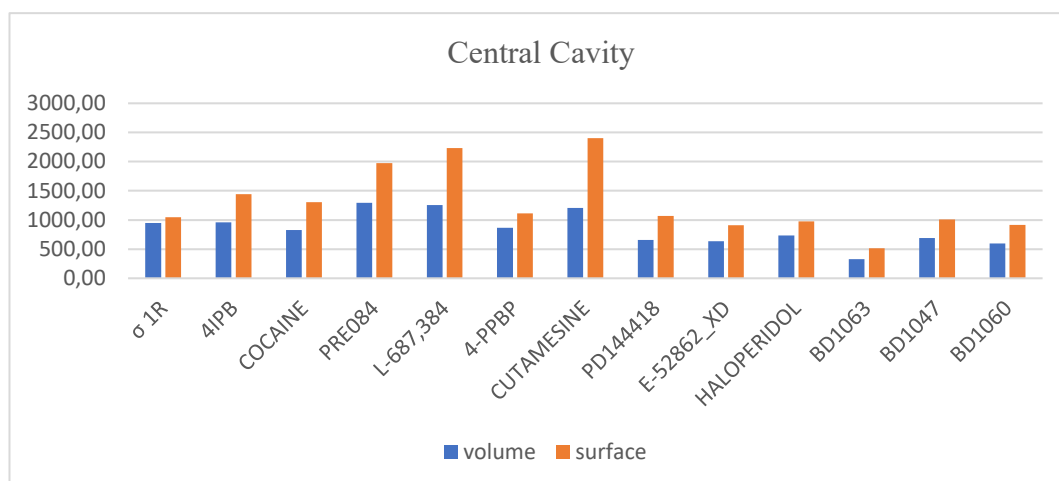


**Figure 4.13.** Volume and surface area of the central cavity after 50 ns of MD simulation.

The homotrimer system of the  $\sigma_1$  receptor forms a central cavity on the opposite side of the cytoplasmic membrane. It has been observed that this cavity may vary depending on the function of the ligand interacting with the receptor, further confirming how the trimer system can be perturbed or stabilized according to the function of the ligands. An average increase of 43.30% of the surface of the cavity in the presence of the agonists was observed, demonstrating the removal of the single monomers to favor low molecular weight oligomeric states. Instead, in the presence of antagonists, the cavity has a smaller size with an average volume of  $606.29 \text{ \AA}^3$ .

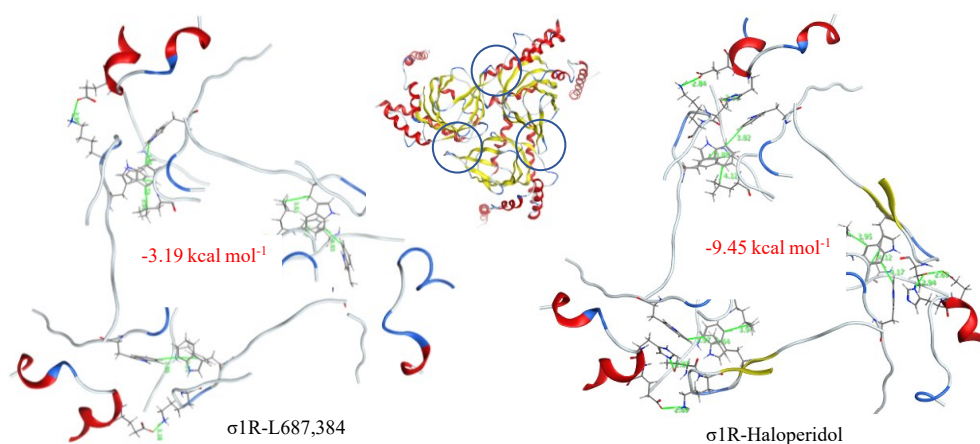


**Figure 4.14.** View of the  $\sigma_1R$  trimerization interface in the presence of L-687,384 and Haloperidol.

The trimerization interface is a hinge point in the  $\sigma_1R$  oligomerization process, with the residues Glu54, Glu55, Phe83, Leu111, Trp136, Lys142, and Trp169, responsible for hydrogen bonds, hydrophobic interactions, and ionic bonds affecting this receptor region (Figure 4.14).

The interaction of the ligand with the top of the receptor pocket may be responsible for the receptor complex's stability, influencing the protein-protein interactions. The MD simulation has shown that Haloperidol maintains in all the monomers of the complex the hydrogen bonds between the residues His54-Thr141 and Glu55-Lys142, the hydrophobic interactions between the Phe83-Thr136, Leu111-Thr136, Trp169-Trp136 residues and the ionic bonds between Glu54-Lys142 and Glu55-Lys142. Instead, the L-687,384 agonist interrupts 29.5% of these interactions, with an energy binding protein-protein of  $-3.19 \text{ kcal mol}^{-1}$  compared with  $-9.45 \text{ kcal mol}^{-1}$  of the Haloperidol- $\sigma_1R$  complex. These data suggest that agonists can disrupt the interactions between residues of contact surfaces by disfiguring the oligomerization process, increasing the average distance of  $0.7 \text{ \AA}$  between the individual monomers. Moreover, also a possible electrostatic interaction between the Cl atom of the Haloperidol and the nitrogen

Gln135, stabilized by a hydrogen bond with the His154 residue. This interaction breaks the hydrogen bond between Gln135 and Glu144, present in the receptor in the native state, favoring greater flexibility of the loop and, therefore, the protein region responsible for the stabilizing interactions. The root mean square deviation (RMSD) of the affected residues is 1.8–2.5 Å.

#### 4.6 CONCLUSION AND PERSPECTIVE

The  $\sigma_1$  receptor is an essential multifunctional protein. Changes in its function and/or expression caused by binding to certain compounds (agonists and antagonists) have been associated with various neurological disorders, including amyotrophic lateral sclerosis/frontotemporal dementia, Alzheimer's and Huntington's disease and retinal degeneration.  $\sigma_1$ R agonists are largely neuroprotective, and this is achieved through a variety of  $\sigma_1$  receptor-mediated signaling functions that are generally pro-survival and anti-apoptotic; however, data on the exact mechanisms of receptor functioning at the molecular level are still limited.

The new synthesized hybrid ligands allow having both a  $\sigma_1$  ligand and a NO donor fraction in the same scaffold. In this preliminary phase, the synthesized compounds were evaluated both for their ability to bind the sigma receptors and for the release of NO. Molecular docking and MD simulation studies demonstrated that aliphatic linker length plays an essential role in ligand orientation within the receptor pocket and for  $\sigma_1/\sigma_2$  selectivity. The nitrate group stabilizes the ligand/receptor complex at the cationic- $\pi$  interaction with the His154 residue in the  $\sigma_1$  receptor, confirmed by the MD simulation, and with the Phe71 and Pro113 residues in the  $\sigma_2$  receptor.

Preliminary data suggest that the designed compounds have an excellent *in-silico* affinity with the human  $\beta_2$ -adrenergic receptor. Biological assays for

---

the determination of the inhibition constants are currently being evaluated. Therefore, the synthesized ligands could be promising multitarget drugs, capable of inhibiting both the  $\sigma_1$  receptor and the human  $\beta_2$ -adrenergic receptor and releasing bioactive NO at the same time.

Obtaining structural data of unbound and agonist- and antagonist-bound  $\sigma_1$  receptors is a crucially important step that could be achieved to better understand the ligand binding affinity of the  $\sigma_1$  receptor. For this reason, we pursued structural studies of several well-known  $\sigma_1$  ligands, agonist and antagonist, and their interaction in complex with the  $\sigma_1$  receptor using the MD simulations of the  $\sigma_1$  receptor-ligand system based on the  $\sigma_1$  receptor crystal structure. We carry out independent MD simulations, examining the frequency of contacts and determining the  $\Delta G$  between them and the individual monomer constituted the trimeric organization of the  $\sigma_1$  receptor.

Finally, to evaluate these results, we decided to realize additional structural studies of a  $\sigma_1$  receptor agonist previously synthesized by our research group and subjected to a specific biological test to define the antagonist or agonist profile.

---

---

## CHAPTER 5 EXPERIMENTAL PART

### GENERAL INFORMATION

All the required chemicals were purchased from Fluorochem and Merck and Aldrich Chemical Company. Pre-coated aluminum sheets (silica gel 60 F<sub>254</sub>, Merck) were used for thin-layer chromatography (TLC), and spots were visualized under UV light. Silica gel column chromatography was performed using silica gel 60–120 mesh size (RANKEM Limited). <sup>1</sup>H NMR and <sup>13</sup>C NMR spectra were recorded on Varian UNITY Inova spectrometer using CDCl<sub>3</sub> as a solvent and tetramethylsilane (TMS) as an internal standard, at 200 or 500 MHz for <sup>1</sup>H NMR and 125 MHz for <sup>13</sup>C NMR. <sup>13</sup>C NMR spectra were <sup>1</sup>H decoupled, and multiplicities were determined by the APT pulse sequence. Chemical shift (δ) values are given in ppm.

#### *General procedure for the synthesis of Timolol-BN*

To a cold solution (0 °C) of Timolol (1.0 g, 3.16 mmol) in DMF (20 mL) was added NaH (83.4 mg, 3.45 mmol). The mixture was stirred at 0 °C to room temperature for 30 min. After cooling the reaction mixture to 0 °C, benzyl bromide (0.45 mL, 3.79 mmol) was added successively, and the mixture was stirred at room temperature for 12 h. The reaction was quenched with saturated NH<sub>4</sub>Cl aqueous solution, and the reaction mixture was extracted with DCM three times. The combined organic phase was dried over MgSO<sub>4</sub>, and the solvents were evaporated. The crude product was purified by flash chromatography, eluting with CH<sub>2</sub>Cl<sub>2</sub>/MeOH 9/1 to afford colorless oil (1.092 g, 85%). <sup>1</sup>H NMR (500 MHz, Chloroform-*d*): δ 7.33–7.34 (m, 5H), 4.63 (2H,s), 4.39–4.43 (2H, ddq, J=8.0 Hz), 4.01 (1H, s), 3.81 (4H,t, J=4.6 Hz), 3.52 (4H,t, J=6.0 Hz), 2.78 (2H, m), 1.17 (9H, s). <sup>13</sup>C NMR (50 MHz, Chloroform-*d*): δ 153.8, 149.75, 137.2, 128.4, 127.8, 127.3, 72.73, 72.1, 66.43, 66.10, 50.24, 47.80, 44.53, 28.95.

---

---

*General procedure for the synthesis of 5-((3a*S*,4*S*,6a*R*)-2-oxohexahydro-1*H*-thieno[3,4-*d*]imidazol-4-yl)pentanoyl chloride (2a)*

A solution of biotin **1** (300 mg, 1.23 mmol, 1 equiv) in 5 mL (69 mmol, 56 equiv) of SOCl<sub>2</sub> was stirred at room temperature for 1 hour. The volatiles were evaporated in vacuo and then co-evaporated with toluene (3 × 15 mL) to yield the chloride **2** directly used in the subsequent reaction.

*General procedure for the synthesis of 4-formylphenyl 5-((3a*S*,4*S*,6a*R*)-2-oxohexahydro-1*H*-thieno[3,4-*d*]imidazol-4-yl)pentanoate (3a)*

4-hydroxy benzaldehyde (165 mg, 1.35 mmol, 1 equiv) and DIPEA (0.265 mL, 1.49 mmol) were dissolved in THF dry (5 mL). To this solution of biotin carbonyl chloride (322.13 mg, 1.23 mmol, 0.9 equiv) in THF (3 mL) was added dropwise at 0 °C under nitrogen atmosphere. The resulting mixture was stirred for 12 h and was further diluted with water (2 mL) and sat. NaCl (25 mL). The aqueous layer was extracted with EtOAc (3 × 10 mL). The combined organic layers were collected, dried over Na<sub>2</sub>SO<sub>4</sub> and evaporated under reduced pressure. The residue was purified over silica gel column (hexane/EtOAc 10%) to afford the colorless solid compound **3** (360.46 mg, 85%). <sup>1</sup>H NMR (500 MHz, Chloroform-*d*): δ 9.85 (1 H, s), 7.81 (2H, d, J=8.8 Hz, Ar-H), 6.97 (2H, d, J=6.8, Ar-H), 4.31 (1H, s), 4.21-4.07 (1 H, m), 3.13 (1H, s), 2.82 (1H, dd, J=5.3, 11.9), 2.72 (1H, t, J=7.0 Hz), 2.58 (1H, d, J=12.5), 2.29 (1H, t, J=6.1 Hz), 1.65 (3H, t, J=6.6 Hz), 1.56–1.32 (3H, m); <sup>13</sup>C NMR (50 MHz, Chloroform-*d*): δ 189.0, 174.6, 166.2, 158.0, 134.2, 131.5, 121.8, 63.5, 61.8, 57.0, 41.1, 37.7, 29.8, 29.6, 26.9.

*General procedure for the synthesis of 4-(hydroxymethyl)phenyl 5-((3a*S*,4*S*,6a*R*)-2-oxohexahydro-1*H*-thieno[3,4-*d*]imidazol-4-yl)pentanoate (4a)*

To a stirring solution of aldehyde (350 mg, 1 mmol, 1.0 equiv) in 5 mL of THF dry (10 mL), NaBH<sub>4</sub> (75.66 mg, 2 mmol, 2.0 equiv) was added portion-

---



wise at 0 °C over 5 min, and stirring was continued for another 15 min at room temperature. After completing the reaction (monitored by TLC), the mixture was cooled to 0 °C; the reaction was carefully quenched with 0.5 mL of acetic acid, followed by 3 mL of water; and the mixture was extracted with ethyl acetate (3 × 5 mL). The organic layer was dried over anhydrous Na<sub>2</sub>SO<sub>4</sub> and concentrated under reduced pressure. Column chromatography with silica gel and a gradient solvent system of 10–30% ethyl acetate/hexane. The yields were 309 mg, 88%. <sup>1</sup>H NMR (500 MHz, Chloroform-*d*): δ 7.72 (2H, d, J=8.8 Hz, Ar-H), 6.69 (2H, d, J=6.8, Ar-H), 4.66 (2H, s, CH<sub>2</sub>-O) 4.31 (1H, s), 4.21–4.07 (1 H, m), 3.13 (1H, s), 2.82 (1H, dd, J=5.3, 11.9), 2.72 (1H, t, J=7.0 Hz), 2.58 (1H, d, J=12.5), 2.20 (1H, t, J=6.1 Hz), 1.60 (3H, t, J=6.6 Hz), 1.56–1.32 (3H, m); <sup>13</sup>C NMR (50 MHz, Chloroform-*d*): δ 174.1, 165.9, 150.0, 138.2, 128.8, 121.8, 72.4, 63.5, 61.8, 57.0, 41.1, 37.7, 29.8, 29.6, 26.9.

*General procedure for the synthesis of 4-(((chlorocarbonyl)oxy)methyl)phenyl 5-((3a*S*,4*S*,6a*R*)-2-oxohexahydro-1*H*-thieno[3,4-*d*]imidazol-4-yl)pentanoate (5a)*

To a cold solution (0 °C) of compound 4 (300 mg, 0.86 mmol, 1 eq) in THF (10 mL) and DIPEA (0.165 mL, 0.94 mmol, 1.1 equiv) was added triphosgene (305.48 mg, 1.03 mmol, 1.2 equiv). The reaction mixture was allowed to warm to room temperature and left to stir for 1 h. After completing the reaction (monitored by TLC), the mixture was directly used in the subsequent reaction.

---

*General procedure for the synthesis of 4-((((S)-2-(benzyloxy)-3-((4-morpholino-1,2,5-thiadiazol-3-yl)oxy)propyl)(tert-butyl)carbamoyl)oxy)methyl)phenyl 5-((3aS,4S,6aR)-2-oxohexahydro-1H-thieno[3,4-d]imidazol-4-yl)pentanoate (6a)*

To a solution of timolol-BN (250.0 mg, 0.61 mmol) and DIPEA (0.13 mL, 0.74 mmol) in THF (15 mL) a mixture of 5 (254 mg, 0.61 mmol) of the previous reaction in crude was added dropwise. The reaction was stirred for 24 hours at room temperature. The mixture was washed with water (10 mL), saturated sodium bicarbonate (10 mL x 2) and brine (10 mL), dried (Na<sub>2</sub>SO<sub>4</sub>), and flash chromatographed purified by flash chromatography, eluting with CH<sub>2</sub>Cl<sub>2</sub>/MeOH 9/1 to afford the white solid compound 6 (321 mg, 65%). <sup>1</sup>H NMR (500 MHz, Methanol-*d*): δ 7.77 (2H, d, J=8.8 Hz), 7.33–7.34 (m, 5H), 6.87 (2H, d, J=6.8), 4.95 (2H, s), 4.63 (2H,s), 4.31 (1H, s), 4.43 (2H, m), 4.21–4.07 (1 H, m), 3.93 (1H, m), 3.81 (4H,t, J=4.6 Hz), 3.52 (4H,t, J=6.0 Hz), 3.13 (1H, s), 2.82 (1H, dd, J=5.3, 11.9), 2.72 (1H, t, J=7.0 Hz), 2.68 (2H, m), 2.58 (1H, d, J=12.5), 2.29 (1H, t, J=6.1 Hz), 1.65 (3H, t, J=6.6 Hz), 1.56–1.32 (3H, m), 1.40 (9H, s); <sup>13</sup>C NMR (50 MHz, Chloroform-*d*): δ 174.1, 166.5,158.0, 157.6, 153.1, 147.7, 137.8, 134.2, 128.4, 127.8, 127.2, 121.8, 72.1, 69.2, 68.6, 67.1, 66.4, 63.5, 61.8,57.2, 57.0, 47.8, 42.5, 41.1, 37.7, 29.8, 29.6, 26.9, 25.8.

*General procedure for the synthesis of 4-(((tert-butyl((S)-2-hydroxy-3-((4-morpholino-1,2,5-thiadiazol-3-yl)oxy)propyl)carbamoyl)oxy)methyl)phenyl 5-((3aS,4S,6aR)-2-oxohexahydro-1H-thieno[3,4-d]imidazol-4-yl)pentanoate (7a)*

To a solution of 6 (200.0 mg, 0.25 mmol) in MeOH (10 mL) was added Pd/C (20 mg), under an atmosphere of hydrogen (1 atm). The reaction was stirred for 12 hours at room temperature. After completion of the reaction (monitored by TLC), the solution was filtered on celite. The residue was purified by flash chromatography, eluting with CH<sub>2</sub>CH<sub>2</sub>/MeOH 9/1 to

---

afford a colorless oil (157.0 mg, 90%).  $^1\text{H}$  NMR (500 MHz, Methanol-*d*):  $\delta$  7.77 (2H, d,  $J=8.8$  Hz), 6.87 (2H, d,  $J=6.8$ ), 4.95 (2H, s), 4.31 (1H, s), 4.43 (2H, m), 4.21-4.07 (1 H, m), 3.93 (1H, m), 3.81 (4H,t,  $J=4.6$  Hz,), 3.52 (4H,t,  $J=6.0$  Hz,), 3.13 (1H, s), 2.82 (1H, dd,  $J=5.3, 11.9$ ), 2.72 (1H, t,  $J=7.0$  Hz), 2.68 (2H, m), 2.58 (1H, d,  $J=12.5$ ), 2.29 (1H, t,  $J=6.1$  Hz), 1.65 (3H, t,  $J=6.6$  Hz), 1.56–1.32 (3H, m), 1.40 (9H, s);  $^{13}\text{C}$  NMR (50 MHz, Methanol-*d*):  $\delta$  174.1, 166.5, 158.0, 157.6, 153.2, 147.7, 134.2, 128.5, 121.8, 69.2, 68.6, 67.1, 66.4, 63.5, 61.8, 57.2, 57.0, 47.8, 42.5, 41.1, 37.7, 29.8, 29.6, 26.9, 25.8.

***General procedure for the synthesis of 4-formylphenyl acetate (9a)***

To a solution of 4-hydroxybenzaldehyde (2 g, 16.38 mmol) and  $\text{Et}_3\text{N}$  (2.74 mL, 19.65 mmol) in anhydrous  $\text{CH}_2\text{Cl}_2$  (30 mL) was added acetic anhydride (1.86 mL, 19.65 mmol) at 0 °C, and the reaction mixture was warmed to room temperature. The reaction was monitored by TLC, and after 2 hours, starting material was completely consumed. Then the reaction was quenched by the addition of  $\text{H}_2\text{O}$  (3 mL), and the organic layer was washed with 1 N HCl (20 mL  $\times$  2) and saturated aq.  $\text{NaHCO}_3$  (15 mL  $\times$  2) and brine. The organic layer was dried over  $\text{Na}_2\text{SO}_4$ , the bulk solvent was removed under vacuum, and the crude product was used for the next step without further purification. The product was obtained as a white solid (2.42 g, 90% yield).  $^1\text{H}$  NMR (500 MHz, Chloroform-*d*):  $\delta$  9.98 (s, 1H), 7.91 (d, 2H), 7.27 (d, 2H), 2.31 (s, 3H).  $^{13}\text{C}$  NMR (50 MHz, Methanol-*d*):  $\delta$  191.1, 169.3, 156.9, 133.9, 131.5, 122.0, 19.6.

***General procedure for the synthesis of 4-(hydroxymethyl)phenyl acetate (10a)***

To a stirring solution of 4-formylphenyl acetate (9) (1.00 g, 6.02 mmol) in 5 mL of MeOH (10 mL),  $\text{NaBH}_4$  (113.85 mg, 3.01 mmol) was added portion-wise at 0 °C under stirring for 1 hour. After completion of the reaction (monitored by TLC), the mixture was cooled to 0 °C; the reaction was

carefully quenched with 0.5 mL of acetic acid, followed by 3 mL of water; and the mixture was extracted with ethyl acetate (3 × 5 mL). The organic layer was dried over anhydrous Na<sub>2</sub>SO<sub>4</sub> and concentrated under reduced pressure. Column chromatography with silica gel and a gradient solvent system of 10–30% ethyl acetate/hexane. The yields were 0.96 g, 95%. <sup>1</sup>H NMR (500 MHz, Chloroform-*d*): δ 7.37 (d, 2H), 7.06 (d, 2H), 4.59 (s, 2H), 2.29 (s, 3H). <sup>13</sup>C NMR (50 MHz, Methanol-*d*): δ 168.5, 151.2, 138.2, 130.1, 128.7, 121.0, 20.1.

*General procedure for the synthesis of (S)-4-(((2-(benzyloxy)-3-((4-morpholino-1,2,5-thiadiazol-3-yl)oxy)propyl)(tert-butyl)carbamoyl)oxy)methyl)phenyl acetate (11a)*

To a cold solution (0 °C) of compound 10 (200 mg, 1.19 mmol) in THF (10 mL) and DIPEA (0.23 mL, 1.31 mmol) was added triphosgene (423.93 mg, 1.43 mmol). The reaction mixture was allowed to warm to room temperature and left to stir for 1 h. After completing the reaction (monitored by TLC), the mixture was directly used in the subsequent reaction.

To a solution of timolol (374.69 mg, 1.19 mmol) and DIPEA (0.23 mL, 1.31 mmol) in THF (15 mL) a mixture of 5 (355 mg, 0.86 mmol, 1 equiv) of the previous reaction in crude was added dropwise. The reaction was stirred for 24 hours at room temperature. The solution was treated with water and diethyl ether; the organic layers were dried over Sodium sulfate and concentrated under reduced pressure. The residue was purified by flash chromatography, eluting with CH<sub>2</sub>CH<sub>2</sub>/MeOH 9/1 to afford a colorless oil (548.83 mg, 77%). <sup>1</sup>H NMR (500 MHz, Methanol-*d*): δ 7.33–7.34 (m, 5H), 7.21 (2H, d), 6.95 (2H, d), 5.11 (2H, s), 4.67 (2H, s), 4.43 (2H, m), 4.31 (1H, br), 3.81 (4H, t, J=4.6 Hz), 3.52 (4H, t, J=6.0 Hz), 3.21–3.35 (m, 2H), 2.31 (3H, s), 1.46 (9H, s). <sup>13</sup>C NMR (50 MHz, Methanol-*d*): δ 169.1, 157.8, 153.7, 149.81, 150.1,

137.8, 133.1, 128.6, 128.4, 127.8, 127.3, 121.5, 77.3, 72.1, 68.2, 67.5, 67.1, 50.3, 47.8, 44.23, 28.2.

*General procedure for the synthesis of (S)-4-(((tert-butyl(2-hydroxy-3-((4-morpholino-1,2,5-thiadiazol-3-yl)oxy)propyl)carbamoyl)oxy)methyl)phenyl acetate (12a)*

To a solution of **11** (200.00 mg, 0.33 mmol) in MeOH (10 mL) was added Pd/C (20 mg), under an atmosphere of hydrogen (1 atm). The reaction was stirred for 12 hours at room temperature. After completion of the reaction (monitored by TLC), the solution was filtered on celite. The residue was purified by flash chromatography, eluting with CH<sub>2</sub>CH<sub>2</sub>/MeOH 9/1 to afford a colorless oil (161.40 mg, 95%). <sup>1</sup>H NMR (500 MHz, Methanol-*d*): δ 7.21 (2H, d), 6.95 (2H, d), 5.11 (2H, s), 4.43 (2H, m), 4.31 (1H, br), 3.81 (4H, t, J=4.6 Hz), 3.52 (4H, t, J=6.0 Hz), 3.21–3.35 (m, 2H), 2.31 (3H, s), 1.46 (9H, s). <sup>13</sup>C NMR (50 MHz, Methanol-*d*): δ 169.1, 157.8, 153.7, 149.81, 150.1, 133.1, 128.6, 121.5, 77.3, 68.2, 67.5, 67.1, 50.3, 47.8, 44.23, 28.2.

*General procedure for the synthesis of N-((S)-2-(benzyloxy)-3-((4-morpholino-1,2,5-thiadiazol-3-yl)oxy)propyl)-N-(tert-butyl)-5-((3a*S*,4*S*,6a*R*)-2-oxohexahydro-1*H*-thieno[3,4-*d*]imidazol-4-yl)pentanamide (13a)*

To a solution of timolol-BN (150 mg, 0.37 mmol) and DIPEA (0.64 mL, 0.37 mmol) in THF/DMF (16 mL, 1/1) a mixture of **2** (173 mg, 0.47 mmol, 1 equiv) of the previous reaction in crude was added dropwise. The reaction was stirred for 24 hours at room temperature. The mixture was washed with water (10 mL), saturated sodium bicarbonate (10 mL × 2) and brine (10 mL), dried (Na<sub>2</sub>SO<sub>4</sub>), and flash chromatographed purified by flash chromatography, eluting with CH<sub>2</sub>Cl<sub>2</sub>/MeOH 9/1 to afford the white solid compound (145 mg, 62%). <sup>1</sup>H NMR (500 MHz, Methanol-*d*): δ 7.33–7.34 (m, 5H), 4.61 (2H, s), 4.43 (2H, m), 4.31 (1H, s), 4.21 - 4.07 (1 H, m), 3.93 (1H, m),

3.81 (4H,t, J=4.6 Hz,), 3.52 (4H,t, J=6.0 Hz,) 3.13 (1H, s), 2.82 (1H, dd, J=5.3, 11.9), 2.72 (1H, t, J=7.0 Hz), 2.68 (2H, m), 2.58 (1H, d, J=12.5), 2.29 (1H, t, J=6.1 Hz), 1.65 (3H, t, J=6.6 Hz), 1.56-1.32 (3H, m), 1.35 (9H, s). <sup>13</sup>C NMR (50 MHz, Methanol-*d*): δ 171.3, 166.1, 157.8, 147.1, 137.2, 128.2, 127.3, 121.8, 82.0, 72.0, 69.5, 68.6, 66.4, 63.5, 61.8, 57.3, 57.0, 47.8, 41.1, 37.7, 29.8, 29.6, 26.9, 25.8.

***General procedure for the synthesis of N-(tert-butyl)-N-((S)-2-hydroxy-3-((4-morpholino-1,2,5-thiadiazol-3-yl)oxy)propyl)-5-((3a*S*,4*S*,6a*R*)-2-oxohexahydro-1*H*-thieno[3,4-*d*]imidazol-4-yl)pentanamide (14a)***

To a solution of **13** (250.0 mg, 0.40 mmol) in MeOH (10 mL) was added Pd/C (20 mg), under an atmosphere of hydrogen (1 atm). The reaction was stirred for 12 hours at room temperature. After completion of the reaction (monitored by TLC), the solution was filtered on celite. The residue was purified by flash chromatography, eluting with CH<sub>2</sub>CH<sub>2</sub>/MeOH 9/1 to afford a colorless oil (151.0 mg, 94%). <sup>1</sup>H NMR (500 MHz, Methanol-*d*): δ 4.43 (2H, m), 4.31 (1H, s), 4.21–4.07 (1 H, m), 3.93 (1H, m), 3.81 (4H,t, J=4.6 Hz,), 3.52 (4H,t, J=6.0 Hz,) 3.13 (1H, s), 2.82 (1H, dd, J=5.3, 11.9), 2.72 (1H, t, J=7.0 Hz), 2.68 (2H, m), 2.58 (1H, d, J=12.5), 2.29 (1H, t, J=6.1 Hz), 1.65 (3H, t, J=6.6 Hz), 1.56-1.32 (3H, m), 1.35 (9H, s). <sup>13</sup>C NMR (50 MHz, Methanol-*d*): δ 171.3, 166.1, 157.8, 147.1, 121.8, 82.5, 69.5, 68.6, 66.4, 63.5, 61.8, 57.3, 57.0, 47.8, 41.1, 37.7, 29.8, 29.6, 26.9, 25.8.

***General procedure for the synthesis of 2-((2-amino-6-oxo-1,6-dihydro-9*H*-purin-9-yl)methoxy)ethyl 2-bromoacetate (2b)***

A solution of ACV (1 g, 4.44 mmol, 1 equiv) in 0.77 mL (8.88 mmol, 2 equiv) of 2-bromoacetyl bromide was added Cs<sub>2</sub>CO<sub>3</sub> (0.72 g, 2.22 mmol, 0.5 equiv) in DMF dry was stirred at room temperature for 2 hour. The reaction was quenched with dropwise addition of methanol. Ice cold water was added to this mixture and stirred for 30 min. The obtained solid product was filtered and washed with water to afford a white solid (1.2 g, 77%). <sup>1</sup>H

NMR (400 MHz, DMSO-d<sub>6</sub>): 10.6 (br, 1H), 7.83 (s, 1H); 6.52 (s, 2H); 5.36 (s, 2H); 4.19 (t, 2H, J = 3.3 Hz); 4.11 (s, 2H); 3.69 (t, 2H, J = 3.3 Hz).

*General procedure for the synthesis of 2-((2-amino-6-oxo-1,6-dihydro-9H-purin-9-yl)methoxy)ethyl 2-(((3aR,4R,6R,6aR)-6-(2,4-dioxo-3,4-dihydropyrimidin-1(2H)-yl)-2,2-dimethyltetrahydrofuro[3,4-d][1,3]dioxol-4-yl)methoxy)acetate (6b)*

Compound **1** (140 mg, 0.49 mmol, 2 equiv) and Cs<sub>2</sub>CO<sub>3</sub> (100 mg, 0.30 mmol, 1 equiv) were dissolved in DMF dry (3 mL). To this solution of compound **2** (100 mg, 0.29 mmol, 1 equiv) in DMF dry (2 mL) was added dropwise at 0 °C under nitrogen atmosphere. The resulting mixture was stirred for 24 h and was evaporated under reduced pressure. The residue was purified over silica gel column (EtOAc/MeOH 10% to 50%) to afford the white solid compound **6** (180 mg, 75%). <sup>1</sup>H NMR (400 MHz, DMSO-d<sub>6</sub>): 10.6 (br, 1H), 9.30 (s, 1H); 7.83 (s, 1H); 7.30 (d, 1H, J = 7.9); 6.52 (s, 2H); 5.91 (s, 1H); 5.78 (d, 1H, J = 7.8); 5.36 (s, 2H); 5.00 (d, 1H, J = 6.4); 4.82 (t, 1H, J = 3.9); 4.24 (q, 1H, J = 4.9); 4.19 (t, 2H, J = 3.3 Hz); 4.13–3.62 (m, 2H); 3.34 (s, 2H); 3.69 (t, 2H, J = 3.3 Hz), 3H; 1.35 s, 3H.

*General procedure for the synthesis of 2-((2-amino-6-oxo-1,6-dihydro-9H-purin-9-yl)methoxy)ethyl 2-(((2R,3S,4R,5R)-5-(2,4-dioxo-3,4-dihydropyrimidin-1(2H)-yl)-3,4-dihydroxytetrahydrofuran-2-yl)methoxy)acetate (ACV\_URD1)*

To a cold solution (0 °C) of compound **6** (250 mg, 0.45 mmol, 1 equiv) in CF<sub>3</sub>COOH/MeOH (10 mL) was stirred at room temperature for 10 hours. After completion of the reaction (monitored by TLC) the mixture was concentrated under reduced pressure. The residue was purified over silica gel column (EtOAc/MeOH 50%) to afford the white solid ACV\_URD1 (225 mg, 90%). <sup>1</sup>H NMR (400 MHz, DMSO-d<sub>6</sub>): 10.6 (br, 1H), 9.30 (s, 1H); 7.83 (s,

1H); 7.30 (d, 1H, J = 7.9); 6.52 (s, 2H); 5.91 (s, 1H); 5.78 (d, 1H, J = 7.8); 5.34 (s, 2H); 4.48 d, (1H, J = 6.4); 4.85 (t, 1H, J = 3.8); 4.27 (q, 1H, J = 4.9); 4.30 (t, 2H, J = 3.3 Hz); 4.17–3.66 (m, 2H); 3.34 (s, 2H); 3.72 (t, 2H, J = 3.4 Hz).

*General procedure for the synthesis of 2-((2-amino-6-oxo-1,6-dihydro-9H-purin-9-yl)methoxy)ethyl carbonochloridate (7b)*

To a solution of ACV (237.76 mg, 0.83 mmol, 1 equiv) and Cs<sub>2</sub>CO<sub>3</sub> (344 mg, 1.06 mmol, 1 equiv) in DMF (3 mL) was added of Triphosgene (313 mg, 1.06 mmol, 1 equiv). The reaction was stirred for 2 hours at room temperature. After completing the reaction (monitored by TLC), the mixture was directly used in the subsequent reaction.

*General procedure for the synthesis of 2-((2-amino-6-oxo-1,6-dihydro-9H-purin-9-yl)methoxy)ethyl ((3aR,4R,6R,6aR)-6-(2,4-dioxo-3,4-dihydropyrimidin-1(2H)-yl)-2,2-dimethyltetrahydrofuro[3,4-d][1,3]dioxol-4-yl)methyl) carbonate (8b)*

A solution of compound 7 (302 mg, 0.83 mmol, 1 equiv) in DMF and Cs<sub>2</sub>CO<sub>3</sub> (270 mg, 0.30 mmol, 1 equiv) was added solution of compound 1 (235.72 mg, 0.83 mmol, 1 equiv) in DMF dry (2 mL) dropwise at 0 °C under nitrogen atmosphere. The resulting mixture was stirred for 24 h at room temperature. The residue was purified over silica gel column (EtOAc/MeOH 30%) to afford the white solid compound 8 (376 mg, 70%).  
<sup>1</sup>H NMR (400 MHz, DMSO-d<sub>6</sub>): 10.6 (br, 1H), 9.30 (s, 1H); 7.83 (s, 1H); 7.30 (d, 1H, J = 7.9); 6.55 (s, 2H); 5.95 (s, 1H); 5.80 (d, 1H, J = 7.8); 5.36 (s, 2H); 5.08 d, (1H, J = 6.4); 4.85 (t, 1H, J = 3.9); 4.27 (q, 1H, J = 4.9); 4.25–3.75 (m, 2H); 3.34 (s, 2H); 3.76 (t, 2H, J = 3.3 Hz); 1.55 s, 3 H; 1.34 s, 3H.

*General procedure for the synthesis of 2-((2-amino-6-oxo-1,6-dihydro-9H-purin-9-yl)methoxy)ethyl ((2R,3S,4R,5R)-5-(2,4-dioxo-3,4-*



*dihydropyrimidin-1(2H)-yl)-3,4-dihydroxytetrahydrofuran-2-yl)methyl carbonate (ACV\_URD3)*

To a cold solution (0 °C) of compound **8** (250 mg, 0.87 mmol, 1 equiv) in CF<sub>3</sub>COOH/MeOH (10 mL) was stirred at room temperature for 10 hours. After completion of the reaction (monitored by TLC) the mixture was concentrated under reduced pressure. The residue was purified over silica gel column (EtOAc/MeOH 50%) to afford the white solid **ACV\_URD3** (235 mg, 94%). <sup>1</sup>H NMR (400 MHz, DMSO-d<sub>6</sub>): 10.7 (br, 1H), 9.34 (s, 1H); 7.83 (s, 1H); 7.31 (d, 1H, J = 7.9); 6.55 (s, 2H); 5.91 (s, 1H); 5.78 (d, 1H, J = 7.8); 5.34 (s, 2H); 4.48 d, (1H, J = 6.4); 4.85 (t, 1H, J = 3.8); 4.27 (q, 1H, J = 4.9); 4.41 (t, 2H, J = 3.3 Hz); 4.22–3.75 (m, 2H); 3.88 (t, 2H, J = 3.4 Hz).

*General procedure for the synthesis of (2R,3R,4R,5R)-2-((((2-((2-amino-6-oxo-1,6-dihydro-9H-purin-9-yl)methoxy)ethoxy)carbonyl)oxy)methyl)-5-(2,4-dioxo-3,4-dihydropyrimidin-1(2H)-yl)tetrahydrofuran-3,4-diyl diacetate (ACV\_URD5)*

A solution of acetic anhydride (0.030 ml, 0.20 mmol, 1 equiv) and pyridine (0.016 ml, 0.20 mmol, 1equiv) in DMF dry (4 mL) was added to **ACV\_URD3** (100 mg, 0.20 mmol, 1 equiv). The mixture was stirred at room temperature for 10 hour. After the mixture had cooled, the solvent was evaporated under reduced pressure to provide a residue that was columnchromatographed (EtOAc/MeOH 25%) to afford the white solid **ACV\_URD5** (98 mg, 84%). <sup>1</sup>H NMR (400 MHz, DMSO-d<sub>6</sub>): 10.7 (br, 1H), 9.34 (s, 1H); 7.83 (s, 1H); 7.31 (d, 1H, J = 7.9); 6.55 (s, 2H); 5.91 (s, 1H); 5.78 (d, 1H, J = 7.8); 5.34 (s, 2H); 4.48 d, (1H, J = 6.4); 4.81 (t, 1H, J = 3.7); 4.27 (q, 1H, J = 4.9); 4.40 (t, 2H, J = 3.3 Hz); 4.18–3.71 (m, 2H); 3.79 (t, 2H, J = 3.4 Hz); 2.34 (s, 3H); 2.21 (s, 3H).

*General procedure for the synthesis of 2-((2-amino-6-oxo-1,6-dihydro-9H-purin-9-yl)methoxy)ethyl (((3aR,4R,6R,6aR)-6-(2,4-dioxo-3,4-*

*dihydropyrimidin-1(2H)-yl)-2,2-dimethyltetrahydrofuro[3,4-d][1,3]dioxol-4-yl)methyl)glycinate* **5(9b)**

Compound **5** (150 mg, 0.31 mmol, 1 equiv) and Cs<sub>2</sub>CO<sub>3</sub> (101 mg, 0.31 mmol, 1 equiv) were dissolved in DMF dry (4 mL). To this solution of compound **7** (107 mg, 0.31 mmol, 1 equiv) in DMF dry (2 mL) was added dropwise at 0 °C under nitrogen atmosphere. The resulting mixture was stirred for 24 h and was evaporated under reduced pressure. The residue was purified over silica gel column (EtOAc/MeOH 40%) to afford the white solid compound **9** (180 mg, 72%). <sup>1</sup>H NMR (400 MHz, DMSO-d<sub>6</sub>): 10.6 (br, 1H), 9.30 (s, 1H); 7.83 (s, 1H); 7.30 (d, 1H, J = 7.9); 6.52 (s, 2H); 5.91 (s, 1H); 5.78 (d, 1H, J = 7.8); 5.36 (s, 2H); 5.00 (d, 1H, J = 6.4); 4.82 (t, 1H, J = 3.9); 4.24 (q, 1H, J = 4.9); 4.13–3.62 (m, 2H); 4.01 (t, 2H, J = 3.3 Hz); 3.34 (s, 2H); 3.69 (t, 2H, J = 3.3 Hz), 1.55 (s, 3 H); 1.34 (s, 3H).

*General procedure for the synthesis of 2-(((2R,3S,4R,5R)-5-(2,4-dioxo-3,4-dihydropyrimidin-1(2H)-yl)-3,4-dihydroxytetrahydrofuran-2-yl)methyl)glycinate* (ACV\_URD2)

To a cold solution (0 °C) of compound **9** (100 mg, 0.18 mmol, 1 equiv) in CF<sub>3</sub>COOH/MeOH (10 mL) was stirred at room temperature for 10 hours. After completion of the reaction (monitored by TLC) the mixture was concentrated under reduced pressure. The residue was purified over silica gel column (EtOAc/MeOH 55%) to afford the white solid **ACV\_URD2** (235 mg, 94%). <sup>1</sup>H NMR (400 MHz, DMSO-d<sub>6</sub>): 10.6 (br, 1H), 9.30 (s, 1H); 7.83 (s, 1H); 7.30 (d, 1H, J = 7.9); 6.52 (s, 2H); 5.91 (s, 1H); 5.78 (d, 1H, J = 7.8); 5.38 (s, 2H); 5.00 (d, 1H, J = 6.4); 4.92 (t, 1H, J = 3.9); 4.24 (q, 1H, J = 4.9); 4.19–3.62 (m, 2H); 4.05 (t, 2H, J = 3.3 Hz); 3.34 (s, 2H); 3.65 (t, 2H, J = 3.3 Hz);

---

*General procedure for the synthesis of 2-((2-amino-6-oxo-1,6-dihydro-9H-purin-9-yl)methoxy)ethyl (((3aR,4R,6R,6aR)-6-(2,4-dioxo-3,4-dihydropyrimidin-1(2H)-yl)-2,2-dimethyltetrahydrofuro[3,4-d][1,3]dioxol-4-yl)methyl)carbamate (10b)*

A solution of compound **7** (200 mg, 0.70 mmol, 1 equiv) in DMF and Cs<sub>2</sub>CO<sub>3</sub> (270 mg, 0.30 mmol, 1 equiv) was added solution of compound **5** (235.72 mg, 0.70 mmol, 1 equiv) in DMF dry (2 mL) dropwise at 0 °C under nitrogen atmosphere. The resulting mixture was stirred for 24 h at room temperature. The residue was purified over silica gel column (EtOAc/MeOH 30%) to afford the white solid compound **8** (376 mg, 70%). <sup>1</sup>H NMR (400 MHz, DMSO-d<sub>6</sub>): 10.5 (br, 1H), 9.37 (s, 1H); 7.83 (s, 1H); 7.35 (d, 1H, J = 7.9); 6.74 (s, 1H); 6.55 (s, 2H); 5.95 (s, 1H); 5.80 (d, 1H, J = 7.8); 5.36 (s, 2H); 5.08 d, (1H, J = 6.4); 4.65 (t, 1H, J = 3.9); 4.11 (q, 1H, J = 4.9); 4.25–3.75 (m, 2H); 3.34 (s, 2H); 3.77 (t, 2H, J = 3.3 Hz); 1.57 s, 3 H; 1.33 s, 3H.

*General procedure for the synthesis of 2-((2-amino-6-oxo-1,6-dihydro-9H-purin-9-yl)methoxy)ethyl (((2R,3S,4R,5R)-5-(2,4-dioxo-3,4-dihydropyrimidin-1(2H)-yl)-3,4-dihydroxytetrahydrofuran-2-yl)methyl)carbamate (ACV\_URD4)*

To a cold solution (0 °C) of compound **10** (100 mg, 0.18 mmol, 1 equiv) in CF<sub>3</sub>COOH/MeOH (10 mL) was stirred at room temperature for 10 hours. After completion of the reaction (monitored by TLC) the mixture was concentrated under reduced pressure. The residue was purified over silica gel column (EtOAc/MeOH 55%) to afford the white solid ACV\_URD2 (95 mg, 96%). <sup>1</sup>H NMR (400 MHz, DMSO-d<sub>6</sub>): 10.5 (br, 1H), 9.37 (s, 1H); 7.83 (s, 1H); 7.35 (d, 1H, J = 7.9); 6.74 (s, 1H); 6.55 (s, 2H); 5.95 (s, 1H); 5.89 (d, 1H, J = 7.8); 5.35 (s, 2H); 5.11 d, (1H, J = 6.4); 4.67 (t, 1H, J = 3.9); 4.18 (q, 1H, J = 4.9); 4.35–3.77 (m, 2H); 3.34 (s, 2H); 3.55 (t, 2H, J = 3.3 Hz);

---

---

*General procedure for the synthesis of (2R,3R,4R,5R)-2-((((2-((2-amino-6-oxo-1,6-dihydro-9H-purin-9-yl)methoxy)ethoxy)carbonyl)oxy)methyl)-5-(2,4-dioxo-3,4-dihydropyrimidin-1(2H)-yl)tetrahydrofuran-3,4-diyl diacetate (ACV\_URD6)*

A solution of acetic anhydride (0.029 ml, 0.19 mmol, 1 equiv) and pyridine (0.015 ml, 0.19 mmol, 1equiv) in DMF dry (4 ml) was added to **ACV\_URD4** (95 mg, 0.19 mmol, 1 equiv). The mixture was stirred at room temperature for 10 hour. After the mixture had cooled, the solvent was evaporated under reduced pressure to provide a residue that was column chromatographed (EtOAc/MeOH 45%) to afford the white solid **ACV\_URD6** (95 mg, 87%). <sup>1</sup>H NMR (400 MHz, DMSO-d<sub>6</sub>): 10.4 (br, 1H), 9.38 (s 1H); 7.83 (s, 1H); 7.35 (d, 1H, J = 7.9); 6.74 (s, 1H); 6.55 (s, 2H); 5.95 (s, 1H); 5.85 (d, 1H, J = 7.8); 5.35 (s, 2H); 5.17 d, (1H, J = 6.4); 4.62 (t, 1H, J = 3.9); 4.18 (q, 1H, J = 4.9); 4.35–3.77 (m, 2H); 3.37 (s, 2H); 3.56 (t, 2H, J = 3.3 Hz); 2.39 (s, 3H); 2.28 (s, 3H).

#### LIGAND PREPARATION

The 2D chemical structures were built by Marvin Sketch, and all the structures were subjected to molecular mechanics energy minimization using the MMFF94 force field present in the same software.<sup>1</sup> Once obtained the 3D structures of all compounds; geometry was also optimized at the semi-empirical level of theory using the PM3 Hamiltonian, as implemented in the MOPAC 2016 package (vMOPAC2016).<sup>167</sup> The protonation states of the molecules were calculated, assuming a pH of 7.4.

#### RECEPTOR PREPARATION

The receptor's crystalline structure was downloaded from the PDB database (ID PDB: 4PD6). This deposition, published by Lee, SY et al.,<sup>168</sup> contains the homotrimer receptor bound with three ligand uridine molecules. The ligand (uridine) was removed, and the whole homotrimer was included in

---

the 1-palmitoyl-2-oleoyphosphatidylcholine (POPC) lipid bilayer using the Orientation of Proteins in Membranes database for proper membrane positioning. The missing residues at the *N*-terminus of vcCNT in the crystal structure were constructed using the YASARA Structure package (15.3.8).<sup>169</sup>

### **HOMOLOGY MODEL**

All of the simulations and molecular modeling experiments have been conducted with YASARA software (v. 18.4.24, YASARA Biosciences GmbH, Vienna, Austria). The homology model was built starting from the Q9Y289 (SC5A6\_HUMAN) sequence deposited in the UniProt Knowledgebase (<https://www.uniprot.org/uniprot/>) and using the crystallographic structures corresponding to the following PDB IDs as templates: 5NVA, 2XQ2, 3DH4, and 6C3I. To these structures have been added the best two structures obtained by the evolutionary coupling analysis, which were executed with the EVfold web-server (<http://evfold.org/evfold-web/newprediction.do>), and the ensemble has been processed with the hm\_build macro of YASARA. In the end, an optimized hybrid model was built by iteratively replacing bad regions in the top-scoring model with the corresponding fragments from the other models.

This model was docked with the hSMVT transporter ligand biotin (see below for details), and the best pose ligand/receptor complex structure was then immersed in a simulated endoplasmic reticulum membrane (see below for details) in physiological environment conditions and subjected to a molecular dynamics (MD) simulation of 10 ns to accommodate the ligand.

### **DOCKING PROTOCOL**

Docking experiments were effectuated, employing the AutoDock (4.2.5.1, The Scripps Research Institute, San Diego, California Jupiter, Florida, US)

---

software implemented in YASARA. Given that water molecules are directly involved in complex stabilization, they were considered in the docking process. All protein amino acidic residues were kept rigid, whereas all single bonds of the ligands were treated as fully flexible. The maps were generated by the program AutoGrid (4.2.5.2) with a spacing of 0.375 Å and dimensions that encompass all atoms extending 5 Å from the surface of the structure of centered at residue Ser81 for hSMVT ( $x = -2.79$ ,  $y = 2.11$ , and  $z = -3.02$ ) and Glu332 for cvCNT transport ( $x = 15.05$ ,  $y = 4.19$ , and  $z = 10.94$ ) and coordinates with a grid size of  $20 \times 20 \times 20 \text{ \AA}^3$ . All the parameters were inserted at their default settings. In the docking tab, the macromolecule and ligand are selected, and GA parameters are set as  $ga\_runs = 100$ ,  $ga\_pop\_size = 150$ ,  $ga\_num\_evals = 25000000$ ,  $ga\_num\_generations = 27000$ ,  $ga\_elitism = 1$ ,  $ga\_mutation\_rate = 0.02$ ,  $ga\_crossover\_rate = 0.8$ ,  $ga\_crossover\_mode = \text{two points}$ ,  $ga\_cauchy\_alpha = 0.0$ ,  $ga\_cauchy\_beta = 1.0$ , number of generations for picking worst individual = 10.

## MOLECULAR DYNAMICS SIMULATIONS

The MD simulations for the hSMVT-ligand and cvCNT-ligand complexes are described below.

For MD, membrane simulation was set up automatically by first scanning the protein for exposed transmembrane helices [*i.e.*, helices longer than 16 residues, with more than seven hydrophobic residues and more than three exposed ones (accessible side-chain surface area >30% of maximum)]. The major axis vectors of these helices (*i.e.*, the direction vectors of the least-squares lines through the  $C_{\alpha}$  atoms) were summed up to obtain the major axis of the protein, which was then oriented along the Y-axis, generally with respect to the plane of the membrane and the X-Z plane. The best shift of the membrane along this major axis was obtained by scanning the protein for the region with the largest number of exposed hydrophobic residues

---

(see definition above) and a width of 28 Å (corresponding to the membrane core).

Having placed an equilibrated membrane structure (consisting of 55% of phosphatidylcholine, 30% of phosphatidylethanolamine, 10% of phosphatidylserine, and 5% of phosphatidylinositol molecules) at this location named 'MemCenterY', the system was enclosed in a simulation cell of size [X\*Y\*Z] Å, the protein was temporarily scaled by 0.9 along the X–Z axes, and then, strongly clashing membrane lipids were deleted (lipids with an atom closer than 0.75 Å to a protein atom).<sup>170</sup>

The temporary protein scaling needed to avoid the deletion of too many lipids around the protein was then slowly removed during a short simulation at 298 K in vacuum. The protein (with all of the atoms kept fixed) was scaled by 1.02 along the X–Z axes every 200 femtoseconds, while the membrane was allowed to move but was restrained to ideal geometry (by pulling lipid residues with an atom further than 21.5 Å away from MemCenterY back into the membrane, and by pushing phosphorus atoms closer than 14 Å to MemCenterY back outwards). The force field was AMBER14, with Lipid17/GAFF2/AM1BCC parameters for non-standard residues. As soon as the protein had reached its original size again, the protein side-chain pKas were predicted, protonation states were assigned according to pH 7.4, and the simulation cell was filled with water, 0.9% NaCl, and counter ions. The main simulation was then run with PME, and an 8.0 Å cutoff for non-bonded real space forces, a four fs time-step, constrained hydrogen atoms, and at constant pressure and temperature (NPT ensemble), as described in detail previously. During the initial 250 picoseconds, the membrane was restrained to avoid distortions while the simulation cell adapted to the pressure exerted by the membrane (see above); additionally, water molecules that got closer than 14 Å to

---

MemCenterY were pushed outside. The MD simulation was then launched, using the NVT ensemble at 298 K and integration time steps for intramolecular and intermolecular forces every 1.25 and 2.5 fs, respectively. The source code of this simulation protocol and visualizations of the individual steps can be found at [www.yasara.org/membranemd](http://www.yasara.org/membranemd). Finally, 100 ns MD simulations without any restrictions were conducted, and the conformations of each system were recorded every 200 ps. All trajectory analyzes were performed using YASARA source codes.

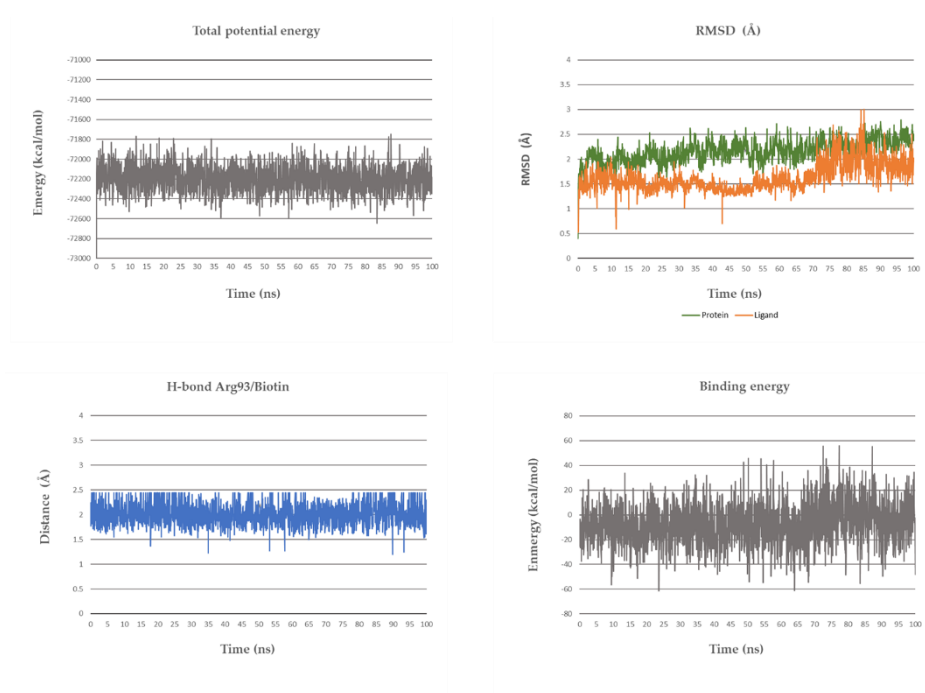


**Figure 5.1. Biotin.** Total energy (up-left) and RMSDs (up-right) of enzyme and its complexes with the ligand. Distance variation of the H-bond during the MD with the residue Arg93. (down-left) and binding energy (downright) according to the Poisson-Boltzmann approach (PBS).



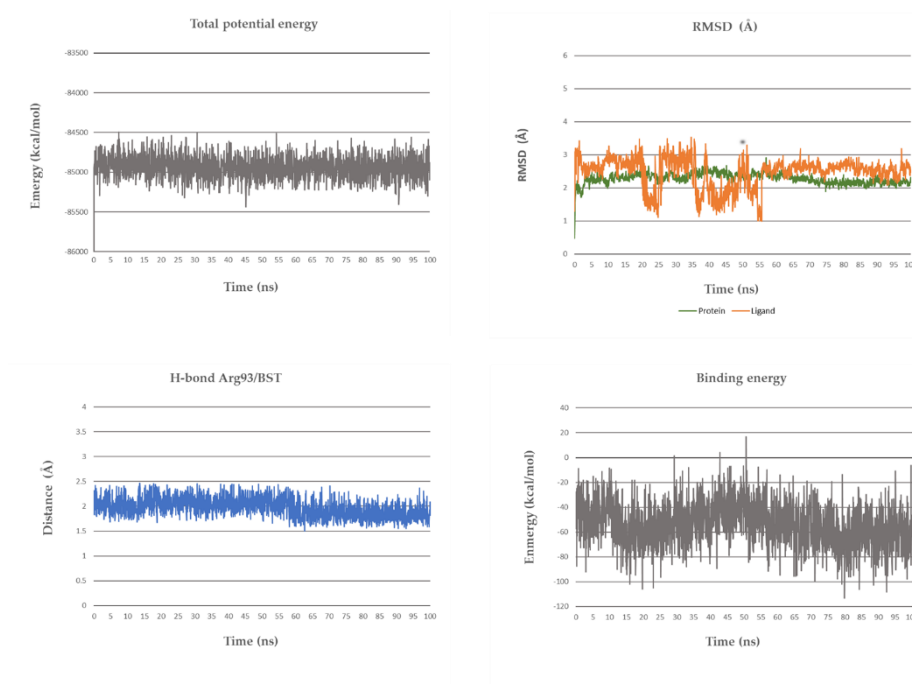


**Figure 5.2.** BST Total energy (up-left) and RMSDs (up-right) of enzyme and its complexes with the ligand. Distance variation of the H-bond during the MD with the residue Arg93. (down-left) and binding energy (downright) according to the Poisson-Boltzmann approach (PBS).

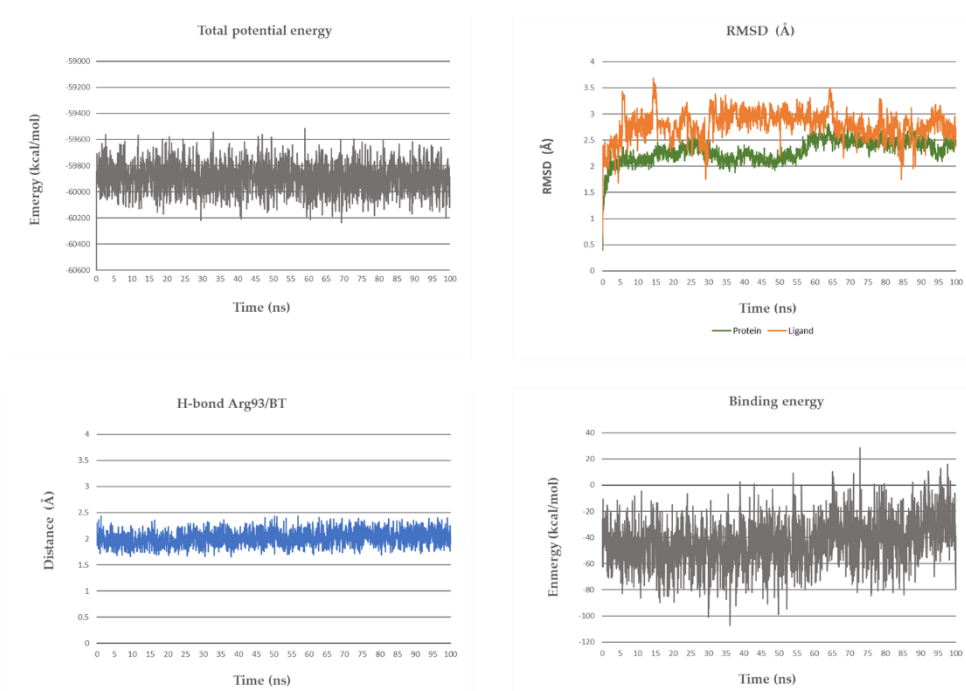


**Figure 5.3.** BT. Total energy (up-left) and RMSDs (up-right) of enzyme and its complexes with the ligand. Distance variation of the H-bond during the MD with the residue Arg93. (down-left) and binding energy (downright) according to the Poisson-Boltzmann approach (PBS).

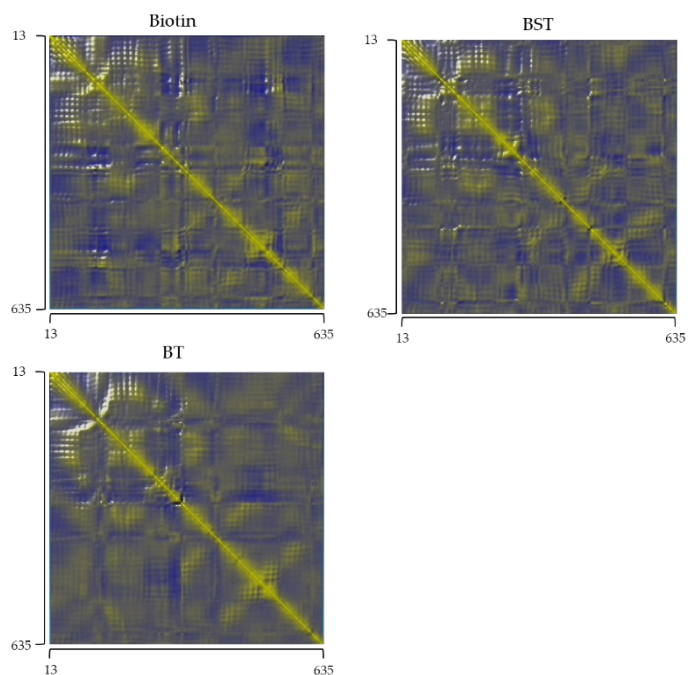


**Figure 5.4.** Dynamic cross-correlation matrix of **biotin**, **BST**, and **BT**. The DCCM is visualized with colors ranging from blue (-1, fully anti-correlated) to yellow (+1, fully correlated).

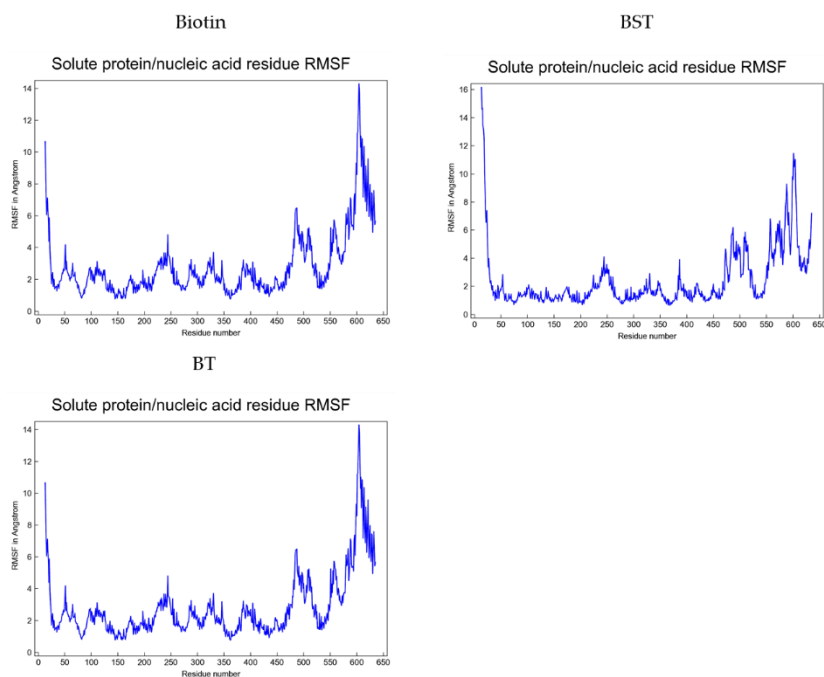


**Figure 5.5** The Root Mean Square Fluctuation [vertical axis] per solute protein/nucleic acid residue [horizontal axis] calculated from the average RMSF of the atoms constituting the residue of **biotin**, **BST**, and **BT**.

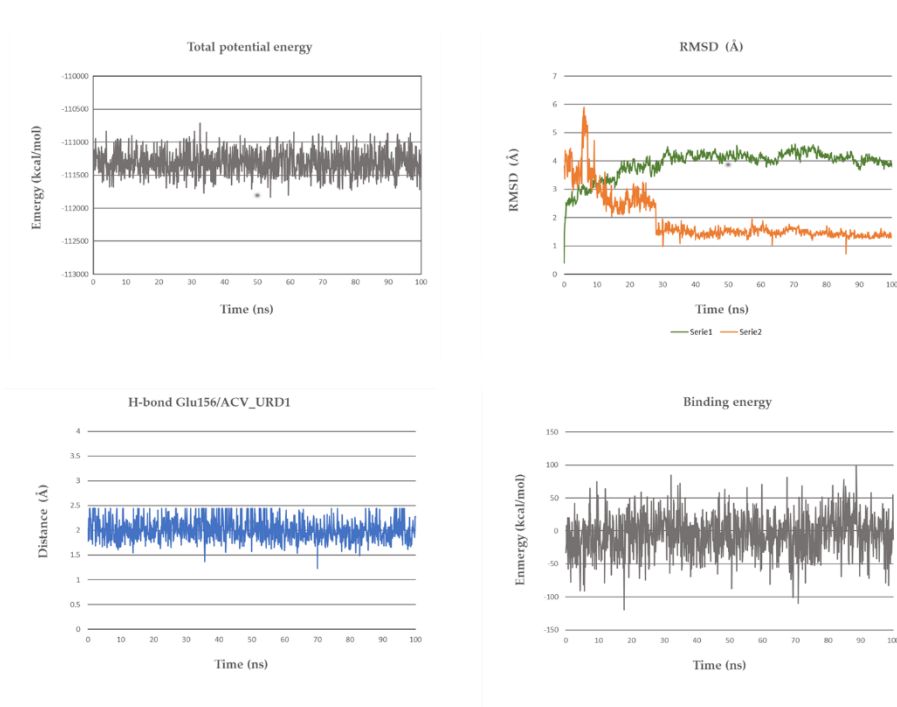


**Figure 5.6. ACV\_URD1.** Total energy (up-left) and RMSDs (up-right) of enzyme and its complexes with the ligand. Distance variation of the H-bond during the MD with the residue Glu156. (down-left) and binding energy (downright) according to the Poisson-Boltzmann approach (PBS).

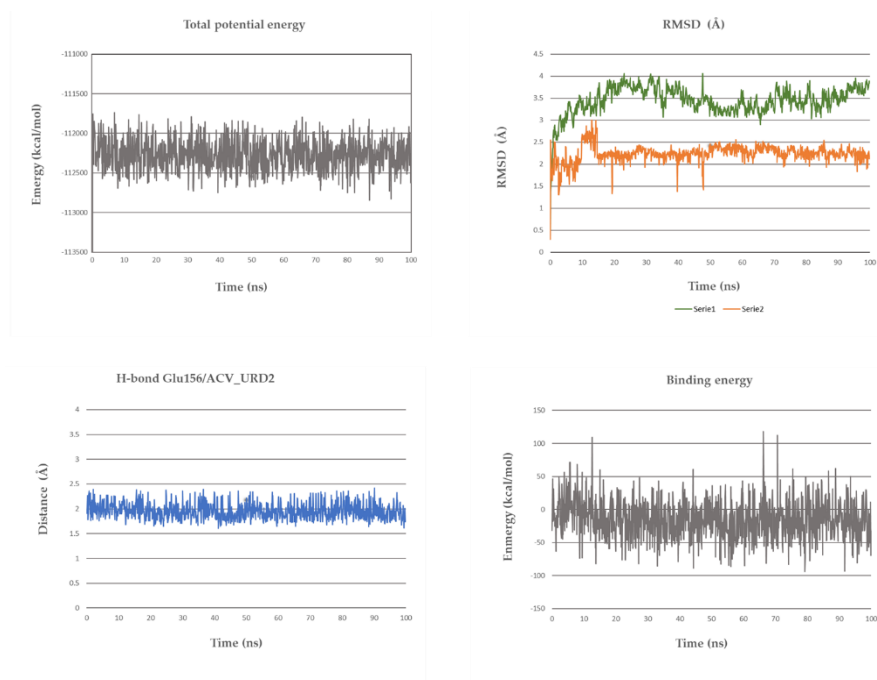


**Figure 5.7. ACV\_URD2.** Total energy (up-left) and RMSDs (up-right) of enzyme and its complexes with the ligand. Distance variation of the H-bond during the MD with the residue Glu156. (down-left) and binding energy (downright) according to the Poisson-Boltzmann approach (PBS).

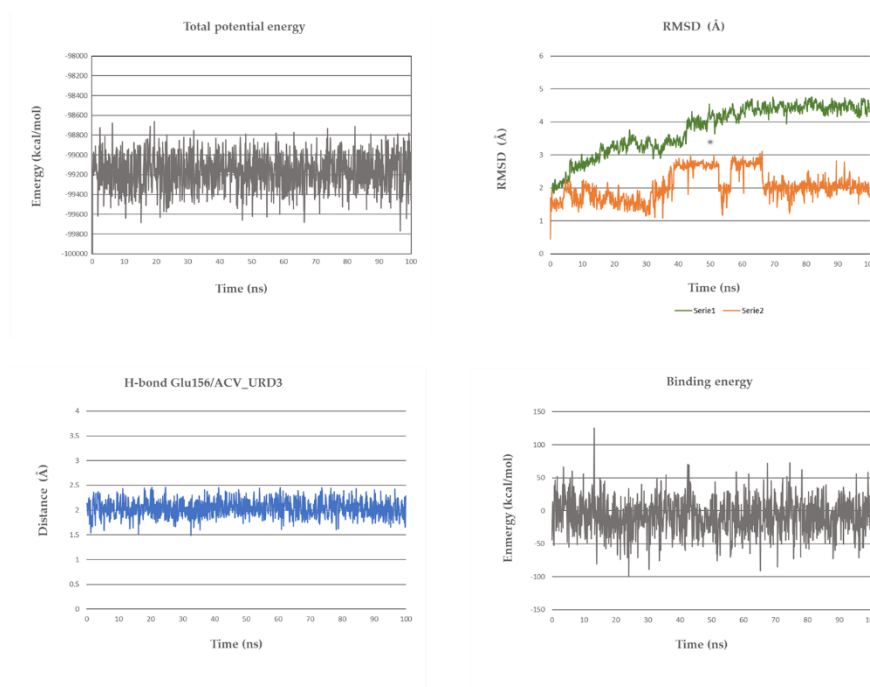


**Figure 5.8.** ACV\_URD3. Total energy (up-left) and RMSDs (up-right) of enzyme and its complexes with the ligand. Distance variation of the H-bond during the MD with the residue Glu156. (down-left) and binding energy (downright) according to the Poisson-Boltzmann approach (PBS).

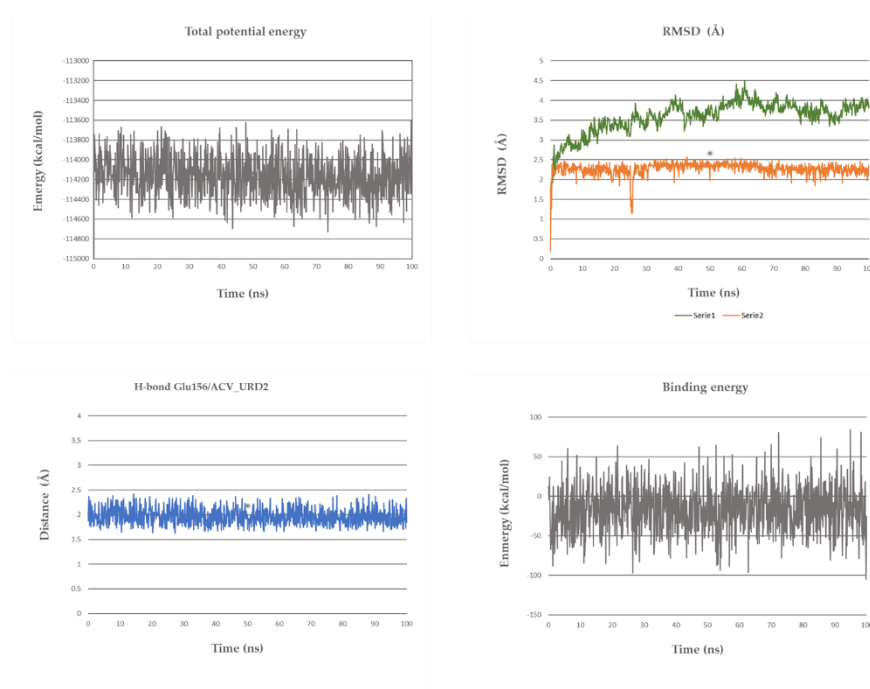


**Figure 5.9.** ACV\_URD4. Total energy (up-left) and RMSDs (up-right) of enzyme and its complexes with the ligand. Distance variation of the H-bond during the MD with the residue Glu156. (down-left) and binding energy (downright) according to the Poisson-Boltzmann approach (PBS).

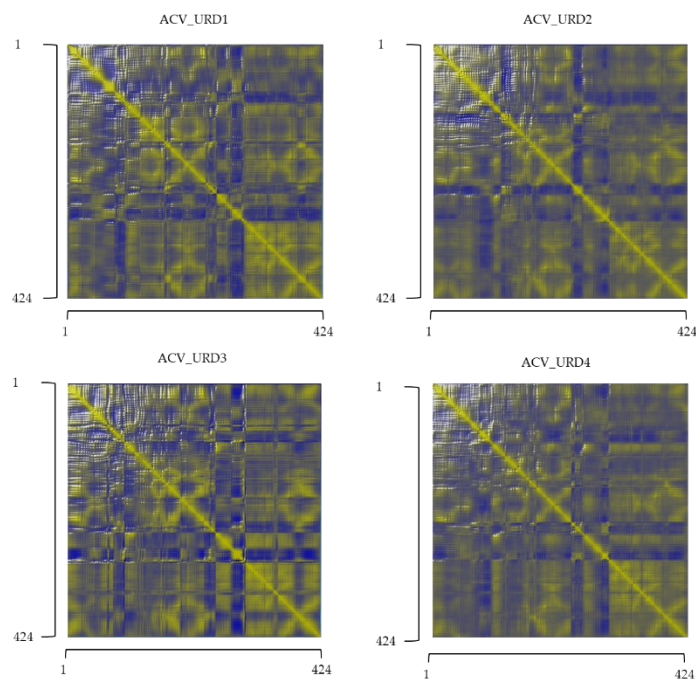


**Figure 5.10.** Dynamic cross-correlation matrix of compounds ACV\_URD 1-4. The DCCM is visualized with colors ranging from blue (-1, fully anti-correlated) to yellow (+1, fully correlated).

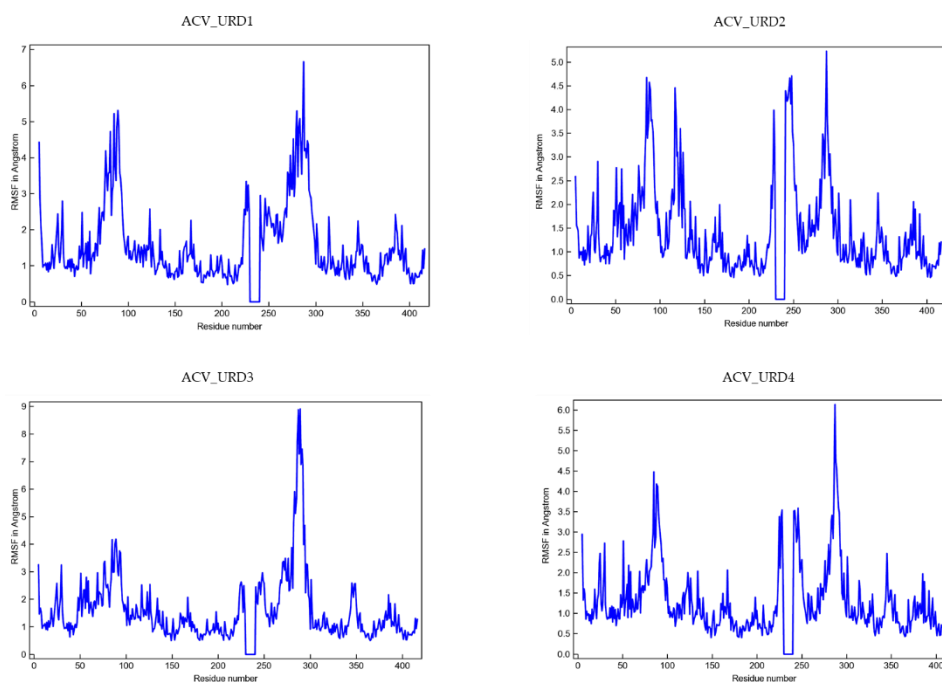


**Figure 5.11** The Root Mean Square Fluctuation [vertical axis] per solute protein/nucleic acid residue [horizontal axis] calculated from the average RMSF of the atoms constituting the residue of compounds ACV\_URD 1-4.

## REFERENCES

- 1 Albert, A. Chemical aspects of selective toxicity. *Nature* **182**, 421-422 (1958).
  - 2 Stella, V. *et al.* *Prodrugs Challenges and Rewards*. Vol. V (2007).
  - 3 Rautio, J. *et al.* Prodrugs: design and clinical applications. *Nat Rev Drug Discov* **7**, 255-270, doi:10.1038/nrd2468 (2008).
  - 4 Rautio, J., Meanwell, N. A., Di, L. & Hageman, M. J. The expanding role of prodrugs in contemporary drug design and development. *Nat Rev Drug Discov* **17**, 559-587, doi:10.1038/nrd.2018.46 (2018).
  - 5 Bodor, N. & Buchwald, P. Soft drug design: general principles and recent applications. *Med Res Rev* **20**, 58-101 (2000).
  - 6 Sun, H. Capture hydrolysis signals in the microsomal stability assay: molecular mechanisms of the alkyl ester drug and prodrug metabolism. *Bioorg Med Chem Lett* **22**, 989-995, doi:10.1016/j.bmcl.2011.12.005 (2012).
  - 7 Vane, J. R. & Botting, R. M. The mechanism of action of aspirin. *Thromb Res* **110**, 255-258 (2003).
  - 8 Sinkula, A. A. & Yalkowsky, S. H. Rationale for design of biologically reversible drug derivatives: prodrugs. *J Pharm Sci* **64**, 181-210 (1975).
  - 9 Stella, V. J. & Nti-Addae, K. W. Prodrug strategies to overcome poor water solubility. *Adv Drug Deliv Rev* **59**, 677-694, doi:10.1016/j.addr.2007.05.013 (2007).
  - 10 Browne, T. R., Kugler, A. R. & Eldon, M. A. Pharmacology and pharmacokinetics of fosphenytoin. *Neurology* **46**, S3-7 (1996).
  - 11 Tsuda, M. *et al.* Transport characteristics of a novel peptide transporter 1 substrate, antihypertensive drug midodrine, and its amino acid derivatives. *J Pharmacol Exp Ther* **318**, 455-460, doi:10.1124/jpet.106.102830 (2006).
  - 12 Nutt, J. G. & Woodward, W. R. Levodopa pharmacokinetics and pharmacodynamics in fluctuating parkinsonian patients. *Neurology* **36**, 739-744 (1986).
  - 13 Nutt, J. G., Woodward, W. R., Hammerstad, J. P., Carter, J. H. & Anderson, J. L. The "on-off" phenomenon in Parkinson's disease. Relation to levodopa absorption and transport. *N Engl J Med* **310**, 483-488, doi:10.1056/NEJM198402233100802 (1984).
  - 14 Persson, B., Pahlm, O. & GnossPELLIUS, Y. Oral bambuterol versus terbutaline in patients with asthma. *Current Therapeutic Research* **65**, 457-465.
  - 15 McCLURE, D. A. The Effect of a Pro-drug of Epinephrine (Dipivalyl Epinephrine) in Glaucoma—General Pharmacology, Toxicology, and Clinical Experience. *Pro-drugs as Novel Drug Delivery Systems* **14**, 224-235 (1975).
  - 16 DelMonte, D. W. & Kim, T. Anatomy and physiology of the cornea. *J Cataract Refract Surg* **37**, 588-598, doi:10.1016/j.jcrs.2010.12.037 (2011).
  - 17 Komai, Y. & Ushiki, T. The three-dimensional organization of collagen fibrils in the human cornea and sclera. *Invest Ophthalmol Vis Sci* **32**, 2244-2258 (1991).
-

- 
- 18 Dingeldein, S. A. & Klyce, S. D. Imaging of the cornea. *Cornea* **7**, 170-182 (1988).
- 19 Iveson-Iveson, J. [Anatomy and physiology of the eye]. *Xianggang Hu Li Za Zhi*, 47-50 (1983).
- 20 Cunha-Vaz, J. G. The blood-ocular barriers: past, present, and future. *Doc Ophthalmol* **93**, 149-157 (1997).
- 21 Mannermaa, E., Vellonen, K. S. & Urtti, A. Drug transport in corneal epithelium and blood-retina barrier: emerging role of transporters in ocular pharmacokinetics. *Adv Drug Deliv Rev* **58**, 1136-1163, doi:10.1016/j.addr.2006.07.024 (2006).
- 22 Tamm, E. R., Braunger, B. M. & Fuchshofer, R. Intraocular Pressure and the Mechanisms Involved in Resistance of the Aqueous Humor Flow in the Trabecular Meshwork Outflow Pathways. *Prog Mol Biol Transl Sci* **134**, 301-314, doi:10.1016/bs.pmbts.2015.06.007 (2015).
- 23 Basu, S. K., Haworth, I. S., Bolger, M. B. & Lee, V. H. Proton-driven dipeptide uptake in primary cultured rabbit conjunctival epithelial cells. *Invest Ophthalmol Vis Sci* **39**, 2365-2373 (1998).
- 24 Halestrap, A. P. & Price, N. T. The proton-linked monocarboxylate transporter (MCT) family: structure, function and regulation. *Biochem J* **343 Pt 2**, 281-299 (1999).
- 25 Prasad, P. D. *et al.* Molecular and functional characterization of the intestinal Na<sup>+</sup>-dependent multivitamin transporter. *Arch Biochem Biophys* **366**, 95-106, doi:10.1006/abbi.1999.1213 (1999).
- 26 Ghosal, A. & Said, H. M. Structure-function activity of the human sodium-dependent multivitamin transporter: role of His<sup>185</sup>; and His<sup>209</sup>; and His<sup>(2)(5)(4)</sup>. *Am J Physiol Cell Physiol* **300**, C97-104, doi:10.1152/ajpcell.00398.2010 (2011).
- 27 Lee, T. K., Koh, A. S., Cui, Z., Pierce, R. H. & Ballatori, N. N-glycosylation controls functional activity of Oatp1, an organic anion transporter. *Am J Physiol Gastrointest Liver Physiol* **285**, G371-381, doi:10.1152/ajpgi.00358.2002 (2003).
- 28 Roth, M., Obaidat, A. & Hagenbuch, B. OATPs, OATs and OCTs: the organic anion and cation transporters of the SLCO and SLC22A gene superfamilies. *Br J Pharmacol* **165**, 1260-1287, doi:10.1111/j.1476-5381.2011.01724.x (2012).
- 29 Hrycyna, C. A. *et al.* Structural flexibility of the linker region of human P-glycoprotein permits ATP hydrolysis and drug transport. *Biochemistry* **37**, 13660-13673, doi:10.1021/bi9808823 (1998).
- 30 Liederer, B. M. & Borchardt, R. T. Enzymes involved in the bioconversion of ester-based prodrugs. *J Pharm Sci* **95**, 1177-1195, doi:10.1002/jps.20542 (2006).
- 31 Macha, S., Duvvuri, S. & Mitra, A. K. Ocular disposition of novel lipophilic diester prodrugs of ganciclovir following intravitreal administration using microdialysis. *Curr Eye Res* **28**, 77-84, doi:10.1076/ceyr.28.2.77.26233 (2004).
- 32 Tirucherai, G. S., Dias, C. & Mitra, A. K. Corneal permeation of ganciclovir: mechanism of ganciclovir permeation enhancement by acyl ester prodrug design. *J Ocul Pharmacol Ther* **18**, 535-548, doi:10.1089/108076802321021081 (2002).
-

- 
- 33 Russo, A., Riva, I., Pizzolante, T., Noto, F. & Quaranta, L. Latanoprost ophthalmic solution in the treatment of open angle glaucoma or raised intraocular pressure: a review. *Clin Ophthalmol* **2**, 897-905 (2008).
- 34 Suzuki, E. R., Jr. & Suzuki, C. L. Efficacy and safety of travoprost alone or in combination with other agents for glaucoma and ocular hypertension: patient considerations. *Clin Ophthalmol* **4**, 1165-1171, doi:10.2147/OPTH.S6289 (2010).
- 35 Sjoquist, B. & Stjernschantz, J. Ocular and systemic pharmacokinetics of latanoprost in humans. *Surv Ophthalmol* **47 Suppl 1**, S6-12 (2002).
- 36 Juntunen, J., Vepsalainen, J., Niemi, R., Laine, K. & Jarvinen, T. Synthesis, in vitro evaluation, and intraocular pressure effects of water-soluble prodrugs of endocannabinoid noladin ether. *J Med Chem* **46**, 5083-5086, doi:10.1021/jm030877j (2003).
- 37 Simplicio, A. L., Clancy, J. M. & Gilmer, J. F. Prodrugs for amines. *Molecules* **13**, 519-547 (2008).
- 38 Farag, H. H. *et al.* Ocular-specific chemical delivery systems of betaxolol for safe local treatment of glaucoma. *Drug Des Discov* **15**, 117-130 (1997).
- 39 Bodor, N. Retrometabolic approaches for drug design and targeting. *Pharmazie* **52**, 491-494 (1997).
- 40 Bodor, N., ElKoussi, A., Kano, M. & Nakamura, T. Improved delivery through biological membranes. 26. Design, synthesis, and pharmacological activity of a novel chemical delivery system for beta-adrenergic blocking agents. *J Med Chem* **31**, 100-106 (1988).
- 41 Hans, B. & Marianne, J. Pro-drugs as drug delivery systems XX. Oxazolidines as potential pro-drug types for  $\beta$ -aminoalcohols, aldehydes or ketones. *International Journal of Pharmaceutics* **10**, 165-175 (1982).
- 42 Drustrup, J. & Bundgaard, L. Prodrug forms for the sulfonamide group. III. Chemical and enzymatic hydrolysis of various N-sulfonyl imidates—a novel prodrug form for a sulfonamide group or an ester function. *International Journal of Pharmaceutics* **51**, 27-38 (1989).
- 43 Garcia, G. A., Ngai, P., Mosaed, S. & Lin, K. Y. Critical evaluation of latanoprostene bunod in the treatment of glaucoma. *Clin Ophthalmol* **10**, 2035-2050, doi:10.2147/OPTH.S103985 (2016).
- 44 Janoria, K. G., Boddu, S. H., Natesan, S. & Mitra, A. K. Vitreal pharmacokinetics of peptide-transporter-targeted prodrugs of ganciclovir in conscious animals. *J Ocul Pharmacol Ther* **26**, 265-271, doi:10.1089/jop.2009.0123 (2010).
- 45 Kansara, V., Hao, Y. & Mitra, A. K. Dipeptide monoester ganciclovir prodrugs for transscleral drug delivery: targeting the oligopeptide transporter on rabbit retina. *J Ocul Pharmacol Ther* **23**, 321-334, doi:10.1089/jop.2006.0150 (2007).
- 46 Patel, K. *et al.* Synthesis, physicochemical properties and antiviral activities of ester prodrugs of ganciclovir. *Int J Pharm* **305**, 75-89, doi:10.1016/j.ijpharm.2005.08.024 (2005).
- 47 Janoria, K. G. *et al.* Vitreal pharmacokinetics of biotinylated ganciclovir: role of sodium-dependent multivitamin transporter expressed on retina. *J Ocul Pharmacol Ther* **25**, 39-49, doi:10.1089/jop.2008.0040 (2009).
- 48 Vadlapudi, A. D. *et al.* Targeted lipid based drug conjugates: a novel strategy for drug delivery. *Int J Pharm* **434**, 315-324, doi:10.1016/j.ijpharm.2012.05.033 (2012).
-



- 49 Carl, P. L., Chakravarty, P. K. & Katzenellenbogen, J. A. A novel connector linkage applicable in prodrug design. *J Med Chem* **24**, 479-480 (1981).
- 50 Papot, S., Tranoy, I., Tillequin, F., Florent, J. C. & Gesson, J. P. Design of selectively activated anticancer prodrugs: elimination and cyclization strategies. *Curr Med Chem Anticancer Agents* **2**, 155-185 (2002).
- 51 Lee, H. Y., Jiang, X. & Lee, D. Kinetics of self-immolation: faster signal relay over a longer linear distance? *Org Lett* **11**, 2065-2068, doi:10.1021/ol900433g (2009).
- 52 Alouane, A. *et al.* Disassembly kinetics of quinone-methide-based self-immolative spacers that contain aromatic nitrogen heterocycles. *Chem Asian J* **9**, 1334-1340, doi:10.1002/asia.201400051 (2014).
- 53 Erez, R. & Shabat, D. The azaquinone-methide elimination: comparison study of 1,6- and 1,4-eliminations under physiological conditions. *Org Biomol Chem* **6**, 2669-2672, doi:10.1039/b808198k (2008).
- 54 Hay, M. P., Anderson, R. F., Ferry, D. M., Wilson, W. R. & Denny, W. A. Synthesis and evaluation of nitroheterocyclic carbamate prodrugs for use with nitroreductase-mediated gene-directed enzyme prodrug therapy. *J Med Chem* **46**, 5533-5545, doi:10.1021/jm030308b (2003).
- 55 Niculescu-Duvaz, D. *et al.* Self-immolative nitrogen mustards prodrugs cleavable by carboxypeptidase G2 (CPG2) showing large cytotoxicity differentials in GDEPT. *J Med Chem* **46**, 1690-1705, doi:10.1021/jm020462i (2003).
- 56 Chang, T. K., Weber, G. F., Crespi, C. L. & Waxman, D. J. Differential activation of cyclophosphamide and ifosfamide by cytochromes P-450 2B and 3A in human liver microsomes. *Cancer Res* **53**, 5629-5637 (1993).
- 57 Niculescu-Duvaz, D. *et al.* Self-immolative nitrogen mustard prodrugs for suicide gene therapy. *J Med Chem* **41**, 5297-5309, doi:10.1021/jm980425k (1998).
- 58 Gesson, J. P. *et al.* Prodrugs of anthracyclines for chemotherapy via enzyme-monoclonal antibody conjugates. *Anticancer Drug Des* **9**, 409-423 (1994).
- 59 Ohwada, J. *et al.* Design, synthesis and antifungal activity of a novel water soluble prodrug of antifungal triazole. *Bioorg Med Chem Lett* **13**, 191-196 (2003).
- 60 M. Eigen & Mayer, L. d. Technique of organic chemistry. *Elucidation of Structures by Physical and Chemical Methods* **44**, 895-1054 (1955).
- 61 Schmid, K. M., Jensen, L. & Phillips, S. T. A self-immolative spacer that enables tunable controlled release of phenols under neutral conditions. *J Org Chem* **77**, 4363-4374, doi:10.1021/jo300400q (2012).
- 62 Hay, M. P., Sykes, B. M., Denny, W. A. & O'Connor, C. J. Substituent effects on the kinetics of reductively-initiated fragmentation of nitrobenzyl carbamates designed as triggers for bioreductive prodrugs. *Journal of the Chemical Society, Perkin Transactions 1* **0**, 2759-2770  
doi:10.1039 / A904067F.
- 63 Robbins, J. S., Schmid, K. M. & Phillips, S. T. Effects of electronics, aromaticity, and solvent polarity on the rate of azaquinone-methide-mediated depolymerization of aromatic carbamate oligomers. *J Org Chem* **78**, 3159-3169, doi:10.1021/jo400105m (2013).

- 
- 64 Weinert, E. E. *et al.* Substituents on quinone methides strongly modulate formation and stability of their nucleophilic adducts. *J Am Chem Soc* **128**, 11940-11947, doi:10.1021/ja062948k (2006).
- 65 Perry-Feigenbaum, R., Baran, P. S. & Shabat, D. The pyridinone-methide elimination. *Org Biomol Chem* **7**, 4825-4828, doi:10.1039/b915265b (2009).
- 66 Tham, Y. C. *et al.* Global prevalence of glaucoma and projections of glaucoma burden through 2040: a systematic review and meta-analysis. *Ophthalmology* **121**, 2081-2090, doi:10.1016/j.ophtha.2014.05.013 (2014).
- 67 Casson, R. J., Chidlow, G., Wood, J. P., Crowston, J. G. & Goldberg, I. Definition of glaucoma: clinical and experimental concepts. *Clin Exp Ophthalmol* **40**, 341-349, doi:10.1111/j.1442-9071.2012.02773.x (2012).
- 68 The Glaucoma Laser Trial (GLT). 2. Results of argon laser trabeculoplasty versus topical medicines. The Glaucoma Laser Trial Research Group. *Ophthalmology* **97**, 1403-1413 (1990).
- 69 Hoyng, P. F. & van Beek, L. M. Pharmacological therapy for glaucoma: a review. *Drugs* **59**, 411-434 (2000).
- 70 Camras, C. B. Travoprost compared with latanoprost and timolol in patients with open-angle glaucoma or ocular hypertension. *Am J Ophthalmol* **133**, 732; author reply 732-733 (2002).
- 71 Sharif, N. A., Kelly, C. R., Crider, J. Y., Williams, G. W. & Xu, S. X. Ocular hypotensive FP prostaglandin (PG) analogs: PG receptor subtype binding affinities and selectivities, and agonist potencies at FP and other PG receptors in cultured cells. *J Ocul Pharmacol Ther* **19**, 501-515, doi:10.1089/108076803322660422 (2003).
- 72 Chatterjee, N. S., Kumar, C. K., Ortiz, A., Rubin, S. A. & Said, H. M. Molecular mechanism of the intestinal biotin transport process. *Am J Physiol* **277**, C605-613, doi:10.1152/ajpcell.1999.277.4.C605 (1999).
- 73 Alvan, G., Calissendorff, B., Seideman, P., Widmark, K. & Widmark, G. Absorption of ocular timolol. *Clin Pharmacokinet* **5**, 95-100 (1980).
- 74 Chang, S. C., Bundgaard, H., Buur, A. & Lee, V. H. Improved corneal penetration of timolol by prodrugs as a means to reduce systemic drug load. *Invest Ophthalmol Vis Sci* **28**, 487-491 (1987).
- 75 Brigitte, P., Olivier, D., Pascal, R. & Jean-Pierre, B. A timolol prodrug for improved ocular delivery: Synthesis, conformational study and hydrolysis of palmitoyl timolol malonate. *International Journal of Pharmaceutics* **128**, 179-188 (1996).
- 76 Alexander, J., Cargill, R., Michelson, S. R. & Schwam, H. (Acyloxy)alkyl carbamates as novel bioreversible prodrugs for amines: increased permeation through biological membranes. *J Med Chem* **31**, 318-322 (1988).
- 77 Nair, B. Final report on the safety assessment of Benzyl Alcohol, Benzoic Acid, and Sodium Benzoate. *Int J Toxicol* **20 Suppl 3**, 23-50 (2001).
- 78 Pacheco-Alvarez, D., Solorzano-Vargas, R. S. & Del Rio, A. L. Biotin in metabolism and its relationship to human disease. *Arch Med Res* **33**, 439-447 (2002).
- 79 Janoria, K. G., Hariharan, S., Paturi, D., Pal, D. & Mitra, A. K. Biotin uptake by rabbit corneal epithelial cells: role of sodium-dependent multivitamin transporter (SMVT). *Curr Eye Res* **31**, 797-809, doi:10.1080/02713680600900206 (2006).
-

- 
- 80 Ghosal, A., Subramanian, V. S. & Said, H. M. Role of the putative N-glycosylation and PKC-phosphorylation sites of the human sodium-dependent multivitamin transporter (hSMVT) in function and regulation. *Biochim Biophys Acta* **1808**, 2073-2080, doi:10.1016/j.bbame.2011.04.014 (2011).
- 81 Gentile, D. *et al.* Cucurbit[7]uril as a catalytic nanoreactor for one-pot synthesis of isoxazolidines in water. *Org Biomol Chem* **18**, 1194-1203, doi:10.1039/c9ob02352f (2020).
- 82 Floresta, G. *et al.* Fourfold Filtered Statistical/Computational Approach for the Identification of Imidazole Compounds as HO-1 Inhibitors from Natural Products. *Mar Drugs* **17**, doi:10.3390/md17020113 (2019).
- 83 Verma, J., Khedkar, V. M. & Coutinho, E. C. 3D-QSAR in drug design--a review. *Curr Top Med Chem* **10**, 95-115, doi:10.2174/156802610790232260 (2010).
- 84 Gentile, D. *et al.* Putative Inhibitors of SARS-CoV-2 Main Protease from A Library of Marine Natural Products: A Virtual Screening and Molecular Modeling Study. *Mar Drugs* **18**, doi:10.3390/md18040225 (2020).
- 85 Vyas, V. K., Ukawala, R. D., Ghate, M. & Chintha, C. Homology modeling a fast tool for drug discovery: current perspectives. *Indian J Pharm Sci* **74**, 1-17, doi:10.4103/0250-474X.102537 (2012).
- 86 Hopf, T. A. *et al.* Sequence co-evolution gives 3D contacts and structures of protein complexes. *Elife* **3**, doi:10.7554/eLife.03430 (2014).
- 87 Laskowski, R. A., Rullmann, J. A., MacArthur, M. W., Kaptein, R. & Thornton, J. M. AQUA and PROCHECK-NMR: programs for checking the quality of protein structures solved by NMR. *J Biomol NMR* **8**, 477-486, doi:10.1007/BF00228148 (1996).
- 88 Griffith, D. A. & Jarvis, S. M. Nucleoside and nucleobase transport systems of mammalian cells. *Biochim Biophys Acta* **1286**, 153-181, doi:10.1016/s0304-4157(96)00008-1 (1996).
- 89 Kraupp, M. & Marz, R. Nucleobase and nucleoside transport in mammalian cells. *Wien Klin Wochenschr* **107**, 677-680 (1995).
- 90 de Koning, H. & Diallinas, G. Nucleobase transporters (review). *Mol Membr Biol* **17**, 75-94 (2000).
- 91 Leung, G. P., Ward, J. L., Wong, P. Y. & Tse, C. M. Characterization of nucleoside transport systems in cultured rat epididymal epithelium. *Am J Physiol Cell Physiol* **280**, C1076-1082, doi:10.1152/ajpcell.2001.280.5.C1076 (2001).
- 92 Vickers, M. F. *et al.* Comparison of the interaction of uridine, cytidine, and other pyrimidine nucleoside analogues with recombinant human equilibrative nucleoside transporter 2 (hENT2) produced in *Saccharomyces cerevisiae*. *Biochem Cell Biol* **80**, 639-644, doi:10.1139/o02-148 (2002).
- 93 Balimane, P. V. & Sinko, P. J. Involvement of multiple transporters in the oral absorption of nucleoside analogues. *Adv Drug Deliv Rev* **39**, 183-209 (1999).
- 94 Borgland, S. L. & Parkinson, F. E. Uptake and release of [3H]formycin B via sodium-dependent nucleoside transporters in mouse leukemic L1210/MA27.1 cells. *J Pharmacol Exp Ther* **281**, 347-353 (1997).
- 95 Hosoya, K. *et al.* MCT1-mediated transport of L-lactic acid at the inner blood-retinal barrier: a possible route for delivery of monocarboxylic acid
-

- 
- drugs to the retina. *Pharm Res* **18**, 1669-1676, doi:10.1023/a:1013310210710 (2001).
- 96 Li, Y. H. *et al.* Mechanism of intestinal absorption of an orally active beta-lactam prodrug: uptake and transport of carindacillin in Caco-2 cells. *J Pharmacol Exp Ther* **290**, 958-964 (1999).
- 97 Li, Y. H., Tanno, M., Itoh, T. & Yamada, H. Role of the monocarboxylic acid transport system in the intestinal absorption of an orally active beta-lactam prodrug: carindacillin as a model. *Int J Pharm* **191**, 151-159, doi:10.1016/s0378-5173(99)00299-9 (1999).
- 98 Tsuji, A., Tamai, I., Nakanishi, M., Terasaki, T. & Hamano, S. Intestinal brush-border transport of the oral cephalosporin antibiotic, cefdinir, mediated by dipeptide and monocarboxylic acid transport systems in rabbits. *J Pharm Pharmacol* **45**, 996-998, doi:10.1111/j.2042-7158.1993.tb05645.x (1993).
- 99 Hosoya, K., Horibe, Y., Kim, K. J. & Lee, V. H. Nucleoside transport mechanisms in the pigmented rabbit conjunctiva. *Invest Ophthalmol Vis Sci* **39**, 372-377 (1998).
- 100 Majumdar, S., Gunda, S. & Mitra, A. Functional expression of a sodium dependent nucleoside transporter on rabbit cornea: Role in corneal permeation of acyclovir and idoxuridine. *Curr Eye Res* **26**, 175-183, doi:10.1076/ceyr.26.3.175.14895 (2003).
- 101 Sharma, H. P., Halder, N., Singh, S. B. & Velpandian, T. Involvement of nucleoside transporters in the transcorneal permeation of topically instilled substrates in rabbits in-vivo. *Eur J Pharm Sci* **114**, 364-371, doi:10.1016/j.ejps.2017.12.027 (2018).
- 102 Catron, T. & Hern, H. G. Herpes zoster ophthalmicus. *West J Emerg Med* **9**, 174-176 (2008).
- 103 Liesegang, T. J. Herpes zoster ophthalmicus natural history, risk factors, clinical presentation, and morbidity. *Ophthalmology* **115**, S3-12, doi:10.1016/j.ophtha.2007.10.009 (2008).
- 104 Insinga, R. P., Itzler, R. F., Pellissier, J. M., Saddier, P. & Nikas, A. A. The incidence of herpes zoster in a United States administrative database. *J Gen Intern Med* **20**, 748-753, doi:10.1111/j.1525-1497.2005.0150.x (2005).
- 105 Cobo, M. *et al.* Observations on the natural history of herpes zoster ophthalmicus. *Curr Eye Res* **6**, 195-199, doi:10.3109/02713688709020090 (1987).
- 106 Zaal, M. J., Volker-Dieben, H. J. & D'Amaro, J. Prognostic value of Hutchinson's sign in acute herpes zoster ophthalmicus. *Graefes Arch Clin Exp Ophthalmol* **241**, 187-191, doi:10.1007/s00417-002-0609-1 (2003).
- 107 Harding, S. P., Lipton, J. R. & Wells, J. C. Natural history of herpes zoster ophthalmicus: predictors of postherpetic neuralgia and ocular involvement. *Br J Ophthalmol* **71**, 353-358, doi:10.1136/bjo.71.5.353 (1987).
- 108 Roesel, M., Heiligenhaus, A. & Messmer, E. M. [Clinical presentation of zoster ophthalmicus]. *Klin Monbl Augenheilkd* **227**, 370-374, doi:10.1055/s-0029-1245329 (2010).
- 109 McGill, J. The enigma of herpes stromal disease. *Br J Ophthalmol* **71**, 118-125, doi:10.1136/bjo.71.2.118 (1987).
- 110 Puri, L. R., Shrestha, G. B., Shah, D. N., Chaudhary, M. & Thakur, A. Ocular manifestations in herpes zoster ophthalmicus. *Nepal J Ophthalmol* **3**, 165-171, doi:<http://dx.doi.org/10.3126/nepjoph.v3i2.5271> (2011).
-

- 
- 111 Buchi, E. R., Herbort, C. P. & Ruffieux, C. Oral acyclovir in the treatment of acute herpes zoster ophthalmicus. *Am J Ophthalmol* **102**, 531-532, doi:10.1016/0002-9394(86)90086-3 (1986).
- 112 Colin, J. *et al.* Comparison of the efficacy and safety of valaciclovir and acyclovir for the treatment of herpes zoster ophthalmicus. *Ophthalmology* **107**, 1507-1511, doi:10.1016/s0161-6420(00)00222-0 (2000).
- 113 Tyring, S. *et al.* Famciclovir for ophthalmic zoster: a randomised aciclovir controlled study. *Br J Ophthalmol* **85**, 576-581, doi:10.1136/bjo.85.5.576 (2001).
- 114 Morfin, F. & Thouvenot, D. Herpes simplex virus resistance to antiviral drugs. *J Clin Virol* **26**, 29-37 (2003).
- 115 Bundgaard, H., Jensen, E. & Falch, E. Water-soluble, solution-stable, and biolabile N-substituted (aminomethyl)benzoate ester prodrugs of acyclovir. *Pharm Res* **8**, 1087-1093, doi:10.1023/a:1015837931256 (1991).
- 116 Richards, D. M. *et al.* Acyclovir. A review of its pharmacodynamic properties and therapeutic efficacy. *Drugs* **26**, 378-438, doi:10.2165/00003495-198326050-00002 (1983).
- 117 Sanitato, J. J., Asbell, P. A., Varnell, E. D., Kissling, G. E. & Kaufman, H. E. Acyclovir in the treatment of herpetic stromal disease. *Am J Ophthalmol* **98**, 537-547, doi:10.1016/0002-9394(84)90237-x (1984).
- 118 Hughes, P. M. & Mitra, A. K. Effect of acylation on the ocular disposition of acyclovir. II: Corneal permeability and anti-HSV 1 activity of 2'-esters in rabbit epithelial keratitis. *J Ocul Pharmacol* **9**, 299-309 (1993).
- 119 Hughes, P. M., Krishnamoorthy, R. & Mitra, A. K. Effect of acylation on the ocular disposition of acyclovir. I: Synthesis, physicochemical properties, and antiviral activity of 2'-esters. *J Ocul Pharmacol* **9**, 287-297 (1993).
- 120 Anand, B. S., Patel, J. & Mitra, A. K. Interactions of the dipeptide ester prodrugs of acyclovir with the intestinal oligopeptide transporter: competitive inhibition of glycylsarcosine transport in human intestinal cell line-Caco-2. *J Pharmacol Exp Ther* **304**, 781-791, doi:10.1124/jpet.102.044313 (2003).
- 121 Gray, J. H., Owen, R. P. & Giacomini, K. M. The concentrative nucleoside transporter family, SLC28. *Pflugers Arch* **447**, 728-734, doi:10.1007/s00424-003-1107-y (2004).
- 122 Slugoski, M. D. *et al.* Conserved glutamate residues Glu-343 and Glu-519 provide mechanistic insights into cation/nucleoside cotransport by human concentrative nucleoside transporter hCNT3. *J Biol Chem* **284**, 17266-17280, doi:10.1074/jbc.M109.009613 (2009).
- 123 Nayal, M. & Di Cera, E. Valence screening of water in protein crystals reveals potential Na<sup>+</sup> binding sites. *J Mol Biol* **256**, 228-234, doi:10.1006/jmbi.1996.0081 (1996).
- 124 Johnson, Z. L., Cheong, C. G. & Lee, S. Y. Crystal structure of a concentrative nucleoside transporter from *Vibrio cholerae* at 2.4 Å. *Nature* **483**, 489-493, doi:10.1038/nature10882 (2012).
- 125 Hirschi, M., Johnson, Z. L. & Lee, S. Y. Visualizing multistep elevator-like transitions of a nucleoside transporter. *Nature* **545**, 66-70, doi:10.1038/nature22057 (2017).
-

- 
- 126 Urtti, A. & Salminen, L. Minimizing systemic absorption of topically administered ophthalmic drugs. *Surv Ophthalmol* **37**, 435-456, doi:10.1016/0039-6257(93)90141-s (1993).
- 127 Sai, Y. & Tsuji, A. Transporter-mediated drug delivery: recent progress and experimental approaches. *Drug Discov Today* **9**, 712-720, doi:10.1016/S1359-6446(04)03198-8 (2004).
- 128 Oosterhuis, J. A., van Ganswijk, R. & Versteeg, J. Acyclovir treatment in stromal herpetic keratitis. *Doc Ophthalmol* **56**, 81-88, doi:10.1007/BF00154713 (1983).
- 129 Katragadda, S., Gunda, S., Hariharan, S. & Mitra, A. K. Ocular pharmacokinetics of acyclovir amino acid ester prodrugs in the anterior chamber: evaluation of their utility in treating ocular HSV infections. *Int J Pharm* **359**, 15-24, doi:10.1016/j.ijpharm.2008.03.015 (2008).
- 130 Young, J. D., Yao, S. Y., Sun, L., Cass, C. E. & Baldwin, S. A. Human equilibrative nucleoside transporter (ENT) family of nucleoside and nucleobase transporter proteins. *Xenobiotica* **38**, 995-1021, doi:10.1080/00498250801927427 (2008).
- 131 Zhang, J. *et al.* Uridine binding motifs of human concentrative nucleoside transporters 1 and 3 produced in *Saccharomyces cerevisiae*. *Mol Pharmacol* **64**, 1512-1520, doi:10.1124/mol.64.6.1512 (2003).
- 132 Trott, O. & Olson, A. J. AutoDock Vina: improving the speed and accuracy of docking with a new scoring function, efficient optimization, and multithreading. *J Comput Chem* **31**, 455-461, doi:10.1002/jcc.21334 (2010).
- 133 Zhou, Y. *et al.* Cryo-EM structure of the human concentrative nucleoside transporter CNT3. *PLoS Biol* **18**, e3000790, doi:10.1371/journal.pbio.3000790 (2020).
- 134 Nagai, K., Nagasawa, K. & Fujimoto, S. Uptake of the anthracycline pirarubicin into mouse M5076 ovarian sarcoma cells via a sodium-dependent nucleoside transport system. *Cancer Chemother Pharmacol* **55**, 222-230, doi:10.1007/s00280-004-0861-7 (2005).
- 135 Cobos, E. J., Entrena, J. M., Nieto, F. R., Cendan, C. M. & Del Pozo, E. Pharmacology and therapeutic potential of sigma(1) receptor ligands. *Curr Neuropharmacol* **6**, 344-366, doi:10.2174/157015908787386113 (2008).
- 136 Brune, S., Priehl, S. & Wunsch, B. Structure of the sigma1 receptor and its ligand binding site. *J Med Chem* **56**, 9809-9819, doi:10.1021/jm400660u (2013).
- 137 Fishback, J. A., Robson, M. J., Xu, Y. T. & Matsumoto, R. R. Sigma receptors: potential targets for a new class of antidepressant drug. *Pharmacol Ther* **127**, 271-282, doi:10.1016/j.pharmthera.2010.04.003 (2010).
- 138 Matsumoto, R. R., Liu, Y., Lerner, M., Howard, E. W. & Brackett, D. J. Sigma receptors: potential medications development target for anti-cocaine agents. *Eur J Pharmacol* **469**, 1-12, doi:10.1016/s0014-2999(03)01723-0 (2003).
- 139 Kashiwagi, H. *et al.* Selective sigma-2 ligands preferentially bind to pancreatic adenocarcinomas: applications in diagnostic imaging and therapy. *Mol Cancer* **6**, 48, doi:10.1186/1476-4598-6-48 (2007).
-

- 
- 140 Vilner, B. J., John, C. S. & Bowen, W. D. Sigma-1 and sigma-2 receptors are expressed in a wide variety of human and rodent tumor cell lines. *Cancer Res* **55**, 408-413 (1995).
- 141 Bowen, W. D. Sigma receptors: recent advances and new clinical potentials. *Pharm Acta Helv* **74**, 211-218, doi:10.1016/s0031-6865(99)00034-5 (2000).
- 142 Hayashi, T. & Su, T. P. Sigma-1 receptor chaperones at the ER-mitochondrion interface regulate Ca(2+) signaling and cell survival. *Cell* **131**, 596-610, doi:10.1016/j.cell.2007.08.036 (2007).
- 143 Mavlyutov, T. A., Nickells, R. W. & Guo, L. W. Accelerated retinal ganglion cell death in mice deficient in the Sigma-1 receptor. *Mol Vis* **17**, 1034-1043 (2011).
- 144 Ola, M. S. *et al.* Expression pattern of sigma receptor 1 mRNA and protein in mammalian retina. *Brain Res Mol Brain Res* **95**, 86-95, doi:10.1016/s0169-328x(01)00249-2 (2001).
- 145 Cuenca, N. *et al.* Cellular responses following retinal injuries and therapeutic approaches for neurodegenerative diseases. *Prog Retin Eye Res* **43**, 17-75, doi:10.1016/j.preteyeres.2014.07.001 (2014).
- 146 Dun, Y., Thangaraju, M., Prasad, P., Ganapathy, V. & Smith, S. B. Prevention of excitotoxicity in primary retinal ganglion cells by (+)-pentazocine, a sigma receptor-1 specific ligand. *Invest Ophthalmol Vis Sci* **48**, 4785-4794, doi:10.1167/iovs.07-0343 (2007).
- 147 Martin, P. M., Ola, M. S., Agarwal, N., Ganapathy, V. & Smith, S. B. The sigma receptor ligand (+)-pentazocine prevents apoptotic retinal ganglion cell death induced in vitro by homocysteine and glutamate. *Brain Res Mol Brain Res* **123**, 66-75, doi:10.1016/j.molbrainres.2003.12.019 (2004).
- 148 Tchandre, K. T. & Yorio, T. sigma-1 receptors protect RGC-5 cells from apoptosis by regulating intracellular calcium, Bax levels, and caspase-3 activation. *Invest Ophthalmol Vis Sci* **49**, 2577-2588, doi:10.1167/iovs.07-1101 (2008).
- 149 Senda, T. *et al.* Ameliorative effect of SA4503, a novel cognitive enhancer, on the basal forebrain lesion-induced impairment of the spatial learning performance in rats. *Pharmacol Biochem Behav* **59**, 129-134, doi:10.1016/s0091-3057(97)00385-7 (1998).
- 150 Bucolo, C. & Drago, F. Effects of neurosteroids on ischemia-reperfusion injury in the rat retina: role of sigma1 recognition sites. *Eur J Pharmacol* **498**, 111-114, doi:10.1016/j.ejphar.2004.06.067 (2004).
- 151 Cantarella, G. *et al.* Protective effects of the sigma agonist Pre-084 in the rat retina. *Br J Ophthalmol* **91**, 1382-1384, doi:10.1136/bjo.2007.118570 (2007).
- 152 Zhao, J. *et al.* Sigma receptor ligand, (+)-pentazocine, suppresses inflammatory responses of retinal microglia. *Invest Ophthalmol Vis Sci* **55**, 3375-3384, doi:10.1167/iovs.13-12823 (2014).
- 153 Zhang, D., Wlodawer, A. & Lubkowski, J. Crystal Structure of a Complex of the Intracellular Domain of Interferon lambda Receptor 1 (IFNLR1) and the FERM/SH2 Domains of Human JAK1. *J Mol Biol* **428**, 4651-4668, doi:10.1016/j.jmb.2016.10.005 (2016).
- 154 Kurcinski, M., Jaronczyk, M., Lipinski, P. F. J., Dobrowolski, J. C. & Sadlej, J. Structural Insights into sigma(1) Receptor Interactions with
-

- Opioid Ligands by Molecular Dynamics Simulations. *Molecules* **23**, doi:10.3390/molecules23020456 (2018).
- 155 Cheng, K. J., Hsieh, C. M., Nepali, K. & Liou, J. P. Ocular Disease Therapeutics: Design and Delivery of Drugs for Diseases of the Eye. *J Med Chem* **63**, 10533-10593, doi:10.1021/acs.jmedchem.9b01033 (2020).
- 156 Costa, V. P. *et al.* Ocular perfusion pressure in glaucoma. *Acta Ophthalmol* **92**, e252-266, doi:10.1111/aos.12298 (2014).
- 157 Amata, E. *et al.* Sigma Receptor Ligands Carrying a Nitric Oxide Donor Nitrate Moiety: Synthesis, In Silico, and Biological Evaluation. *ACS Med Chem Lett* **11**, 889-894, doi:10.1021/acsmchemlett.9b00661 (2020).
- 158 Floresta, G. *et al.* A Structure- and Ligand-Based Virtual Screening of a Database of "Small" Marine Natural Products for the Identification of "Blue" Sigma-2 Receptor Ligands. *Mar Drugs* **16**, doi:10.3390/md16100384 (2018).
- 159 Martin, W. R., Eades, C. G., Thompson, J. A., Huppler, R. E. & Gilbert, P. E. The effects of morphine- and nalorphine- like drugs in the nondependent and morphine-dependent chronic spinal dog. *J Pharmacol Exp Ther* **197**, 517-532 (1976).
- 160 Nguyen, L. *et al.* Role of sigma-1 receptors in neurodegenerative diseases. *J Pharmacol Sci* **127**, 17-29, doi:10.1016/j.jphs.2014.12.005 (2015).
- 161 Mei, J. & Pasternak, G. W. Sigma1 receptor modulation of opioid analgesia in the mouse. *J Pharmacol Exp Ther* **300**, 1070-1074 (2002).
- 162 Gromek, K. A. *et al.* The oligomeric states of the purified sigma-1 receptor are stabilized by ligands. *J Biol Chem* **289**, 20333-20344, doi:10.1074/jbc.M113.537993 (2014).
- 163 Navarro, G. *et al.* Direct involvement of sigma-1 receptors in the dopamine D1 receptor-mediated effects of cocaine. *Proc Natl Acad Sci U S A* **107**, 18676-18681, doi:10.1073/pnas.1008911107 (2010).
- 164 Carnally, S. M., Johannessen, M., Henderson, R. M., Jackson, M. B. & Edwardson, J. M. Demonstration of a direct interaction between sigma-1 receptors and acid-sensing ion channels. *Biophys J* **98**, 1182-1191, doi:10.1016/j.bpj.2009.12.4293 (2010).
- 165 Balasuriya, D. *et al.* The sigma-1 receptor binds to the Nav1.5 voltage-gated Na<sup>+</sup> channel with 4-fold symmetry. *J Biol Chem* **287**, 37021-37029, doi:10.1074/jbc.M112.382077 (2012).
- 166 Van Durme, J. *et al.* A graphical interface for the FoldX forcefield. *Bioinformatics* **27**, 1711-1712, doi:10.1093/bioinformatics/btr254 (2011).
- 167 Stewart, J. J. Optimization of parameters for semiempirical methods IV: extension of MNDO, AM1, and PM3 to more main group elements. *J Mol Model* **10**, 155-164, doi:10.1007/s00894-004-0183-z (2004).
- 168 Johnson, Z. L. *et al.* Structural basis of nucleoside and nucleoside drug selectivity by concentrative nucleoside transporters. *Elife* **3**, e03604, doi:10.7554/eLife.03604 (2014).
- 169 Krieger, E. & Vriend, G. YASARA View - molecular graphics for all devices - from smartphones to workstations. *Bioinformatics* **30**, 2981-2982, doi:10.1093/bioinformatics/btu426 (2014).
- 170 van Meer, G., Voelker, D. R. & Feigenson, G. W. Membrane lipids: where they are and how they behave. *Nat Rev Mol Cell Biol* **9**, 112-124, doi:10.1038/nrm2330 (2008).
-